Aerosol Effects on Mesoscale Convective Systems: Can Urban Regions Affect Severe Weather?

by

Stacey Kawecki

A dissertation submitted in partial fulfillment
of the requirements for the degree of
Doctor of Philosophy in
(Atmospheric, Oceanic, and Space Sciences)
The University of Michigan
2017

Doctoral Committee:

Associate Professor Allison Steiner, Chair
Associate Professor J. Tim Dvonch
Professor Joyce Penner
Associate Professor Derek Posselt

Stacey Kawecki

slekaw@umich.edu

ORCIC iD: 0000-0003-2677-2191

DEDICATION

To my Jia Jia, Daniel Kawecki. He always believed in me, encouraged my curiosity, and gave me my very first lesson on clouds and thunderstorms.

ACKNOWLEDGEMENTS

The well of gratitude I have for those who guided me through this academic adventure is seemingly bottomless. This experience has been transformative and I would like to express my appreciation for the individuals who have aided me during this process. First and foremost, I would like to thank my advisor, Dr. Allison Steiner. To this day, I marvel at how the puzzle pieces fit into place such that we could work together. Working with Allison has been a privilege. She always values my contributions and ideas; weekly meetings felt like collaborations. Her unfailing confidence in me inspired and encouraged me to keep going, even when it felt like I could never complete the task, like when I was afraid to edit model code. She always encouraged me to dig for an answer, and guided me through the process of learning how to debug, both code and academic life.

Next I would like to recognize my first advisor and mentor, Frank Marsik. The very week I started thinking about pursuing a PhD, he told me "I think you'd make a great PhD student". He always had a moment when I needed it and provided much-needed encouragement when I accidentally g-chatted him instead of a fellow student about how I couldn't possibly ever graduate. Thank you, Frank, for always listening.

To each of my committee members, your feedback has been invaluable and you have each inspired me academically. Derek Posselt, your Clouds and Precipitation class may have changed my life. I always knew I liked clouds, but while taking your class, I learned that modeling clouds was fascinating. Tim Dvonch provided me with an amazing opportunity in the

Air Quality lab my first summer in Ann Arbor, where my curiosity about the data being collected lead to my inevitable pursuit of a PhD. Joyce Penner taught me about aerosol processes, but our first interaction occurred when she guest lectured in the clouds and precipitation course. She discussed how clouds are represented in global models, and when I asked a question, knowing absolutely nothing about modeling at the time, her answer surprised me – using cloud resolving models in global models is actually an active area of research! Thank you to each of my committee members – who push me towards the best work I can produce, leading me by example.

To my fellow Steinerites! Every one of you has left a lasting impression. Alex, you were always ready to help me with NCL, chemistry, or life. You provided a wonderful aura of positivity and light. Yang – as my PhD buddy, we've seen a lot. From fluids and Rad-Tran, all the way to dissertation writing. These last five years you've been my constant companion and I wouldn't have it any other way. Susan – our g-chat conversations could probably fill up hundreds of pages. You are always there for me, whether it's as a paragraph editor, a shoulder to cry on, a friend to laugh with, or a Yin yoga companion. Matt, your outlook on life is contagious, in the best way. I'm so glad we have had the opportunity to work together and learn from each other. Ahmed, you were the first one to tell me to not be afraid to break the code. Kirsti, you always provided excellent feedback, timely encouragement, and perfectly composed sarcasm. Samantha, fellow meteorologist, feminist and lover of Gilmore Girls – your thoughtful approach to your work and your friendships are greatly appreciated.

The administrative staff has always been so helpful and responsive. I've had the opportunity to work with many of you, through my work with GUStO and MGU, so I want to thank you all for making those endeavors much more pleasant and efficient. Specifically, I'd like

to thank Sandra Pytlinski, for all the time you have put into my paperwork. I definitely could not graduate without you. Tonya, you are always so helpful and prompt.

Friends are the family you choose, and I chose some pretty awesome family, my fellow scoobies. Anne, you are the Willow to my Buffy. The support and inspiration you have provided me these last years has been incredible, and I'm so lucky to have found you! Beth, you always provide a hug when I need it. Your heart is so big, and I'm grateful to have you as a friend. Lizzi, you are my partner in dining and cartoon watching. Chris, my OG lady, your positivity and encouragement have fueled this academic fire. To Adam, my homework buddy turned friend, your love of Michigan athletics has definitely rubbed off on me. Thank you for always being my sports-watching buddy and for providing a laid back presence to counteract my anxious tendencies. Jen, thank you for all the fun, all the understanding, and all the wine. And all the Halloweens! While our domestic partnership might be coming to an end, our friendship will not, plus there's that whole dog mom thing. The fine folks of Red Zeppelin and Molecular Thunder deserve a shout out for helping me stay active and competitive in the world of intramural sports. And thanks to Greg and Jared, who always listen and never judge – even when I'm being really weird.

The love and support from my family has been amazing. Mom you are the Lorelai to my Rory. You have always believed in me, supported me, and encouraged me to be who I am. Dad, you inspired me to look at the sky and ask why. Michelle and Tim, you are my pillars, the support that never waivers. You both inspire me every single day. Jerry, you always invite me to think about things from different perspectives and Justin, you have always inspired me to be my best self. Thank you to everyone who has helped me through this process. It is only with your guidance, inspiration, support and friendships that I have been able to come this far.

Table of Contents

List of Tables

List of Figures

Abstract

Aerosols affect the climate system via directly reflecting or absorbing incoming or outgoing short or long-wave radiation, or by affecting cloud albedo and precipitation processes. In this dissertation, I focus on the role of aerosols as cloud condensation nuclei and their impact on precipitation patterns and cloud lifetimes (i.e., the second indirect effect). I hypothesize that anthropogenic and natural aerosols originating from the Great Plains region have the ability to affect severe weather through the magnitude, composition and source of aerosol emissions. These influences are addressed using the Weather Research and Forecasting model coupled with chemistry (WRF-Chem 3.6), including the development of a new ice nucleation parameterization for dust aerosol. The first chapter examines the impact of the magnitude of urban aerosol emissions on a squall line in the Central Great Plains. Changes in urban emissions and the resulting aerosol loading drive changes in cloud microphysics, which alter the Mesoscale convective system (MCS) propagation and strength via cold pool strength, and trigger large-scale changes in storm morphology and precipitation patterns. These results show that urban emissions can play an important role in mesoscale weather systems. The second chapter investigates the role of aerosol composition on the precipitation patterns and intensity resulting from the same squall line. By changing the prescribed default hygroscopicity values to updated values from laboratory studies, model assumptions about individual component hygroscopicity are tested for anthropogenic aerosols such as ammonium, sulfate, nitrate, and organic species. The sensitivity simulations yield changes in the distribution of high-intensity precipitation events, indicating that

aerosol composition plays an important role in predicting high intensity events. Finally, the third chapter investigates the role of dust on ice nucleation and deep convection. One of the major limitations of WRF-Chem is that it does not include the effects of heterogeneous ice nucleation in cold clouds. We implement the Phillips et al (2008) and DeMott et.al (2010) parameterization in the Morrison microphysics scheme of WRF-Chem with interactive dust aerosols to improve these model processes. Including dust as ice-nucleating particles (INPs) affects important microphysical characteristics, where ice crystals and snowflakes tend to increase effective radii and decrease number concentrations. These changes in cloud properties signify that including dust as IN in WRF-Chem can aid in decreasing uncertainty surrounding the aerosol-cloud interactions effects on climate. Overall, this work highlights the role of aerosol composition and magnitude on cloud microphysical processes. These processes are substantial enough, even during severe weather events, to influence the placement and intensity of simulated precipitation, and an improved representation of these aerosol-cloud interactions will likely improve the predictability of precipitation in this region.

Chapter I

Overview of Cloud and Aerosol Interactions

1.0 Introduction

1.1 Atmospheric Aerosols

Aerosols are defined as fine solid or liquid particles suspended in a gas. In the Earth's atmosphere, they can be defined by size, composition, and emission sources. Typically, four size modes are used to represent the range of aerosol diameters in the atmosphere (Figure 1.1). The nucleation mode is the smallest mode, with aerosol diameters up to approximately 10 nanometers, followed by the Aitken mode (10 nm – 100 nm diameters). The nucleation mode represents processes of new particle formation from the condensation of vapors (e.g., sulfur dioxide oxygenated volatile organic compounds), and the coagulation of condensed vapors to form aerosols. The Aitken mode aerosols are usually emitted as particles and provide a surface onto which gases can condense, leading to the formation of larger particles. The third mode is the accumulation mode (100 nm – 2.5 microns), thus named because atmospheric removal processes (e.g., dry deposition; wet deposition) are not as efficient in this size range and therefore cause particles of this size to accumulate in the atmosphere. Many of these particles are the result of primary emissions from biogenic and anthropogenic activity, and are subject to further growth in

the atmosphere after the condensation of atmospheric gases onto particles. Finally, the fourth mode is the coarse mode (> 2.5 microns). Because of their size, these aerosols have relatively large sedimentation velocities and tend to settle out of the atmosphere quickly (Seinfeld and Pandis 2006). Two common approaches exist to represent aerosol size and number concentrations in models, the modal approach and the sectional approach. The modal approach uses a lognormal distribution for each mode: the Aitken, accumulation, and coarse mode, like the MADE-SORGAM model ((Ackermann et al. 1998). Modal representations enable the efficient tracking of aerosol number concentrations, sizes, and composition. The sectional approach is more computationally expensive and uses bins, integrated over size ranges, to track aerosol size, number, and composition, like the MOSAIC model (Zaveri et al. 2008).

Aerosol sources can be either natural or anthropogenic as well as emitted primarily from the Earth's surface or formed by secondary processes in the atmosphere. Natural sources are vast and include sea salt from oceans, dust from deserts and dry soil, organic matter from biomass burning, and pollen and spores from the biosphere. Anthropogenic sources include primary particles produced by power generation, engine combustion, agriculture, anthropogenic burning, and industry. In addition to their source attribution to a specific process, the mechanism of emission and/or formation is also important. Primary emissions are direct emission from the surface (Prospero et al. 2002), where as secondary production can occur based on chemical processes in the atmosphere. This second mechanism relies on the emission of gases such as sulfur dioxide (SO_2) and volatile organic compounds (VOCs), which can be oxidized to form lower volatility products that partition in to the aerosol phase (Kanakidou et al. 2005). They can also condense and/or coagulate with other particles to make clusters and larger particles in the atmosphere. The combination of natural versus anthropogenic, and primary versus secondary,

determine their population characteristics of size, number, and composition. In turn, these characteristics define and determine how aerosols interact with the atmosphere.

1.2 Aerosol-Cloud-Climate Interactions

Atmospheric aerosols can affect clouds, weather and climate, but their influence on cloud processes at varying spatial and temporal scales is highly uncertain (Stevens and Feingold 2009; Boucher et al. 2013; Fan et al. 2016). Aerosols can alter the climate directly, by influencing the transfer of radiation through the atmosphere (Figure 1.2) Composition and size determine whether an aerosol will either reflect or absorb the incoming or outgoing short or long-wave radiation. For example, fine particles (e.g., the accumulation mode with diameters < 2.5 microns) interact with shortwave radiation from the sun, scattering incoming solar radiation and cooling the Earth's surface (known as the direct effect). Additionally, some chemical components of aerosols can absorb incoming solar radiation, such as black carbon (Andreae and Gelencsér 2006) brown carbon (Liu et al. 2014) and other weakly absorbing organics (Zhang et al. 2013).

Aerosols can also indirectly influence climate through the modification of clouds (Figure 1.2). The addition of aerosols as cloud condensation nuclei (CCN) affects the albedo of clouds, known as the first indirect effect (Twomey 1977). Increasing concentrations of atmospheric aerosols can also influence precipitation processes and cloud lifetimes, known as the second indirect effect (Albrecht 1989). The number concentration and size distribution are the dominant factors in determining aerosol effects on precipitation and cloud lifetime (Khain et al. 2000; Dusek et al. 2006). However, the aerosol chemical composition also influences its ability to act as a CCN (Ekman et al. 2004; Fan et al. 2007; Shrivastava et al. 2013), where increasing the amount of soluble chemical species leads to an increase in the aerosols' ability to activate as a CCN. On shorter time scales, studies show that aerosols can affect weather on timescales that

govern deep convection and severe weather (Andreae et al. 2004; Tao et al. 2012; Saide et al. 2015). The amount and composition of aerosol in a given meteorological system affects the efficiency of cloud microphysics and precipitation development, thereby altering the cloud macrostructure and lifetime (Stevens and Feingold 2009). For example, anthropogenic aerosols from a New York City, NY can lead to increases in downwind precipitation, updraft velocities and overall increased organized convection (Ntelekos et al. 2009). Increases in elemental carbon, which is light absorbing and does not act as a CCN leads to more intense flooding events due to radiation effects (Fan et al. 2015).

1.3 Cloud Microphysics

1.3.1 Cloud Drop Formation

To understand the implications aerosols have on clouds and precipitation and their indirect climate effects, fundamental cloud and precipitation processes are described here. The most basic element of a cloud is a cloud drop. In warm clouds (temperature > 0°C), the first step in initiating cloud and precipitation processes is the activation of aerosols as cloud condensation nuclei (CCN) (Hudson 1993). The ability of an aerosol to act as a good CCN depends on its size, composition, and the environmental factors. Once formed, a drop will grow or decay based on the balance between the evaporation and condensation rates between the droplet and the surrounding atmosphere (Mason,1971). These rates depend on the temperature, the amount of water vapor in the atmosphere, the size of the drop, and the composition of the aerosol on which the water condenses. After water condenses on the aerosol, the aerosol can dissolve into the cloud drop, so the cloud drop becomes a solution. The number of ions in this solution partially determines the growth rate of a cloud drop; more ions would lead to faster growth (known as the "solute" effect). However, the size of

the newly formed cloud drop also affects the drop growth rate. The curvature effect is a function of surface tension and how a curved surface changes the supersaturation vapor pressure, $\frac{e_s'}{e_s(\infty)}$. Köhler Theory (Equation 1) describes these competing effects of size and composition (Köhler 1936):

$$\frac{e_s'}{e_s(\infty)} \cong 1 + \frac{a}{r} - \frac{b_a}{r^3}, a = \frac{2\sigma_{lv}}{R_v \rho_L T}, b_a = \frac{3 i m_L M_a}{4\pi \rho_L m_a} \quad \text{(Eq 1)}$$

where $\frac{a}{r}$ is the curvature effect and $\frac{b_a}{r^3}$ is the solute effect. The curvature effect is a function of the surface tension of water (σ_{lv}) and the drop size (r), which increases the saturation vapor pressure above the surface of the drop. The solute effect is a function of the number of ions, i, the liquid mass m_L, the mass of the aerosol M_a, and the molecular weight of the aerosol, m_a. Therefore, the more ions an aerosol has, the more soluble it is and the more likely it will reduce the vapor pressure, leading to quicker growth (Rogers and Yau 1989). Figure 1.3 illustrates cloud droplet growth as described by Köhler theory, where very high supersaturations are required to allow cloud droplets to grow when they are small, until they reach a critical supersaturation (Sc), after which droplet growth for larger sizes requires lower supersaturations.

1.3.2 Cloud droplet activation

Because CCN activation is the first step in cloud formation, representation of this activation step is important in models that simulate cloud drop formation and also represents a key uncertainty in how climate models simulate clouds (Kreidenweis and Asa-Awuku 2014; Farmer et al. 2015; Ruehl et al. 2016; Zhou et al. 2016). Hygroscopicity is a lab-derived characteristic that describes how readily a particular chemical species will take up water, and is commonly used in models to determine supersaturation values that will

trigger aerosols to activate as CCN. Higher values of hygroscopicity would correspond to a quicker activation of smaller aerosols at lower supersaturation. (Petters and Kreidenweis 2007) formulated a CCN activation model parameterization that accounts for the hygroscopicity, dry diameter size of a particle and the environmental supersaturation, known as the "kappa" parameterization (Figure 1.4). In WRF-Chem, hygroscopicity is calculated by mode for modal aerosol representation (Ackermann et al. 1998; Schell et al. 2001) (or bins, if it is a sectional approach; e.g., MOSAIC (Zaveri et al. 2008)), and volumetrically averaged to create a bulk hygroscopicity value for each size mode. This value is then used with grid-cell supersaturation and updraft velocity to determine how many aerosols will activate as cloud drops (Chapman et al. 2009). While size is an important parameterization, the kappa formulation allows the inclusion of aerosol composition on the formation of cloud drops.

By relating the hygroscopicity of aerosols derived from WRF-Chem to the kappa values used in the Regional Atmospheric Modeling System (RAMS; (Pielke et al. 1992)), (Ward and Cotton 2011) demonstrate that including hygroscopicity in the CCN activation leads to a better spatial and temporal representation of CCN. Using observed hygroscopicity values also leads to an improved prediction of cloud macrostrucre characteristics, like cloud optical depth and liquid water path (Yang et al. 2011). Additionally, the ability to represent the organic aerosol hygroscopicities is also a necessary for more accurate CCN predictions (Shrivastava et al. 2013), however there are still large uncertainties surrounding organic aerosols in modeling their formation.

1.3.3. Cloud and Rain Drop Formation Processes

Within the cloud, updrafts and downdrafts can move cloud droplets and other hydrometeors, where the speed of motion depends on the hydrometeor size. These size differences are important, because of the process of collision and coalescence of cloud droplets can alter the overall size distribution. Collision and coalescence is the primary process for rain formation in warm clouds. Increasing the number of hygroscopic aerosols in warm clouds leads to an increase in the number of smaller cloud drops, decreasing the collision and coalescence efficiency and leading to longer cloud lifetimes (Albrecht 1989). This effect has been investigated substantially, via both modeling and observational studies (Rosenfeld 1999, 2000; Sekiguchi et al. 2003; Kaufman et al. 2005; Morrison and Grabowski 2007; Rosenfeld et al. 2008; Wang et al. 2012)). Understanding the effects aerosol composition and magnitude have on warm clouds is imperative for better quantifying the aerosol-cloud second indirect effect, especially considering deep convection. Aerosol-cloud interactions within deep convective systems are still uncertain (Fan et al. 2016), and these uncertainties propagate into the quantification of climate effects (Regayre et al. 2014; Seinfeld et al. 2016).

Theoretically, increases in cloud drop number and the associated decreases in size can lead to more water being lofted above the freezing line, which increases latent heat release when compared to an unpolluted system. The proposed increase in latent heat fuels updraft intensity and enhances precipitation in a process called convective invigoration (Andreae et al. 2004; Lebo and Seinfeld 2011; Rosenfeld and Bell 2011). Idealized modeling studies indicate this process does occur within deep convective cloud systems (Morrison and Grabowski 2013; Lebo and Morrison 2014). Additionally, several modeling studies investigate the more complex feedbacks of aerosols and deep convection (Van den Heever et al. 2006; van den Heever and Cotton 2007; Wang et al. 2009; Cheng et al. 2010; Storer and Van den Heever 2013). These effects are

difficult to quantify because increasing hygroscopic aerosol can lead to precipitation enhancement and suppression, depending on environmental factors (Khain et al. 2005; Fan et al. 2009; Storer et al. 2010; Han et al. 2012).

Deep convective clouds are additionally complex because water exists in all three phases, where temperatures can range from very warm near the cloud base (> 25°C) to very cold (< -40°C) in anvil-forming cirrus clouds. Therefore, understanding of the processes that occur in both warm and cold clouds is required. In these mixed phase clouds, the interactions between warm and cold phases are important as ice crystals (snow) can grow at the expense of liquid water (cloud drops) as a result of the Wegener-Bergeron-Findeisen (WBF) process (Storelvmo and Tan 2015). All phases of hydrometeors (cloud drops, raindrops, snow, graupel, hail, ice crystals, etc.) are transported in the updrafts and downdrafts and can collide with other hydrometeors of both phases in the collision and coalescence, and accretion. The interactions and representations of these interactions drive changes in cloud structure and ultimately can affect storm dynamics (Grant and van den Heever 2015).

1.3.4 Ice formation processes

Because of the wide range of temperatures within the troposphere, clouds can exist at very different temperature conditions and aerosol effects are important for ice and mixed-phased microphysical processes as well as warm phase clouds. Ice freezing in the atmosphere can proceed through several physical mechanisms, including homogeneous and heterogeneous freezing ((Cantrell and Heymsfield 2005); Figure 1.5). Homogeneous freezing occurs when liquid aerosols, usually either a mixture of ammonium sulfate or cloud drops, spontaneously freeze and form ice crystals at very cold (<-40°C) temperatures with high ice supersaturation (>150%). These conditions limit the locations and circumstances for this freezing process.

Heterogeneous processes, or those processes that involve particles or ice-nucleating particles (INPs), are more typical. There are four types of heterogeneous freezing processes: deposition, immersion, condensation, and contact freezing. These INP processes occur within a wide temperature range from 0°C to -40°C and supersaturation with respect to water and ice in the range of 100-140% (Figure 1.5). In deposition freezing, vapor deposits onto an ice-nucleating particle when ice supersaturation is roughly 200% at temperatures ranging from -30 to -40°C. In immersion freezing, an ice-nucleating particle is immersed in a cloud drop and it freezes at -40°C with ice supersaturation > 200% and water sub-saturation. Immersion freezing also occurs in warmer temperature regimes (-15 to -30°C) at water saturation. Condensation freezing is similar to immersion freezing, although at slightly warmer temperatures 25 to -35°C) and lower water saturation, where water will condense on an ice-nucleating particle and freeze. Finally, contact freezing, which occurs at the lowest ice supersaturation values (> 100%) and warmest temperatures (> 0°C), is when a super-cooled water drop comes into contact with an ice-nucleating particle and freezes on contact (Cantrell and Heymsfield 2005). Studies of anvil-cirrus clouds show that dust is an effective INP and is important in the aforementioned heterogeneous freezing processes (Figure 1.5, (Cziczo et al. 2013).

1.4 Meteorology of Severe Weather events

Severe weather is defined as a storm producing at least one of the following three criteria: hail 1.0 inch (2.54 cm) or greater in diameter, winds exceeding 58 mph (26 m s^{-1}), or a tornado. Several storm types resulting from a variety of synoptic conditions can produce this type of event, from supercell thunderstorms and mesoscale convective complexes to derechoes. In this work we focus primarily on two types of mesoscale convective systems (MCS), including a squall line and a supercell. First, we examine the effects of aerosol magnitude and composition

on a squall line that crossed Kansas City, MO on May 27, 2013. A squall line is a linear MCS characterized by strong thunderstorms with heavy precipitation, damaging straight-line winds, hail, and occasionally tornadoes (Markowski and Richardson 2011).

Within a squall line, there is usually a warm, moist inflow near the surface (Figure 1.6, red arrows). As the warm, moist air is lifted, it expands adiabatically and cools to its dew point, allowing the condensation of water to cloud drops and releasing latent heat. The latent heat fuels updraft strength, which leads to strong vertical velocities. Hydrometeors caught in this strong updraft have sufficient time to grow by collision, coalescence and accretion (Dudhia 1996). On the rear side of the squall line, a rear inflow jet forms, as winds bring cooler and drier air into the system at mid and upper levels. The falling hydrometeors then fall through the sub-saturated air brought in by the rear-inflow, resulting in hydrometeor sublimation and evaporation that further cool the rear-inflow air, creating a cold pool (Houze, 2004). Cold pools are an important aspect of squall line development and propagation and are defined as evaporatively-cooled areas of downdraft air that spread out horizontally underneath a precipitating cloud (Engerer et al. 2008). Idealized simulations indicate that the organization and maintenance of a squall line is a balance between the vorticity produced by cold pools and environmental wind shear (Rotunno et al. 1988). Cold pool strength is determined by the environment of the middle troposphere, the temperature and humidity stratification (Alfaro and Khairoutdinov 2015) and by microphysical processes within the cloud, such as sublimation, melting, and evaporation of precipitation falling through unsaturated air (Corfidi 2003). Because of this dependence on the microphysical processes and the relationship of aerosols with cloud and ice nucleation, we hypothesize that aerosols can affect severe weather by altering the microphysical aspects that feed into the dynamical aspects of squall lines.

Supercell thunderstorms often occur in the Central Great Plains and are of particular interest because their intense nature usually leads to the most extreme severe weather, such as significant tornadoes (>F2; (Bunkers et al. 2006)). The defining feature of a supercell is the presence of a persistent, rotating updraft, spanning the middle troposphere, from 2-8 km above ground level (Browning 1964; Weisman and Klemp 1984; Bunkers et al. 2006). These storms can be long lived and produce an associated large cirrus anvil cloud. Figure 1.7 illustrates the structure of a typical supercell. Converging warm, moist surface winds combined with vertical significant vertical wind shear provides the dynamic environment necessary to enable the rotating updraft. The rotating updraft, like the tilted updraft in a squall line, causes precipitation to fall away from the updraft, allowing longer-lived convection.

1.5 Current Understanding of Urban Region – Meteorology Interactions

Urban regions have been hypothesized to affect weather and climate via a variety of physical and chemical mechanisms. Compared to surrounding rural areas, cities have an increased surface roughness, which drives an increase in low-level convergence and convection (Thielen et al. 2000; Niyogi et al. 2006). The urban heat island (UHI) effect can cause a destabilization of the boundary layer, which can trigger localized circulations or UHI-generated convective clouds (Shepherd 2005). Modeling and observational studies suggest there is an increase in precipitation downwind of urbanized regions (Changnon Jr 1981; Carrió et al. 2010; Schmid and Niyogi 2013). Furthermore, the morphology of a storm can change as it traverses across a city (Niyogi et al. 2011). The physical features of urban areas have been shown to account for some of these precipitation changes (Carrió et al. 2010). More recently, studies indicate emissions of aerosols in urban environment can increase the number of CCN that may interact with clouds and suppress precipitation over urban regions and enhance precipitation

downwind of urban regions (Zhong et al. 2015; Schmid and Niyogi 2017). In the Central Great Plains (CGP), mesoscale convective systems are responsible for more than 10% of precipitation in June, the growing season (Ashley et al. 2003). Because the CGP are subject to frequent severe weather events, this region provides a natural laboratory for investigating the effects that anthropogenic urban and agricultural aerosols have on severe weather.

1.6 Dissertation Overview

In this dissertation, we investigate the role of aerosols on mesoscale convective systems in the Central Great Plains of the United States. We utilize the state of the art Weather Research and Forecasting model, fully coupled with online chemistry (WRF-Chem), as the online-coupled chemistry and meteorology model provides a realistic approach to the formation, evolution, and transport of aerosols. To date, other studies have used highly idealized models and do not take into account the complexity of aerosol composition, especially in an urban region (Van den Heever et al. 2006; van den Heever and Cotton 2007). The CGP region is dominated by natural gas power generation and agriculture, which leads to relatively low amounts of sulfur dioxide (SO_2) emissions and relatively large amounts of ammonia (NH_3) emissions. Additionally, agricultural activity by humans leads to soil and dust emissions, which are notably efficient INPs. Considering the urban regions in the CGP are surrounded by agriculture, this land use mix provides an interesting opportunity for investigation of aerosol-cloud interactions on mesoscale convective systems. This dissertation is divided into three chapters (Chapters 2, 3 and 4) as described below.

Chapter 2: *Effects of urban plume aerosols on a mesoscale convective system.*

Science Question: Can the aerosols from an urban region affect a mesoscale convective system?

In this chapter, we examine urban anthropogenic emissions in the Kansas City, MO region and investigate the impacts of different aerosol concentrations on a severe squall line that crossed Kansas City, MO on May 27, 2013. We hypothesize that when accounting for realistic and dynamic aerosol concentrations from urban areas, they will impact the timing and spatial distribution of precipitation. We link the resulting aerosol concentration changes to changes in hydrometeors, which leads to changes in the cold pool strength and propagation speed. We are able to demonstrate that increasing emissions leads to a stronger and longer-lived squall line, while decreasing emissions leads to a weakened squall line.

Chapter 3: *The influence of aerosol hygroscopicity on precipitation intensity during a mesoscale convective event.*

Science Question: Are the spatial patterns and intensity of precipitation sensitive to aerosol composition?

In this chapter, we examine the effects of hygroscopicity on the squall line that occurred in Kansas City, MO on May 27, 2013. Because volumetric bulk hygroscopicity is the characteristic used to determine aerosol activation to cloud drops within the model parameterizations, we hypothesize that this model characteristic will influence the simulation of precipitation intensity. We systematically change the default hygroscopicity values for sulfate, ammonium, and organics from the WRF-Chem modal aerosol model default values to values that reflect those derived in laboratory studies. We find that precipitation intensity is sensitive to the bulk hygroscopicity values. Increasing the sulfate and ammonium values leads to a greater probability of both weaker and more intense rainfall. A similar pattern exists for decreasing hygroscopicity in the organics, although a much larger probability occurs for weaker intensity rain events. Including all the lab-

derived values leads to a decrease in the weaker and stronger intensity events but an increase in the mid-range intensity rainfall, which more closely represents the observed data. Testing the model's assumptions about hygroscopicity provides insight into how a region's aerosol composition could affect precipitation intensity and the capacity for flooding.

Chapter 4: *Dust as ice nuclei: Implications for a mesoscale convective event in the Central Great Plains.*

Science Question: How does including dust as INP affect solid-phase hydrometeors, precipitation patterns, and thunderstorm intensity?

Finally, to address this final science question, we add a new model parameterization to the WRF-Chem model to replace the current ice nucleation rate. The current parameterization for INP is temperature dependent only, and we update this with a new parameterization that allows dust concentrations to influence the ice nucleation rate. We simulate a supercell that occurred on May 29-30, 2012, which was observed during the Deep Convective Clouds and Chemistry (DC3) campaign. We find that including dust as INPs significantly alters the ice and snow hydrometeors. Both hydrometeors have smaller number concentrations and larger radii yet overall, these changes in the microphysical characteristics have little effect on storm intensity. However, there is a significant effect on outgoing long-wave radiation, where including dust as INP leads to more OLR, signaling a difference in anvil cirrus characteristics. Laying the groundwork for including dust as INP within this modeling framework is a necessary step in mitigating the aerosol-cloud-climate radiation uncertainty, especially the longer-term effects of deep convection associated with anvils.

Figures

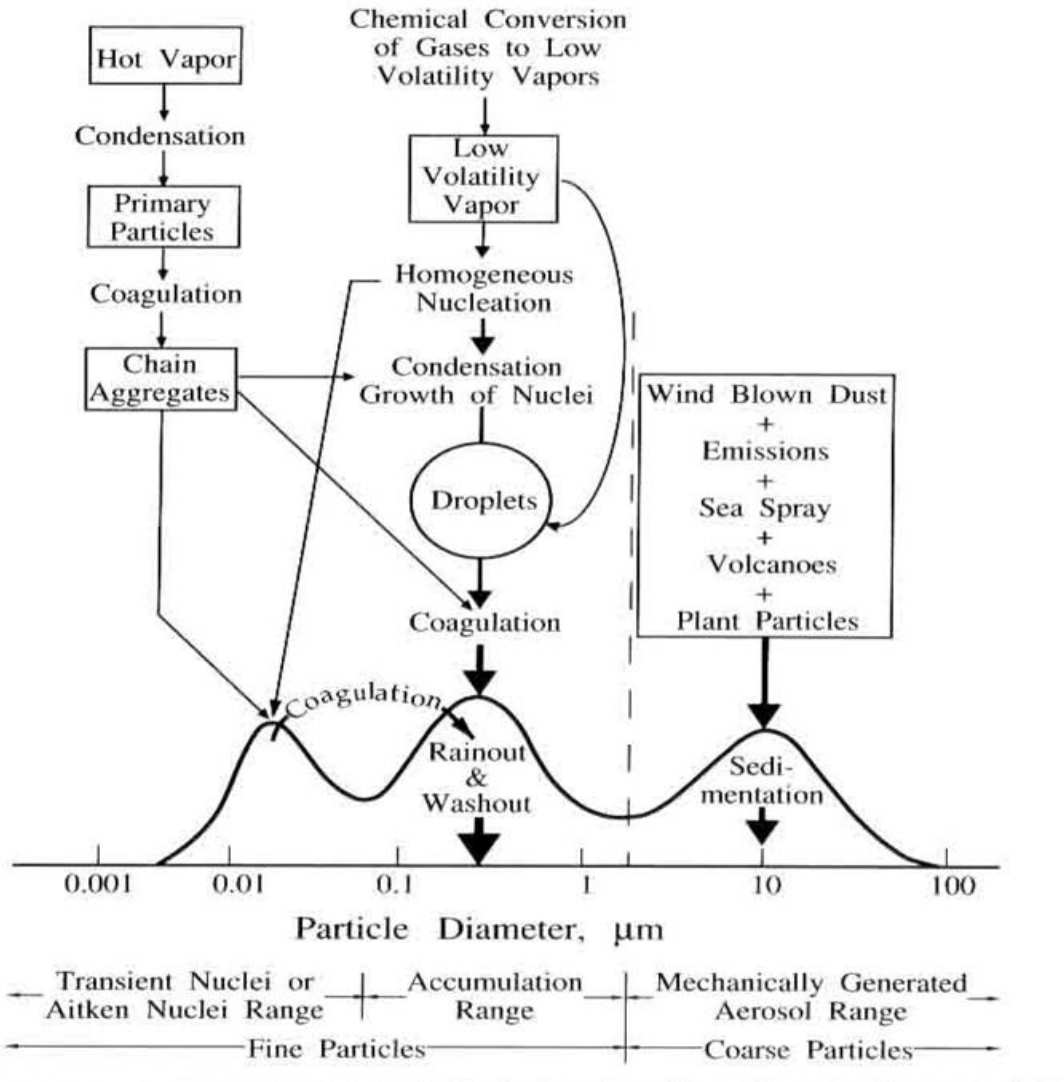

Figure 1.1: Description of atmospheric aerosol size distributions, including the common sources and sinks for each particle diameter and mode. (Seinfeld and Pandis 2006).

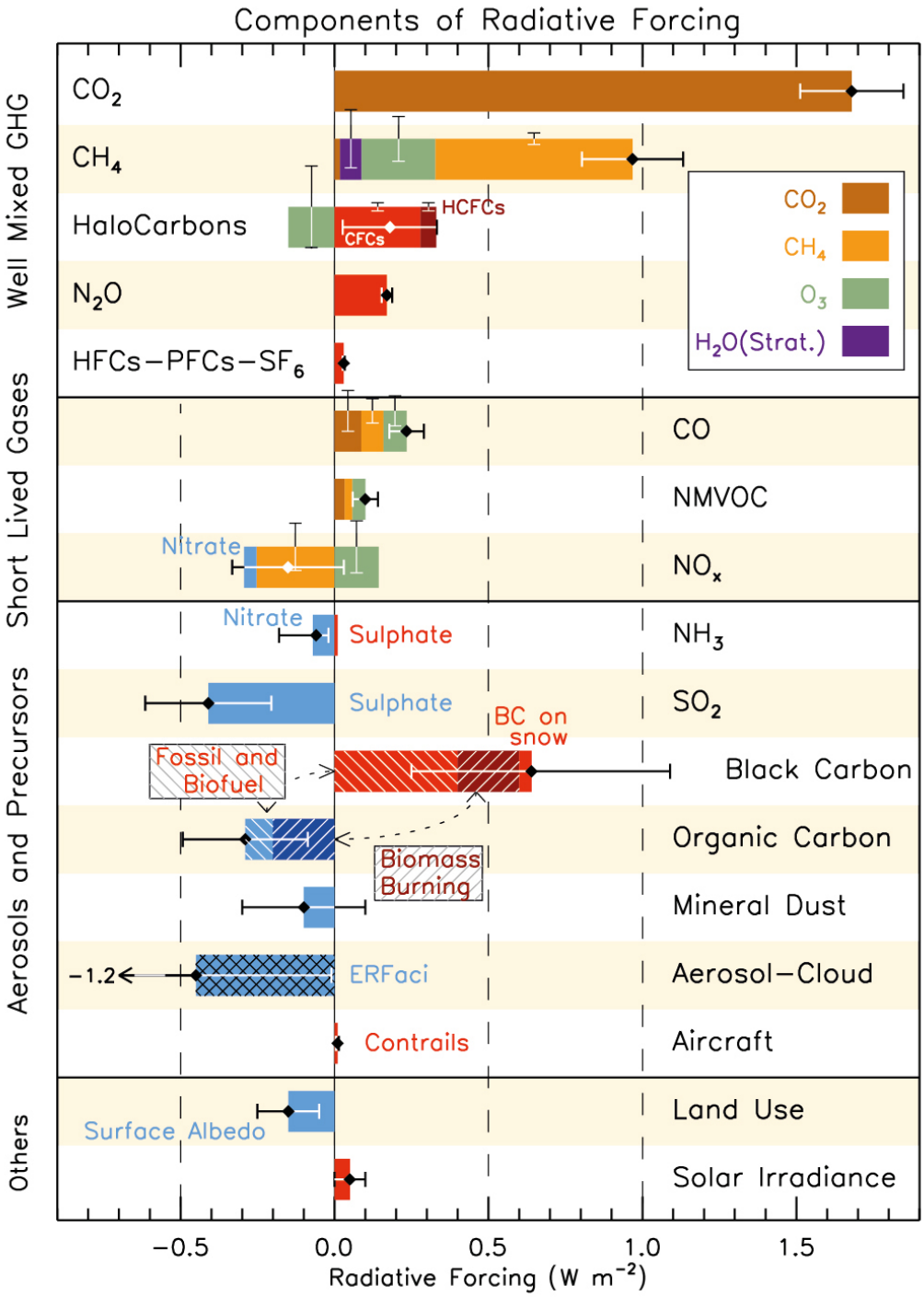

Figure 1.2: Radiative forcing (RF) diagram, Intergovernmental Program on Climate Change AR5 report (2013). Error bars indicate amount of uncertainty associated with the appropriation of RF to a particular forcing agent. Notice the relatively large uncertainty for aerosol-cloud interactions.

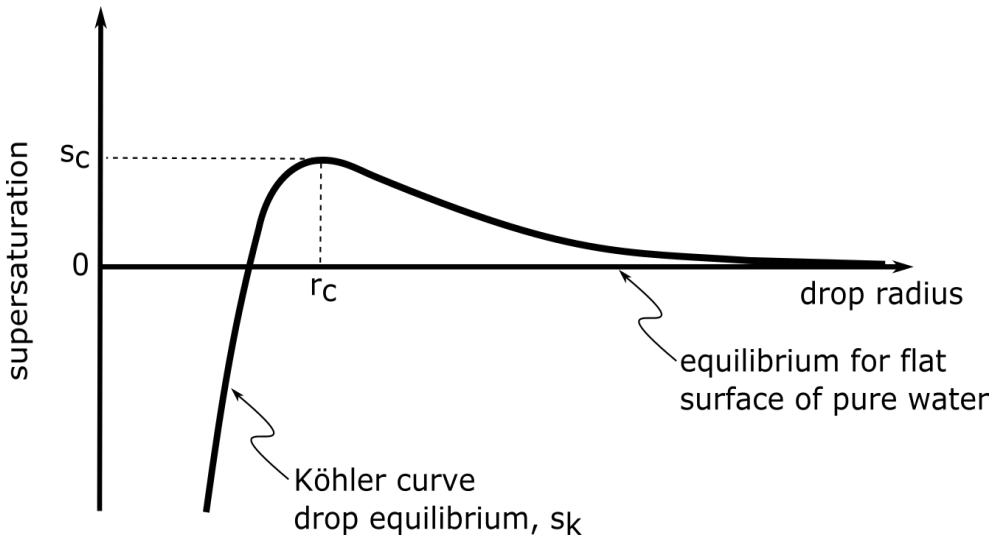

Figure 1.3: Köhler curve (Kohler, 1936) demonstrating the droplet growth or decay as a function of size (x-axis) and atmospheric supersaturation (y-axis). (Brune)

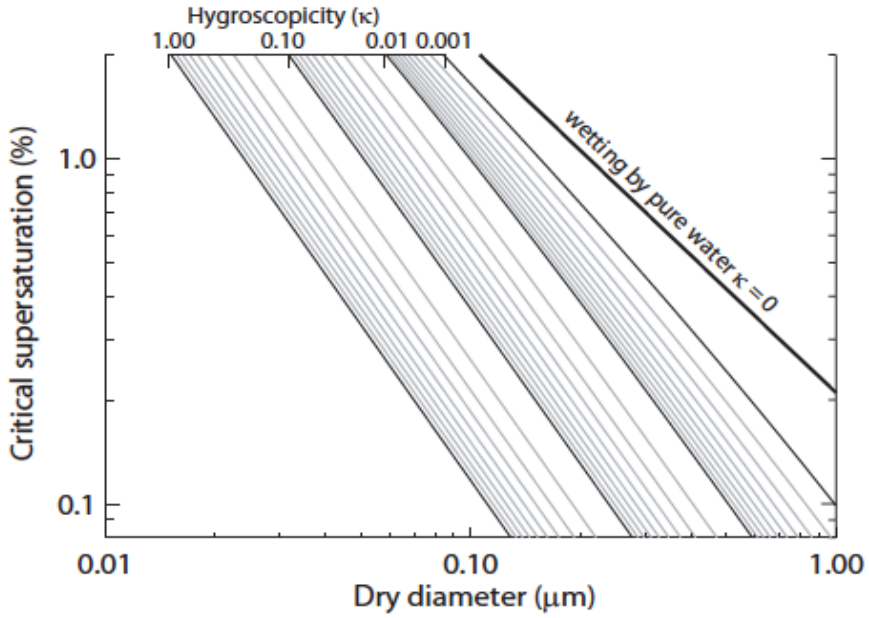

Figure 1.4: Kappa (κ) parameterization showing the relationship between hygroscopicity, dry diameter size and supersaturation (Petters and Kreidenweiss, 2007).

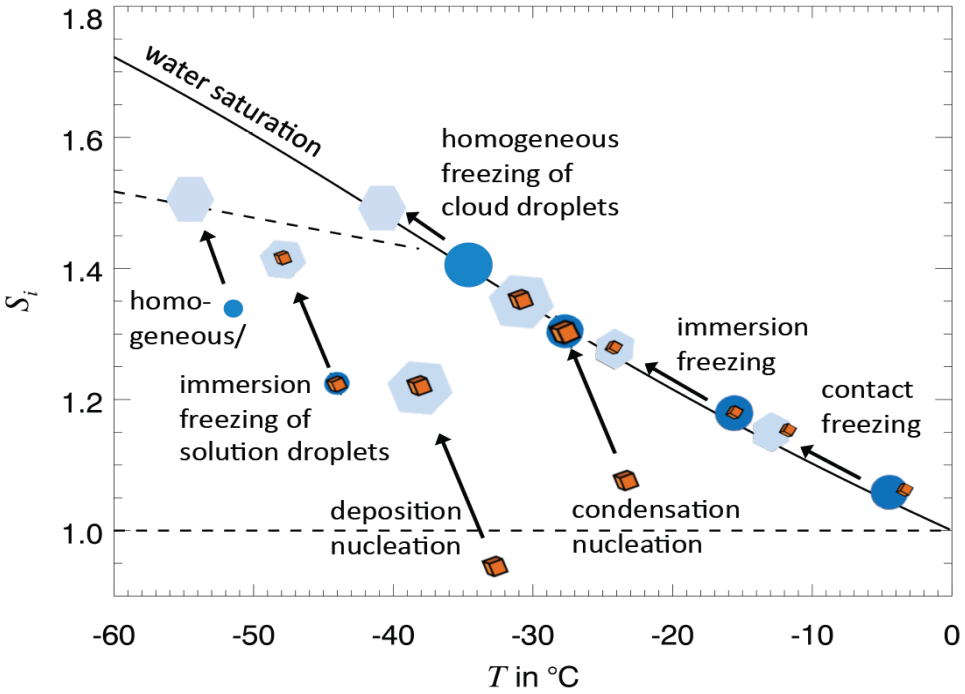

Figure 1.5: Ice nucleation processes, as described by the relationship between temperature and saturation with respect to ice and water (S_i, S_w). (WELTI 2012)

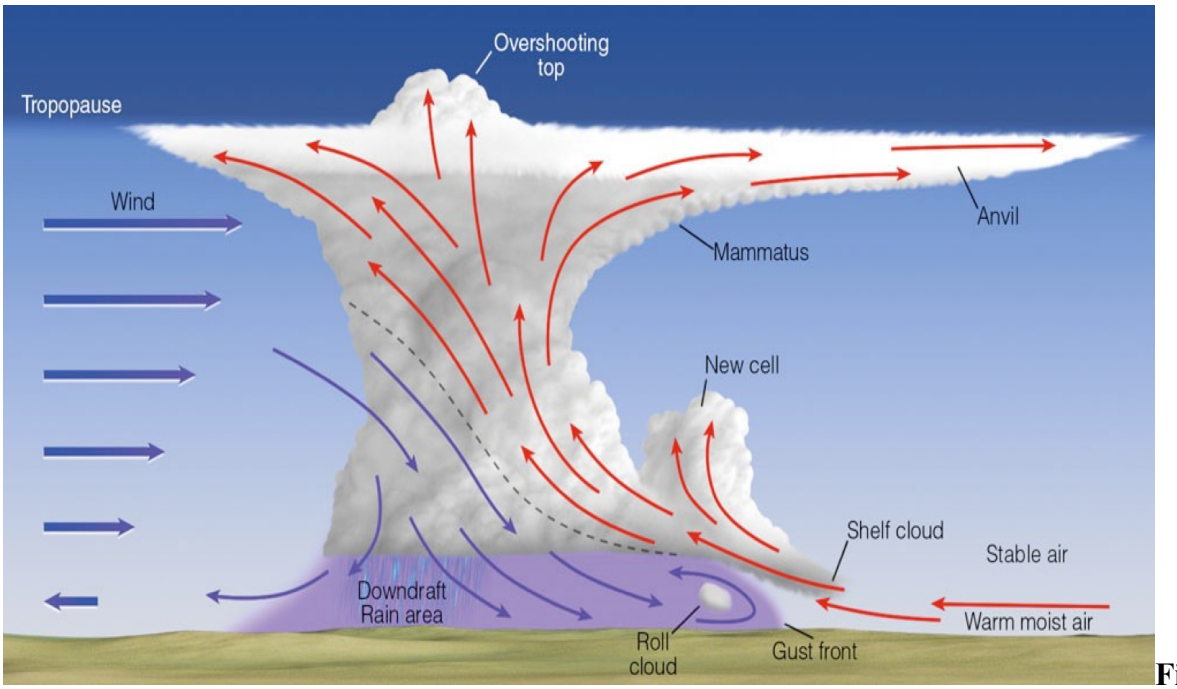

Figure 1.6: Schematic of a squall line (Ahrens 2011).

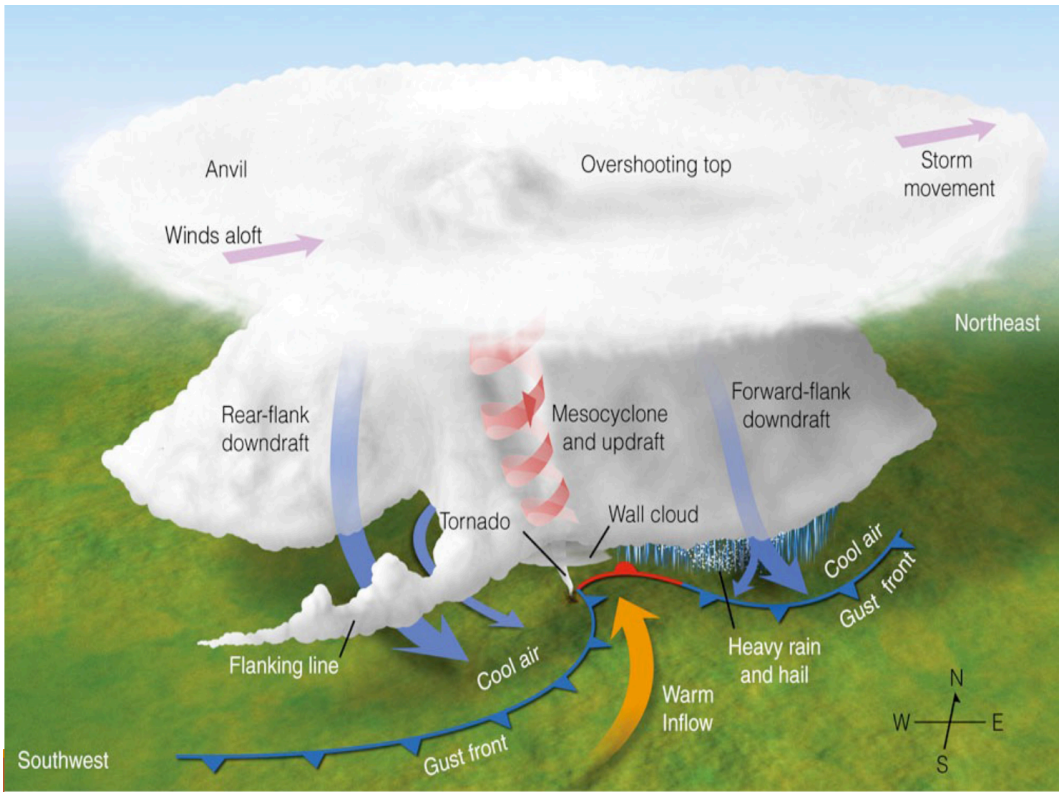

Figure 1.7: Schematic of a supercell (Ahrens 2011).

References

Ackermann, I. J., H. Hass, M. Memmesheimer, A. Ebel, F. S. Binkowski, and U. Shankar, 1998: Modal aerosol dynamics model for Europe: Development and first applications. *Atmospheric environment*, **32,** 2981-2999 %@ 1352-2310.

Ahrens, C. D., 2011: *Essentials of meteorology: an invitation to the atmosphere.* Cengage Learning.

Albrecht, B. A., 1989: Aerosols, cloud microphysics, and fractional cloudiness. *Science*, **245,** 1227-1230.

Alfaro, D. A., and M. Khairoutdinov, 2015: Thermodynamic Constraints on the Morphology of Simulated Midlatitude Squall Lines. *Journal of the Atmospheric Sciences*, **72,** 3116-3137.

Andreae, M., and A. Gelencsér, 2006: Black carbon or brown carbon? The nature of light-absorbing carbonaceous aerosols. *Atmospheric Chemistry and Physics*, **6,** 3131-3148.

Andreae, M. O., D. Rosenfeld, P. Artaxo, A. Costa, G. Frank, K. Longo, and M. Silva-Dias, 2004: Smoking rain clouds over the Amazon. *science*, **303,** 1337-1342.

Ashley, W. S., T. L. Mote, P. G. Dixon, S. L. Trotter, E. J. Powell, J. D. Durkee, and A. J. Grundstein, 2003: Distribution of mesoscale convective complex rainfall in the United States. *Monthly Weather Review*, **131,** 3003-3017.

Boucher, O., and Coauthors, 2013: Clouds and aerosols. *Climate change 2013: the physical science basis. Contribution of Working Group I to the Fifth Assessment Report of the Intergovernmental Panel on Climate Change*, Cambridge University Press, 571-657.

Browning, K. A., 1964: Airflow and precipitation trajectories within severe local storms which travel to the right of the winds. *Journal of the Atmospheric Sciences*, **21,** 634-639.

Brune, W.

Bunkers, M. J., M. R. Hjelmfelt, and P. L. Smith, 2006: An observational examination of long-lived supercells. Part I: Characteristics, evolution, and demise. *Weather and forecasting*, **21,** 673-688.

Cantrell, W., and A. Heymsfield, 2005: Production of Ice in Tropospheric Clouds: A Review. *Bulletin of the American Meteorological Society*, **86,** 795-807.

Carrió, G. G., W. R. Cotton, and W. Y. Y. Cheng, 2010: Urban growth and aerosol effects on convection over Houston. *Atmospheric Research*, **96,** 560-574.

Changnon Jr, S. A., 1981: METROMEX review and summary. *Meteor. Monogr.*, **40,** 181.

Chapman, E. G., W. Gustafson Jr, R. C. Easter, J. C. Barnard, S. J. Ghan, M. S. Pekour, and J. D. Fast, 2009: Coupling aerosol-cloud-radiative processes in the WRF-Chem model: Investigating the radiative impact of elevated point sources. *Atmospheric Chemistry and Physics*, **9,** 945-964.

Cheng, C.-T., W.-C. Wang, and J.-P. Chen, 2010: Simulation of the effects of increasing cloud condensation nuclei on mixed-phase clouds and precipitation of a front system. *Atmospheric Research*, **96,** 461-476.

Corfidi, S. F., 2003: Cold pools and MCS propagation: Forecasting the motion of downwind-developing MCSs. *Weather and forecasting*, **18,** 997-1017.

Cziczo, D. J., and Coauthors, 2013: Clarifying the dominant sources and mechanisms of cirrus cloud formation. *Science*, **340,** 1320-1324.

Dudhia, J., 1996: Back to basics: thunderstorms: Part 1. *Weather*, **51,** 371-376.

Dusek, U., and Coauthors, 2006: Size matters more than chemistry for cloud-nucleating ability of aerosol particles. *Science*, **312,** 1375-1378 %@ 0036-8075.

Ekman, A., C. Wang, J. Wilson, and J. Ström, 2004: Explicit simulations of aerosol physics in a cloud-resolving model: a sensitivity study based on an observed convective cloud. *Atmospheric Chemistry and Physics*, **4,** 773-791.

Engerer, N. A., D. J. Stensrud, and M. C. Coniglio, 2008: Surface Characteristics of Observed Cold Pools. *Monthly Weather Review*, **136,** 4839-4849.

Fan, J., Y. Wang, D. Rosenfeld, and X. Liu, 2016: Review of Aerosol–Cloud Interactions: Mechanisms, Significance, and Challenges. *Journal of the Atmospheric Sciences*, **73,** 4221-4252.

Fan, J., R. Zhang, G. Li, W. K. Tao, and X. Li, 2007: Simulations of cumulus clouds using a spectral microphysics cloud‐resolving model. *Journal of Geophysical Research: Atmospheres*, **112**.

Fan, J., D. Rosenfeld, Y. Yang, C. Zhao, L. R. Leung, and Z. Li, 2015: Substantial contribution of anthropogenic air pollution to catastrophic floods in Southwest China. *Geophysical Research Letters*, **42,** 6066-6075.

Fan, J., and Coauthors, 2009: Dominant role by vertical wind shear in regulating aerosol effects on deep convective clouds. *Journal of Geophysical Research*, **114**.

Farmer, D. K., C. D. Cappa, and S. M. Kreidenweis, 2015: Atmospheric processes and their controlling influence on cloud condensation nuclei activity. *Chem Rev*, **115,** 4199-4217.

Grant, L. D., and S. C. van den Heever, 2015: Cold pool and precipitation responses to aerosol loading: Modulation by dry layers. *Journal of the Atmospheric Sciences*, **72,** 1398-1408.

Han, J.-Y., J.-J. Baik, and A. P. Khain, 2012: A numerical study of urban aerosol impacts on clouds and precipitation. *Journal of the Atmospheric Sciences*, **69,** 504-520.

Houze, R. A., 2004: Mesoscale convective systems. *Reviews of Geophysics*, **42**.

Jin, M., J. M. Shepherd, and M. D. King, 2005: Urban aerosols and their variations with clouds and rainfall: A case study for New York and Houston. *Journal of Geophysical Research: Atmospheres (1984–2012)*, **110**.

Hudson, J. G., 1993: Cloud condensation nuclei. *Journal of Applied Meteorology*, **32,** 596-607.

Kanakidou, M., and Coauthors, 2005: Organic aerosol and global climate modelling: a review. *Atmospheric Chemistry and Physics*, **5,** 1053-1123.

Kaufman, Y. J., I. Koren, L. A. Remer, D. Rosenfeld, and Y. Rudich, 2005: The effect of smoke, dust, and pollution aerosol on shallow cloud development over the Atlantic Ocean. *Proceedings of the National Academy of Sciences of the United States of America*, **102,** 11207-11212.

Khain, A., D. Rosenfeld, and A. Pokrovsky, 2005: Aerosol impact on the dynamics and microphysics of deep convective clouds. *Quarterly Journal of the Royal Meteorological Society*, **131,** 2639-2663.

Khain, A., M. Ovtchinnikov, M. Pinsky, A. Pokrovsky, and H. Krugliak, 2000: Notes on the state-of-the-art numerical modeling of cloud microphysics. *Atmospheric Research*, **55,** 159-224.

Köhler, H., 1936: The nucleus in and the growth of hygroscopic droplets. *Transactions of the Faraday Society*, **32,** 1152-1161.

Kreidenweis, S., and A. Asa-Awuku, 2014: 5.13-Aerosol hygroscopicity: Particle water content and its role in atmospheric processes.

Lebo, Z. J., and J. H. Seinfeld, 2011: Theoretical basis for convective invigoration due to increased aerosol concentration. *Atmospheric Chemistry and Physics*, **11,** 5407-5429.

Lebo, Z. J., and H. Morrison, 2014: Dynamical Effects of Aerosol Perturbations on Simulated Idealized Squall Lines. *Monthly Weather Review*, **142,** 991-1009.

Liu, J., and Coauthors, 2014: Brown carbon in the continental troposphere. *Geophysical Research Letters*, **41,** 2191-2195.

Markowski, P., and Y. Richardson, 2011: *Mesoscale meteorology in midlatitudes.* Vol. 2, John Wiley & Sons.

Mason, B.: 1971: The Physics of Clouds. Clarendon Press.

Morrison, H., and W. W. Grabowski, 2007: Comparison of bulk and bin warm-rain microphysics models using a kinematic framework. *Journal of the atmospheric sciences*, **64,** 2839-2861.

Morrison, H., and W. W. Grabowski, 2013: Response of Tropical Deep Convection to Localized Heating Perturbations: Implications for Aerosol-Induced Convective Invigoration. *Journal of the Atmospheric Sciences*, **70,** 3533-3555.

Niyogi, D., T. Holt, S. Zhong, P. C. Pyle, and J. Basara, 2006: Urban and land surface effects on the 30 July 2003 mesoscale convective system event observed in the southern Great Plains. *Journal of Geophysical Research: Atmospheres*, **111**.

Niyogi, D., and Coauthors, 2011: Urban Modification of Thunderstorms: An Observational Storm Climatology and Model Case Study for the Indianapolis Urban Region*. *Journal of Applied Meteorology and Climatology*, **50,** 1129-1144.

Ntelekos, A. A., J. A. Smith, L. Donner, J. D. Fast, W. I. Gustafson, E. G. Chapman, and W. F. Krajewski, 2009: The effects of aerosols on intense convective precipitation in the northeastern United States. *Quarterly Journal of the Royal Meteorological Society*, **135,** 1367-1391.

Petters, M. D., and S. M. Kreidenweis, 2007: A single parameter representation of hygroscopic growth and cloud condensation nucleus activity. *Atmospheric Chemistry and Physics*, **7,** 1961-1971 %@ 1680-7316.

Pielke, R. A., and Coauthors, 1992: A comprehensive meteorological modeling system—RAMS. *Meteorology and Atmospheric Physics*, **49,** 69-91 %@ 0177-7971.

Prospero, J. M., P. Ginoux, O. Torres, S. E. Nicholson, and T. E. Gill, 2002: Environmental characterization of global sources of atmospheric soil dust identified with the Nimbus 7 Total Ozone Mapping Spectrometer (TOMS) absorbing aerosol product. *Reviews of geophysics*, **40**.

Regayre, L., and Coauthors, 2014: Uncertainty in the magnitude of aerosol‐cloud radiative forcing over recent decades. *Geophysical Research Letters*, **41,** 9040-9049.

Rogers, R., and M. Yau, 1989: A short course of cloud physics. Pregamon. Oxford.

Rosenfeld, D., 1999: TRMM observed first direct evidence of smoke from forest fires inhibiting rainfall. *Geophysical research letters*, **26,** 3105-3108.

——, 2000: Suppression of rain and snow by urban and industrial air pollution. *Science*, **287,** 1793-1796.

Rosenfeld, D., and T. L. Bell, 2011: Why do tornados and hailstorms rest on weekends? *Journal of Geophysical Research*, **116**.

Rosenfeld, D., and Coauthors, 2008: Flood or drought: how do aerosols affect precipitation? *science*, **321,** 1309-1313.

Rotunno, R., J. B. Klemp, and M. L. Weisman, 1988: A theory for strong, long-lived squall lines. *Journal of the Atmospheric Sciences*, **45,** 463-485.

Ruehl, C. R., J. F. Davies, and K. R. Wilson, 2016: An interfacial mechanism for cloud droplet formation on organic aerosols. *Science*, **351,** 1447-1450 %@ 0036-8075.

Saide, P. E., and Coauthors, 2015: Central American biomass burning smoke can increase tornado severity in the U.S. *Geophysical Research Letters*, **42,** 956-965.

Schell, B., I. J. Ackermann, H. Hass, F. S. Binkowski, and A. Ebel, 2001: Modeling the formation of secondary organic aerosol within a comprehensive air quality model system. *Journal of Geophysical Research: Atmospheres*, **106,** 28275-28293.

Schmid, P. E., and D. Niyogi, 2013: Impact of city size on precipitation-modifying potential. *Geophysical Research Letters*, **40,** 5263-5267.

Schmid, P. E., and D. Niyogi, 2017: Modeling Urban Precipitation Modification by Spatially Heterogeneous Aerosols. *Journal of Applied Meteorology and Climatology*.

Seinfeld, J., and S. Pandis, 2006: Atmospheric chemistry and physics. Hoboken. NJ: Wiley.

Seinfeld, J. H., and Coauthors, 2016: Improving our fundamental understanding of the role of aerosol− cloud interactions in the climate system. *Proceedings of the National Academy of Sciences*, **113,** 5781-5790.

Sekiguchi, M., and Coauthors, 2003: A study of the direct and indirect effects of aerosols using global satellite data sets of aerosol and cloud parameters. *Journal of Geophysical Research: Atmospheres*, **108**.

Shepherd, J. M., 2005: A review of current investigations of urban-induced rainfall and recommendations for the future. *Earth Interactions*, **9,** 1-27.

Shrivastava, M., and Coauthors, 2013: Modeling aerosols and their interactions with shallow cumuli during the 2007 CHAPS field study. *Journal of Geophysical Research: Atmospheres*, **118,** 1343-1360.

Stevens, B., and G. Feingold, 2009: Untangling aerosol effects on clouds and precipitation in a buffered system. *Nature*, **461,** 607-613.

Storelvmo, T., and I. Tan, 2015: The Wegener-Bergeron-Findeisen process–Its discovery and vital importance for weather and climate. *Meteor. Z*, **24,** 455-461.

Storer, R. L., and S. C. Van den Heever, 2013: Microphysical processes evident in aerosol forcing of tropical deep convective clouds. *Journal of the Atmospheric Sciences*, **70,** 430-446.

Storer, R. L., S. C. van den Heever, and G. L. Stephens, 2010: Modeling Aerosol Impacts on Convective Storms in Different Environments. *Journal of the Atmospheric Sciences*, **67,** 3904-3915.

Tao, W.-K., J.-P. Chen, Z. Li, C. Wang, and C. Zhang, 2012: Impact of aerosols on convective clouds and precipitation. *Reviews of Geophysics*, **50**.

Thielen, J., W. Wobrock, A. Gadian, P. Mestayer, and J.-D. Creutin, 2000: The possible influence of urban surfaces on rainfall development: a sensitivity study in 2D in the meso-γ-scale. *Atmospheric Research*, **54,** 15-39.

Twomey, S., 1977: The influence of pollution on the shortwave albedo of clouds. *Journal of the atmospheric sciences*, **34,** 1149-1152.

van den Heever, S. C., and W. R. Cotton, 2007: Urban Aerosol Impacts on Downwind Convective Storms. *Journal of Applied Meteorology and Climatology*, **46,** 828-850.

Van den Heever, S. C., G. G. Carrió, W. R. Cotton, P. J. DeMott, and A. J. Prenni, 2006: Impacts of nucleating aerosol on Florida storms. Part I: Mesoscale simulations. *Journal of the atmospheric sciences*, **63,** 1752-1775.

Wang, J., S. C. van den Heever, and J. S. Reid, 2009: A conceptual model for the link between Central American biomass burning aerosols and severe weather over the south central United States. *Environmental Research Letters*, **4,** 015003.

Wang, M., and Coauthors, 2012: Constraining cloud lifetime effects of aerosols using A‐Train satellite observations. *Geophysical Research Letters*, **39**.

Ward, D., and W. Cotton, 2011: A Method for Forecasting Cloud Condensation Nuclei Using Predictions of Aerosol Physical and Chemical Properties from WRF/Chem. *Journal of Applied Meteorology and Climatology*, **50,** 1601-1615.

Weisman, M. L., and J. B. Klemp, 1984: The structure and classification of numerically simulated convective stormsin directionally varying wind shears. *Monthly Weather Review*, **112,** 2479-2498.

WELTI, A. E., 2012: Experimental studies on deposition and immersion mode ice nucleation on mineral dust, ETH ZURICH.

Yang, Q., and Coauthors, 2011: Assessing regional scale predictions of aerosols, marine stratocumulus, and their interactions during VOCALS-REx using WRF-Chem. *Atmospheric Chemistry and Physics*, **11,** 11951-11975.

Zaveri, R. A., R. C. Easter, J. D. Fast, and L. K. Peters, 2008: Model for simulating aerosol interactions and chemistry (MOSAIC). *Journal of Geophysical Research: Atmospheres*, **113**.

Zhang, X., Y.-H. Lin, J. D. Surratt, and R. J. Weber, 2013: Sources, composition and absorption Ångstrom exponent of light-absorbing organic components in aerosol extracts from the Los Angeles Basin. *Environmental science & technology*, **47,** 3685-3693.

Zhong, S., Y. Qian, C. Zhao, R. Leung, and X. Q. Yang, 2015: A case study of urbanization impact on summer precipitation in the Greater Beijing Metropolitan Area: Urban heat island versus aerosol effects. *Journal of Geophysical Research: Atmospheres*, **120**.

Zhou, C., X. Zhang, S. Gong, Y. Wang, and M. Xue, 2016: Improving aerosol interaction with clouds and precipitation in a regional chemical weather modeling system. *Atmospheric Chemistry and Physics*, **16,** 145-160.

Chapter II

Effects of urban plume aerosols on a mesoscale convective system

Stacey Kawecki, Department of Climate and Space Sciences and Engineering, University of Michigan, Ann Arbor, MI 48109

Geoffrey M. Henebry, Geospatial Sciences Center of Excellence, South Dakota State University, Brookings, SD 57007-3510

Allison L. Steiner, Department of Climate and Space Sciences and Engineering, University of Michigan, Ann Arbor, MI 48109

2.0 Abstract

This study examines the effects of urban aerosols on a mesoscale convective system (MCS) in the Central Great Plains with the Weather Research and Forecasting Chemistry model (WRF-Chem). Urban emissions from Kansas City, Missouri were scaled by factors of 0.5, 1.0, and 2.0 to investigate the impact of urban aerosol load on MCS propagation and strength. The first half of the storm development is characterized by a stationary front to the north of Kansas City (Phase I; 5-26-18:00 UTC – 5-27-06:00 UTC), which develops into a squall line south of the urban area (Phase II; 5-27-06:00 – 18:00 UTC). During Phase I, doubling urban emissions shifts the precipitation accumulation, with enhancement downwind of the storm propagation and

suppression upwind. During Phase II, a squall line develops in the baseline and doubled emissions scenarios but not when emissions are halved. These changes in MCS propagation and strength are a function of cold pool strength, which is determined by microphysical processes and directly influenced by aerosol load. Overall, changes in urban emissions drive changes in cloud microphysics, which trigger large-scale changes in storm morphology and precipitation patterns. These results show that urban emissions can play an important role in meso-scale weather systems.

2.1 Introduction

Aerosols impact the Earth's climate by reducing incoming solar radiation and altering cloud properties (Boucher et al. 2013). Depending on aerosol size and composition, these particles can act as cloud condensation nuclei (CCN) in warm clouds and/or ice nuclei (IN) in cold clouds, affecting the cloud microphysics and resulting precipitation (Stevens and Feingold 2009). Increasing aerosol concentrations can increase cloud drop number and decrease cloud drop size, which can affect cloud optical properties (the first indirect effect; (Twomey 1977)). Through decreasing cloud drop size, the number of CCN can also change precipitation patterns and cloud lifetimes, which can increase the lifetime of the cloud (the second indirect effect; (Albrecht 1989)). On weather timescales, the amount of aerosol present in a given meteorological system affects the efficiency of cloud microphysics and precipitation development, thereby altering the macrostructure and lifetime of the cloud (Stevens and Feingold 2009)

Aerosol impacts on cloud microphysics have been documented in observational studies with satellite and ground-based data (Rosenfeld 2000; Yang et al. 2011; Christensen and Stephens 2012; Min et al. 2014; Rosenfeld et al. 2014). In warm, shallow, precipitating clouds, observations and models indicate that the addition of hygroscopic aerosols suppresses precipitation (Lohmann et al. 1999; Rosenfeld 2000), as increased CCN drives competition between drops for water vapor and subsequently reduces drop sizes (Twomey 1974). In mixed-phase clouds, aerosol effects are more complex due to multiple phase changes and the associated thermodynamic processes simultaneously occurring in different locations (Seifert and Beheng 2006). The addition of CCN has competing effects on precipitation depending on whether warm or cold precipitation processes dominate; for example, warm precipitation processes will be suppressed, but cold precipitation processes can either be suppressed or enhanced (Cheng et al. 2010). Theoretically, precipitation enhancement has been explained by the phase change, release

of latent heat, and subsequent ice processes during the transport of liquid mass to freezing levels that increases the updraft velocity (Rosenfeld et al. 2008; Koren et al. 2010; Lebo and Seinfeld 2011; Tao et al. 2012). Stevens and Feingold (2009) theorize that many coarser resolution models may overestimate the sensitivity of cloud microphysics to aerosols because of the assumptions made in the microphysics schemes. These assumptions do not include processes that buffer the effects of aerosol perturbations, which are seen in both the observations and very high-resolution models. For example, a CCN increase can decrease precipitation efficiency but also invigorate convection, which can increase precipitation amounts. These competing or buffering processes can be negligible or impactful, depending on the atmospheric state and synoptic conditions (Peters et al. 2014). In severe weather systems, these effects likely become more complex as aerosols can invigorate deep convection (Andreae et al. 2004; Fan et al. 2013; Storer et al. 2014) and influence intense convective precipitation events (Ntelekos et al. 2009). These nonlinear relationships between the microphysics and dynamics of aerosol-cloud interactions become more complex during strong convective events (Seifert et al. 2012).

Severe weather is defined as an event with any of three features: (1) hail equal to or exceeding 1.0 inch (2.54 cm) in diameter, (2) wind speeds exceeding 58 miles hour-1 (26 m s^{-1}), or (3) a tornado. For each of these three cases, the atmospheric environment must be highly unstable with large amounts of Convective Available Potential Energy (CAPE) and wind shear values of 15-20 m s^{-1} over a depth of 0-6 km (Thompson et al. 2003). One type of system that often results in severe weather is the mesoscale convective system (MCS) (Maddox 1980; Houze 2004). MCSs are responsible for a large amount of growing season precipitation in the Central Great Plains (CGP) (Ashley et al. 2003). They frequently form squall lines, or linear MCSs characterized by strong thunderstorms with heavy precipitation, damaging straight-line winds,

hail, and occasionally tornadoes (Markowski and Richardson 2011). Idealized simulations indicate that the organization and maintenance of a squall line is a balance between the vorticity produced by cold pools and environmental wind shear (Rotunno et al. 1988). Cold pools are an important aspect of squall line development and propagation and are defined as evaporatively-cooled areas of downdraft air that spread out horizontally underneath a precipitating cloud (Engerer et al. 2008). Their strength is determined by the environment of the middle troposphere, the temperature and humidity stratification (Alfaro and Khairoutdinov 2015) and by microphysical processes within the cloud, such as sublimation, melting, and evaporation of precipitation falling through unsaturated air (Corfidi 2003) and is likely influenced by aerosol-cloud interactions (Grant and van den Heever 2015).

Urban areas have been observed to influence local weather and climate by increasing precipitation downwind (Changnon Jr 1981; Shepherd and Burian 2003; Jin et al. 2005; Schmid and Niyogi 2013). Observational and modeling studies have developed several mechanisms to explain this phenomenon as reviewed in Shepherd (2005), including (1) an increase in low-level convergence and convection from the higher surface roughness of urban areas; (2) a destabilization of the boundary layer from the Urban Heat Island (UHI) effect, which can trigger localized circulations or UHI-generated convective clouds, and (3) higher aerosol concentrations over urban areas that increase number of CCN and lifetime of clouds.

Urban aerosol concentrations are typically higher than background aerosol concentrations due to anthropogenic activity, and aerosol-cloud interactions resulting from these emissions have the potential to alter the growth of clouds and precipitation. In one modeling study, an increase in precipitation downwind of Houston, TX was attributed to local meteorological feedbacks (e.g., land use change causing an enhanced sea breeze) over increased urban aerosol concentrations

(Carrió et al. 2010). However, other studies have demonstrated that urban aerosols can increase downwind precipitation through invigoration of convection (van den Heever and Cotton 2007; Han et al. 2012). Additionally, the morphology of a storm can change as it traverses across a city (Niyogi et al. 2011), which can modify when and where severe weather occurs. Ntelekos et al (2009) attributed changes to precipitation patterns in intense convective precipitation to aerosol-induced convective invigoration. A recent study by Fan et al. (2015) found that absorbing aerosols can increase extreme precipitation events. All of these studies suggest that urban aerosols exhibit a range of impacts on precipitation and large-scale systems. Here, we focus on understanding the role of hygroscopic urban aerosols on large systems that produce severe weather, examining not only precipitation patterns but also the relationship between these aerosols, cloud microphysics and storm dynamics.

Understanding the mechanisms that drive the interactive effects of local weather and urbanization on severe weather is critical to predicting the societal impacts of changing urbanization and weather patterns. We explore the role of aerosols on severe storms in the urban area of Kansas City, Missouri, a metropolitan area with a population of over two million in 2013 (http://factfinder.census.gov) located on the eastern edge of the U.S CGP. This region is known for frequent warm season convective weather events such as tornadoes, squall lines, hail, and heavy precipitation. Regional aerosol sources include a combination of anthropogenic sources from mid-sized urban areas, light industries, and energy generation embedded within an agricultural land use matrix. With the combination of unique aerosol sources and frequent severe weather, the CGP region is well-suited to investigate the urban aersosol-weather interaction. To address the question of how urban aerosols affect storm morphology, cloud microphysics, and the potential for severe weather, we scale typical urban emissions during a

severe weather event and evaluate the concurrent aerosol-cloud microphysical processes and characteristics. By taking this sensitivity test approach, we reconcile the fine-scale differences in the precipitation response and address the influence of urban aerosols on severe weather. We describe the experiment and model simulations (Section 2), analyze the precipitation and microphysical differences (Section 3), and provide a discussion of our results and concluding remarks (Section 4).

2.2.0 Model Description

2.2.1 Model and Domain

To produce a realistic evolution of the temporal formation and chemical composition of aerosols, we use the fully interactive Weather Research Forecast (WRF) model with chemistry—WRF-Chem v. 3.6 (Grell et al. 2005)—to simulate aerosol-cloud interactions during a severe weather event over the CGP on May 27, 2013. During this event, several reports of hail (> 1.0 inch in diameter), strong winds (> 60 knots), and tornadoes were recorded (Storm Prediction Center). A model domain with 4 km grid spacing is centered over Kansas City, MO and extends over an area of 988 km X 636 km (158 by 246 rows and columns; Figure 2.1), with 72 vertical levels and a 50 hPa model top. We run continuous simulations from May 25, 0600 UTC through May 27 1800 UTC with a dynamical timestep of 15 seconds and chemistry timestep of 60 seconds. We analyze the last 30 hours of the simulation to allow for chemistry spinup in the model, based on calculations of transport time across the domain and similar studies (Eidhammer et al. 2014). For lateral meteorological boundary conditions, we use NAM-Reanalysis 12 km data (http://nomads.ncdc.noaa.gov/data.php) every six hours. Although a resolution of 250 m may be required to resolve the convective updrafts (Bryan et al. 2003), a 4km grid size has been shown to be sufficient for resolving the potential for severe weather (Weisman et al. 1997) and

we do not incorporate a cumulus scheme based on this horizontal resolution. Table 1 describes the full suite of physical and chemical parameterizations implemented in the simulation.

Simulated atmospheric aerosols are linked to microphysical processes with the Morrison microphysics scheme (Morrison et al. 2005), a two-moment bulk microphysics scheme. Aerosols are activated as CCN in a separate module and provided as condensation nuclei (CN) to the microphysics (Abdul‐Razzak and Ghan 2000), which tracks the mass mixing ratio and number concentration of five hydrometeor species and water vapor (mass only): (1) cloud drop; (2) raindrop; (3) ice; (4) snow and (5) graupel. Sources and sinks of these hydrometeors include accretion, heterogeneous freezing, melting, self-collection, sublimation, evaporation, deposition, condensation, autoconversion (cloud drops to raindrops and ice to snow), homogeneous freezing (cloud drops to ice and rain drops to snow) ice nucleation from freezing of aerosol, droplet activation from aerosol, and ice multiplication (riming processes) (Morrison, 2005). Deposition nucleation is not included, as aerosols are assumed to be coated in sulfate (Cziczo et al. 2009). Ice nucleation is not explicitly included, although this process has been shown to be important for convection (Van den Heever et al. 2006).

We include the direct and indirect radiative effects of aerosols with anthropogenic emissions and on-line chemistry to predict CN. In this version of the model, the chemistry module calculates the number and mass of aerosols that will activate as CCN based on hygroscopicity and supersaturation (Köhler curves), and provides this prognostic CCN to the microphysics module. Gas phase chemistry is simulated with the Regional Acid Deposition Mechanism version 2 (RADM2) chemical mechanism (Stockwell et al. 1990) and particle phase chemistry is simulated with the Modal Aerosol Dynamics model for Europe (Schell et al. 2001) aerosol model, including sulfate, nitrate, ammonium, black carbon, and organic carbon. New

particle formation is included via nucleation of sulfuric acid and the formation of secondary organic aerosol (SOA) are simulated with the Secondary ORGanic Aerosol Model (SORGAM;(Schell et al. 2001)).

2.2.2 Emissions and Chemical Boundary Conditions

We implement the United States Environmental Protection Agency (EPA) 2011 National Emissions Inventory (NEI) re-gridded to the 4km model domain. The NEI includes emissions from point, area, and mobile sources for 57 gas phase species and 19 aerosol species (including sulfate, nitrate, salt, elemental carbon, and un-speciated $PM_{2.5}$). Biogenic emissions of isoprene are estimated using the MEGAN emissions algorithm (Guenther et al. 2006) and are used in the gas-phase chemistry scheme. However, the formation of secondary organic aerosol (SOA) via isoprene is not included in this version of the model. We do not include an interactive, wind-driven source of dust (e.g., GOCART (Zhao et al. 2010)), however the NEI includes emissions of anthropogenic dust from mobile, point, and area sources in the coarse aerosol mode. Chemical boundary conditions are provided every 6 hours from MOZART-4/GEOS5 simulations (Emmons et al. 2010).

To investigate the sensitivity of a MCS to urban emissions and aerosols, we conduct three separate three-member ensemble simulations, each with a different emissions scenario for the Kansas City region: (1) 2011 NEI (hereinafter called the BASE case), (2) doubled NEI emissions (2X case), and (3) halved NEI emissions (HALF case). Because of the complexity of aerosol concentrations on cloud microphysics, especially in severe weather events, we focus on the role of urban aerosols on precipitation in a representative CGP urban environment. Emissions are scaled only in the Kansas City, MO region (black box outlined in Figure 2.2) and all NEI gas and aerosol emissions are scaled equally. Chemical boundary conditions are not altered; therefore, background aerosol and gas phase constituents are consistent across all three simulations.

Ensemble members are created by randomly perturbing the initial condition on model perturbation temperature for every grid cell. Perturbation values are created by a function that generates random numbers using a normal distribution, with a prescribed variance of 0.05 and an average of 0.0. This is slightly modified from the method provided by the WRF Working Group 13 (NOAA 2007), which is designed for operational forecasting and more ensemble members.

2.2.3 Boundary Layer Aerosol Loading and Composition

Boundary layer (surface to approximately 2 km) aerosol is averaged over the second 24-hour period in the simulation (e.g. 06 UTC May 26 – 06 UTC May 27) for the BASE ensemble. This time slice allows time for chemical spin-up yet is before the precipitation begins to accumulate. In the boundary layer, $PM_{2.5}$ concentrations are highest in the northern portion of the domain, with values up to 50 μg m^{-3} in southern Iowa and Nebraska and up to 30 μg m^{-3} along the Missouri River Valley (Figure 2.2a). Much of the $PM_{2.5}$ in the northern portion of the domain is composed of sulfate (Figure 2.2b) and is driven by the interaction of the relatively large amount of ammonia emitted from the agricultural region in the northwest of the domain and incoming sulfate from the northeastern boundary. Evaluations of hourly station data $PM_{2.5}$ in this region of the domain show that the model overproduces $PM_{2.5}$ (https://www.epa.gov/hesc/remote-sensing-information-gateway). However, this pattern is consistent in all simulations. The maximum ammonium aerosol mixing ratios exceed 5 μg m^{-3} in the northwestern portion of the domain along the Missouri River Valley (Figure 2.2c). Distinct nitrate aerosol point sources are visible and originate in northern Oklahoma, spread out and travel north with prevailing southerly wind into Kansas and Missouri (Figure 2.2d). The spatial patterns of nitrate aerosol show well-defined plumes associated with power generation and urban areas (Figure 2.1d), and comprise up to 35% of the $PM_{2.5}$ plumes southwest of Kansas City, MO.

Nitrate concentrations reach a maximum (> 2 μg m^{-3}) in Omaha, NE and just east of Kansas City with relatively little nitrate aerosol in the northern portion of the domain. Directly downwind of Kansas City, there is a local maximum nitrate aerosol concentration of 2 μg m^{-3}, which is on the same order as sulfate concentrations in and near the Kansas City urban region (2 – 4 μg m^{-3}). This pattern reflects the shift from ammonium sulfate in the relatively rural northern portion of the domain to ammonium nitrate near the urban areas.

Modeled aerosol composition in the Kansas City metropolitan area is dominated by ammonium sulfate and ammonium nitrate. In our BASE case ensemble, elemental carbon is less than 0.15 μg m^{-3} (~1% of the $PM_{2.5}$) within the urban region. Studies have shown that a 20% elemental carbon fraction of $PM_{2.5}$ is a lower limit for semi-direct radiative effects to be important (Meier et al. 2012), suggesting that absorption and heating by black carbon (i.e., the semi-direct effect) would be minimal. Simulated organic carbon aerosol concentrations are also relatively low. Organic aerosol is derived from primary emissions and secondary formation in the atmosphere from anthropogenic species, but the SORGAM SOA module is known to under-predict SOA formation (Ahmadov et al. 2012). SOA from biogenic VOC are not included in our organic aerosol estimates, as SORGAM does not calculate isoprene-derived SOA and monoterpene emissions are not included in our MEGAN simulations. Based on the relatively low forest cover in the region (Figure 2.1), the formation of local biogenically-derived SOA is likely not a main driver of the organic aerosol composition.

2.2.4 Evaluation of Modeled Aerosol Composition

Using IMPROVE data (Malm et al. 1994) from the two sites within the modeling domain (El Dorado Springs, MO (EDS) and Lake Seguma, IA (LAKE); Figure 2.1), we compare simulated and observed aerosol composition. Because of the precipitation timing and four-day

interval of the IMPROVE data, we compare the observed versus modeled average composition prior to the synoptic event (e,g., May 22 – 25, 2013, which includes two samples) in Table 2.2. We compare this to a similar model time frame, averaging the simulation hours 12-30, which allows chemical spin-up and is prior to the precipitation event.

At the EDS site, elemental carbon comprises 0.35 μg m^{-3} of the aerosol compared with 0.13 μg m^{-3} simulated by the model. Elemental carbon emissions from the 2011 EPA NEI and chemical boundary conditions are from anthropogenic activity only, and this discrepancy at the rural IMPROVE sites may be due to the lack of biomass burning emissions. Evaluation of thermal anomalies in the region show that sources within the domain are small, but there are indications of biomass burning to the south in Mexico (results not shown). Because the background aerosol is consistent through all simulations and the focus of this work is on the role of urban aerosols, this discrepancy should not significantly affect our sensitivity tests near the urban area. Prior to the storm, the model and observations compare well for ammonium sulfate, with the model contributing to 2.29 μg m^{-3} of aerosol and the observed 1.43 μg m^{-3}. Together, the most hygroscopic aerosols (ammonium sulfate and ammonium nitrate) contribute approximately the same fraction of the mass in both the modeled and the observed composition, which is the primary consideration for activation as CCN and most relevant for our analysis.

In contrast, the Lake Seguma modeled data shows greater discrepancies with the observations. Modeled elemental carbon is 0.09 μg m^{-3}, while observed values are four times as large at 0.34 μg m^{-3}, which we also attribute to the lack of biomass burning emissions in our inventory and an underestimation of the Fire Inventory from NCAR (FINN), which is used to drive the MOZART model (Pereira et al. 2016). Simulated ammonium nitrate (1.45 μg m^{-3}) compares well with observations (0.74 μg m^{-3}); however, the modeled ammonium sulfate (9.81

μg m^{-3}) is nearly eight times larger than the observed value (1.24 μg m^{-3}). This discrepancy is likely due to an interaction between local NH_3 emissions from agriculture with H_2SO_4 (sulfuric acid) entering from the northern boundary. One possible reason for the high ammonium sulfate formed in the model is that the MOZART model implements emissisons from the 2002 EPA NEI (http://bio.cgrer.uiowa.edu/arctas/emission.html; (Lu 2016)) and may not reflect the sulfur dioxide reductions observed in the central US (Hand et al. 2012). However, because we use the same boundary conditions for each simulation and this region is not located near the urban region of our analysis (Figure 2.2), the ammonium sulfate created in the northern portion of the domain does not significantly affect our analysis.

2.3.0 Results

In the Central United States, the Great Plains Low-Level Jet consistently influences the region's weather and climatology (Bonner 1968). The prevailing south-southwestly wind flow transports moisture from the Gulf of Mexico to the north, and has been connected with severe weather systems in the Central United States. Prior to the 27 May 2013 event, the jet transports surface emissions and resulting oxidation products and aerosol from the urban regions northward. This influence is apparent in Figure 2.2d, where visible plumes from the nearby urban areas extend from the point of origin (e.g., Omaha, NE and Kansas City, MO) to the north due to the jet direction. Aloft, the large-scale Mesoscale Convective System (MCS) simulated in this case study originates in the northwest and propagates south-to-southeast. Therefore, because of these two contrasting directions, the MCS interacts with aerosols originating from the urban area well before traversing the Kansas City region. A full description of the case study follows, comparing the BASE ensemble simulation with the HALF and 2X urban emissions ensembles for the meteorology (Section 3.1), the accumulated precipitation (Section 3.2), the microphysics

in Phase I (00-06 UTC; Section 3.3) and Phase II (06-18 UTC; Section 3.4) of the simulation, and the thermodynamics (Section 3.5).

2.3.1 Meteorology of the convective event: May 27, 2013, 00:00 – 18:00 UTC

Observed radar reflectivity (UCAR) shows strong, isolated precipitation occurring in the northeastern portion of the domain (Figure 2.3a). At 04:00 UTC, the precipitation in the northeastern portion of the domain is more organized, and a MCS enters the domain at the northwestern boundary (Figure 2.3b). By 06:00 the MCS has propagated southeast and there is an outflow boundary just north of Kansas City, MO (Figure 2.3c). At 10:00 UTC, the MCS continues to propagate and is now just north of Kansas City, MO (Figure 2.3d). Severe thunderstorms moved across Kansas City on May 27, 2013 (Figure 2.3e&f), 12:00 -14:00 UTC. The model qualitatively simulates these events, as shown in Figure 2.4a-g with the BASE ensemble simulated radar reflectivity, a quantity derived from an NCAR Command Language function (wrf_user_getvar) that computes the maximum radar reflectivity over all model levels. This function uses raindrop, water vapor, graupel, and snow mixing ratios to compute the simulated radar reflectivity. This storm system divides into two distinct meteorological events: (1) a stationary front that dominates precipitation during Phase I [5-26-18:00 UTC – 5-27-06:00 UTC]; and (2) a MCS that propagates through the region in Phase II [5-27-06:00-18:00 UTC]. Phase I begins with several convective cells that occur along a weak stationary front that stretches from northwestern to central Missouri at 02:00 UTC (Figure 2.4a). At 04:00 UTC, an MCS develops in the northwest corner of the domain (Figure 2.4b), and begins to grow and propagate southeast. This system merges with the frontal convection by 05:00 UTC (not shown) forming an outflow boundary that travels south along the Missouri River at 6:00 UTC (Figure 2.4c). This time point is the end of Phase I and the beginning of Phase II. The outflow boundary

crosses the city as it moves southwest, dissipating by 10:00 UTC (Figure 2.4d). Convective cells that originated with the MCS strengthen and develop into a squall line by 12:00 (Figure 2.4e). As this squall line propagates in the southeast direction across the urban region of Kansas City, it strengthens just south of the urban area (14:00 UTC; Figure 2.4f). At 15:00 UTC (Figure 2.4g), the squall line begins to dissipate and travels into eastern Missouri, exiting the domain.

Scaling urban area emissions by factors of two (2X ensemble; Figure 2.4h-n) and one-half (HALF ensemble; Figure 2.4o-u), the model simulates changes in storm morphology. At 04:00 UTC (46 hours into the simulation), all three cases are qualitatively similar, with a developing MCS in the northwestern quadrant and the frontal convection along the Missouri River Valley. The 2X and BASE ensemble simulated radar reflectivities are very similar through 10:00 UTC. After 10:00 UTC, the 2X ensemble diverges from the BASE, and the BASE and HALF simulated radar reflectivities become more similar. Noticeable differences between the BASE and HALF ensembles begin at 06:00 UTC with the progression of the outflow boundary. The HALF case has lower precipitation intensity and smaller spatial extent than the BASE ensemble (Figure 2.4q). From 08:00 – 10:00 UTC, the band of precipitation ranging southwest to northeast of the city dissipates more quickly in the HALF ensemble (Figure 2.4r). In the BASE case, there is an area of precipitation spanning Kansas City (Figure 2.4d), yet this region of precipitation is smaller in the HALF case (Figure 2.4r) and larger, with stronger reflectivities in the 2X case (Figure 2.4k). The strongest winds are still north of the city, with strong winds in the 2X and BASE cases extending eastward (2X further than the BASE) and the HALF slightly further south, covering a smaller area than the other two ensembles.

By 12:00 UTC the strongest reflectivites are north of Kansas City in the BASE case, with a developing system extending southwest of the city. While the system north of the city in the

HALF case is stronger, it lacks the southwestern development seen in both the BASE and 2X (Figure 2.4s). The strongest reflectivities are shifted to the south in the 2X ensemble (Figure 2.4l), indicating a stronger squall line development southwest of Kansas City. This is confirmed by the 12 m s^{-1} contour, where there is a distinct pattern with all three ensembles producing strong winds to the north of the city. However the 2X and BASE ensembles also include strong winds extending from the city center to the southwest, and the HALF ensemble fails to produce this feature (Figure 2.4e,l,s). This pattern persists through 14:00 UTC, where the 2X and BASE ensembles have strong winds southwest of Kansas City, indicating a possible squall line (Figure 2.4f,m). This is not present in the HALF ensemble (Figure 2.4t), and is consistent with the simulated radar reflectivity. By 15:00 UTC, the first pulse of convective activity has dissipated and moved south, and the main squall line crosses the Kansas City, MO region in all three cases (Figure 2.4g,n,u).

2.3.2 Accumulated Precipitation

The total accumulated precipitation pattern can be attributed to the two meteorological events: (1) the stationary front that dominates precipitation during Phase I and (2) the MCS that propagates through the region in Phase II. In the following discussion, we refer to the direction of storm propagation relative to Kansas City; upwind is to the northwest of the city and downwind is to the southeast. Phase I accumulated precipitation is clearly associated with the stationary front (Figure 2.5 a-c), with maximum accumulation exceeding 80 mm in the 12-hour period (Figure 2.5a). The swath of precipitation extends northwest to southeast, with the leading edge of precipitation reaching northeastern Kansas City. In the 2X ensemble, accumulated precipitation is reduced up to 50 mm [80 %] (Figure 2.5b). Differences in the HALF ensemble

exhibit greater spatial variability with no clear pattern associated with the emissions decrease (Figure 2.5c).

For the final twelve hours of the simulation (Phase II; 06:00 -18:00 UTC; Figures 2.5d-f), we focus on the region of precipitation exceeding 65 mm near the Kansas City urban area. This region of precipitation extends east and south over Kansas City and is associated with a squall line development (Figure 2.5d). In the 2X case, there is suppression east of the city (a decrease of 40 mm, or 50%) and enhancement (20 mm, >100%) to the north and south of the urban area (Figure 2.5e). In the HALF case, there is a distinct suppression of precipitation over Kansas City extending east and south, with values exceeding 30 mm (50%). North of Kansas City precipitation is enhanced up to 20 mm (Figure 2.5f). Comparison with the storm morphology suggests that changes in the spatial distribution of precipitation are due to a displacement of the squall line, which occurs north of Kansas City as compared to the BASE case.

2.3.3 Spatial Distribution and Time Series of Hydrometeors: Phase I

By varying the Kansas City anthropogenic emissions, we directly affect aerosol concentrations and therefore the available CCN within and upwind of the city. As described in Sections 3.1 and 3.2, this magnitude change leads to large-scale changes in storm morphology and accumulated precipitation patterns. To understand how scaling urban emissions affects the spatial distribution of hydrometeors on a cloud macroscale, we examine the model microphysics via changes in liquid water path (kg m^{-2}; LWP) and ice water path (kg m^{-2}; IWP). LWP and IWP are each temporally integrated over all hours in Phase I.

During Phase I, LWP and IWP are elevated along the stationary front that extends from the northwest to southeast just to the north of Kansas City (Figure 2.6a). The 2X ensemble LWP decreases to the northeast and increases to the southwest of the front as compared to the BASE

case (Figure 2.6b). This result is consistent with warm rain suppression theory, where more aerosols initially increase the cloud drop number, decreasing the cloud drop size and slowing the autoconversion to rain. The displacement of the system to the south suggests that it takes longer for raindrops to form, and when they do, they drive enhancement downwind compared to the BASE case. Solid phase hydrometeors form via heterogeneous or homogenous ice nucleation. The Morrison microphysics scheme employed considers heterogeneous ice nucleation to occur by condensation freezing of deliquesced, internally mixed particles or homogenous ice nucleation, which is expressed as a probability (Morrison et al. 2005). Homogenous ice nucleation occurs with temperatures colder than -40C, however ice nucleation onto aerosol is not included in the model. As a result of solid phase formation in the microphysics parameterization, the change in IWP is similar to the LWP. In the HALF case, no clear spatial pattern is evident in either LWP (Figure 2.6c) or IWP (Figure 2.6f), although the magnitude of change is comparable to the 2X case. The broader spatial impacts in the IWP versus the LWP are a result of the surface changes propagating to higher altitudes and being dispersed by stronger winds aloft.

Next we compare the temporal changes in the hydrometeors during Phase I. In Figure 2.7, we average over all model vertical levels and over the region shown in Figure 2.5a that encompasses the region where the stationary front occurred and a majority of the accumulated precipitation, while excluding grid cells with less than 1 drop cm^{-3} and the elevated $PM_{2.5}$ in the northern portion of the domain (Figure 2.2a). At the beginning of Phase I, scaling emissions leads to a reduction of precipitation in the 2X ensemble (18 mm; Figure 2.7a) compared to the BASE and HALF ensembles (~20.5 mm; Figure 2.7a). At 5-27 00:00 UTC, all three ensembles have a similar accumulated precipitation (~ 21.5 mm). The HALF ensemble accumulates

precipitation more quickly than the BASE or 2X cases and by the end of Phase 1, the BASE and HALF ensembles have accumulated 39 mm of precipitation, and the 2X ensemble has only accumulated 36 mm of precipitation. The BASE ensemble is usually between the 2X and HALF ensembles with the minimum/maximum shading overlapping, suggesting that these changes may not be significant. The cloud drop number concentration and size are also sensitive to the emissions scaling. The 2X ensemble has the largest concentration (152 cm^{-3}), the BASE ensemble has a concentration of 135 cm^{-3}, and the HALF ensemble starts with 130 cm^{-3} (Figure 2.7b) and the ensemble shading for the 2X case is outside of that for the BASE and HALF cases. This pattern of 2X > BASE & HALF persists until 5-27 00:00 UTC, at which point, the HALF case cloud drop number concentrations decrease more rapidly than the 2X or BASE ensembles. As Phase I progresses, cloud drop sizes grow larger and number concentrations decrease to ~70 cm^{-3}. Droplet size is increasing as number concentrations are decreasing for all ensembles. Raindrop number concentrations and sizes increase for all three ensembles throughout Phase I (Figure 2.7c); raindrop size increases from 100 μm to 430-440 μm. For the first half of Phase I, the 2X ensemble generally has fewer but slightly larger raindrops than the HALF or BASE ensembles; after the halfway mark, the 2X raindrops are more numerous and continue to be larger although this does not exceed the range of variability of the other two ensembles.

Graupel number concentrations remain relatively stable throughout most of Phase I, and decrease to about 13 L^{-1} by the end of Phase I (Figure 2.7d). Initially graupel sizes differ between the ensembles (2X (~400 μm) > BASE & HALF (~50 μm)) but all ensembles are about 450 μm by 5-26 22:00 UTC and remain steady through the end of Phase I. All three ensembles increase in snow number concentrations and size until 5-26-22:00 UTC (Figure 2.7e). The differences in number concentrations and sizes are relatively small, especially after 5-27-00:00 UTC. Finally,

ice hydrometeor number concentrations increase through 5-27-00:00 UTC for all three ensembles (Figure 2.7f) and ice hydrometeor size increases throughout Phase I. Like the snow number concentrations and sizes, differences are especially small between the ensembles after 5-27-00:00 UTC.

To demonstrate how scaling emissions affects the aerosols and subsequently the available CCN, we show the interstitial accumulation mode aerosol number concentrations (Figure 2.7g). Total accumulation mode aerosol number concentration would include the in-cloud category as well, however, those aerosols are passed into the microphysics as activated CCN (i.e. cloud drops). At the beginning of Phase I, all three ensembles have similar aerosol number concentrations (~190 cm^{-3}). As precipitation forms and the sources continually emit, by the end of Phase I, there are more aerosols in the 2X ensemble than in the BASE or HALF ensembles although this is not outside of the model spread.

To summarize Phase I, scaling emissions leads to changes in the liquid phase hydrometeors consistent with current warm-rain theory; increasing emissions leads to increasing the available CCN, which leads to smaller cloud drops and delayed precipitation or suppression upwind and enhancement downwind of the stationary front. For the HALF ensemble, the spatial changes are less coherent, though the time series' indicate that fewer activated CCN lead to larger initial cloud drops and earlier precipitation. However, the changes in the solid-phase hydrometeors are relatively small and do not scale directly with emissions. The rates at which these hydrometeors form and grow set the stage for Phase II.

2.3.4 Spatial Distribution and Time Series of Hydrometeors: Phase II

During Phase II (5-27-06:00 to 18:00 UTC), a squall line develops south of Kansas City in the BASE and 2X ensembles and is weaker in the HALF ensemble. This phenomenon was

shown in the simulated radar reflectivity (Figure 2.4) and the accumulated precipitation differences (Figure 2.5). Here we link these changes in storm morphology and precipitation to the spatial and temporal hydrometeor characteristics during Phase II.

In the BASE ensemble, the temporally integrated LWP and IWPs are associated with the squall line and are largest south of Kansas City of 30 kg m^{-2} and 85 kg m^{-2}, respectively (Figure 2.8a,d). The 2X ensemble LWP and IWP values show suppression of the squall line upwind and enhancement of the squall line downwind of Kansas City (Figures 2.8b and 2.8e), and the HALF ensemble displays a strong reduction of the LWP and the IWP, < 20 kg m^{-2}; ~66% and < 45 kg m^{-2} south of Kansas City (Figure 2.8c,f). The corresponding increase to the north of the city is not as large. The large decrease in IWP in the HALF ensemble is due to the suppressed squall line development.

As in Phase I, we compare the temporal changes in the hydrometeor size and number concentrations. In Figure 2.9, we average over all model vertical levels and over the region shown in Figure 2.5d, which encompasses the region where the squall line occurred and excludes grid cells with less than 1 drop cm^{-3}. At the beginning of Phase II (06:00 UTC), accumulated precipitation is similar for all three ensembles (~13.5 mm; Figure 2.9a). By the end of Phase II, there is a clear enhancement of mean accumulated precipitation in the 2X ensemble outside of the HALF and BASE ensemble spread, and a reduction of precipitation in the HALF ensemble. At 10:00 UTC, cloud drop number concentrations are the same for all three ensembles (70 cm^{-3}), and the 2X drop size is clearly larger than the BASE and HALF ensembles (15 μm vs. 13 μm), which generally persists throughout Phase II. After 11:00 UTC, cloud drop number concentrations decrease for all three ensembles, as cloud drops are converted to rain or solid phase species (Figure 2.9b,c,d,e,f). As a result of less precipitation, the HALF ensemble has

more cloud drops than both the 2X and BASE ensembles from 11:00 UTC through 14:00 UTC with little overlap with the other ensembles. Raindrop number concentrations are increasing (Figure 2.9c), coinciding with the squall line development (06:00 – 12:00 UTC). The raindrop number concentrations are similar until 12:00 UTC, increasing to 130 L^{-1} (BASE and 2X) and 150 L^{-1} (HALF), then the BASE and 2X ensembles continue to increase until 14:00 UTC. The 2X raindrop sizes are consistently larger than the BASE and HALF ensembles. Greater vertical velocities (not shown) in the 2X ensembles can support larger hydrometeors and suggest a more efficient collision and coalescence process. Graupel number concentrations increase through 11:00 UTC, with the 2X ensemble once again being more numerous than the HALF and BASE ensembles during most of that time. After 11:00 UTC, 2X graupel number concentration decreases and is distinct from the other ensembles, but the size increases through 14:00 UTC. Number concentrations of snow and ice are steady throughout Phase II, with 2X number concentrations and sizes of snow and ice generally greater than both BASE and HALF snow and ice number concentrations and sizes, although there is little distinction between the ensembles. The urban emissions scaling is most evident in the 2X ensemble aerosol number concentrations at 06:00 UTC (~160 cm-3 vs. ~125 cm-3; Figure 2.9g). As precipitation increases in the 2X ensemble and ceases in the BASE and HALF ensembles (Figure 2.9a), aerosol number concentrations increase in the BASE and HALF ensembles and decrease in the 2x ensemble until 10:00 UTC. After the squall line passes at 14:00 UTC, 2X ensemble aerosol number concentrations increase much more quickly than in the BASE and HALF ensembles. While meteorology is a strong driver of the diurnal cycle of aerosol number concentrations, they are also influenced by the diurnal pattern of emissions as seen in all three ensembles.

During Phase II, increasing urban emissions leads to convective invigoration, i.e., enhanced precipitation, hydrometeor growth and number concentrations (Figure 2.5e) and decreasing emissions leads to the suppression of the squall line (Figure 2.5f). The 2X ensemble has the largest hydrometeors while the HALF and BASE ensembles are similar. From 10:00 – 14:00 UTC, the HALF ensemble has more numerous and smaller cloud drops, coinciding with and fewer and smaller solid phase hydrometeors (Figure 2.9 b,c,d,e).

In summary, the growth rates of hydrometeors and subsequent timing of the synoptic meteorology drive differences in the simulated squall line development. At the beginning of Phase II, more numerous and smaller raindrops contribute to the development of the squall line differently in the HALF ensemble compared to the 2X or BASE ensembles. This difference leads to more substantial changes in the growth and formation of solid phase hydrometeors in the 2X and BASE ensembles, which feeds back into the formation of rain from cold cloud processes. The link between hydrometeors and the weakened squall line development lies in the connection between microphysics and cold pools. As squall line formation and development is a function of the strength of cold pools and their propagation speeds. We next examine how the rate of hydrometeor evaporation determines cold pool strength.

2.3.5 Dynamics: Cold Pools

Cold pool strength determines the propagation speed of a squall line, which control its development and subsequent propagation. The strength of a cold pool is determined by the thermodynamic profile of the atmospheric column; the difference between the equivalent potential temperature near the surface and at the origin of the downdraft (Schlemmer and Hohenegger 2014). Because the equivalent potential temperature accounts for the condensation of all water vapor, changes in cold pool strength can be related to microphysical processes. Here

we use the perturbation temperature (T'; T_{ref} = 290K) as a proxy for cold pool strength (Kalina et al. 2014). We calculate T' as the difference between the lowest model level perturbation temperature and the domain-averaged lowest model level perturbation temperature, where a larger negative value of T' corresponds to a stronger cold pool. We use T' and the 10-meter maximum wind speed to examine the relationships between the cold pool strength and squall line formation.

Here we show that cold pool magnitude and expanse (location) are sensitive to urban emissions. At 10:00 UTC, a weak cold pool (-2K) northwest of Kansas City develops in the BASE ensemble (Figure 2.10a); this cold pool is much stronger in the 2X ensemble (-6K; Figure 2.10e) and is stronger (-3K) but displaced south in the HALF ensemble (Figure 2.10i). The 12 m s^{-1} contour follows this pattern, encompassing the largest area with the strongest cold pool in the 2X ensemble. By 11:00 UTC, T' decreases to -4 K and to -8 K for the BASE and 2X ensembles respectively (Figure 2.10 c,g). While the strength of the HALF ensemble cold pool is comparable to the BASE ensemble, it continues to be displaced to the south, and is ahead of precipitation (Figure 2.10k, Figure 2.5d). This pattern is reflected in the 12 m s^{-1} contour, which is to the north of Kansas City in the BASE ensemble but extends southward in the HALF ensemble. By 12:00 UTC, the squall line has developed south of Kansas City (Figure 3f), approximately located along the -3 K contour (Figure 2.10d) and along the 12 s^{-1} contour. A similar pattern can be seen in the 2X ensemble, except the cold pool is slightly stronger (-5 K contour; Figure 2.10h). In the HALF ensemble, the cold pool is stronger (-4K) and much further southeast (Figure 2.10k). As a result of this southern displacement of the cold pool the squall line is greatly weakened, leading to reduced amounts of precipitation in the HALF ensemble. Therefore, changes in cold pool

strength and location between ensembles are likely a function of the changes in the diabatic processes driven primarily by changes in the microphysics and aerosol concentrations.

2.4.0 Discussion and Conclusions

This study examined the effects of the magnitude of urban emissions on a severe weather system in the CGP, a region with mid-sized urban areas and subject to a large number of severe weather events. Emissions within the Kansas City urban area (Figure 2.2) were doubled (2X ensemble) and halved (HALF ensemble) from a baseline (BASE) emissions scenario. We examined a specific severe weather event (May 26-27, 2013) and organized the analysis in two phases, referring to a stationary front in the first half of the simulation (Phase I) and the formation and propagation of an MCS in the second half of the simulation (Phase II).

The perturbation to urban emissions directly affects the aerosol concentrations throughout the domain, as the low level jet in the region transports direct aerosol emissions as well as those formed through atmospheric processes from the urban area to the north. The resulting effects of these emissions changes are described here and visually in Figure 2.11. Changes in aerosol concentrations affect the number of CN that activate as CCN, which affects the hydrometeor formation and growth rate. Initially during Phase I, increased aerosol concentrations (2X ensemble) shift the total accumulated precipitation to the southwest, where rainfall is enhanced downwind and suppressed upwind. Later in Phase II, the lack of squall line development in the HALF case leads to the largest differences in accumulated precipitation. Because squall line development and propagation is determined by the cold pool strength, we show that increasing emissions leads to larger hydrometeors, suggesting stronger downdrafts and therefore a stronger and larger cold pool in the 2X ensemble. The more numerous but smaller cloud drops in the HALF case coincides with the cold pool propagating more quickly than in the 2X or BASE

ensembles, driving the southward displacement of the cold pool. The displaced cold pool leads to a reduction in the squall line strength in the HALF ensemble. In our dynamic simulations with evolving aerosols, these changes in precipitation then control the aerosol concentrations themselves by removing aerosols through wet deposition.

In our simulations, we attempt to understand the meteorology associated with realistic atmospheric chemistry simulations that include dynamic aerosol number concentrations, composition and evolution of aerosol burden. Our three-member ensemble approach (e.g., three simulations for each of the three emissions scenarios) lends strength to the consistent response of the meteorology to the change in aerosol magnitude. By showing the variance between the ensemble members, we gain confidence in asserting how the changes between each emissions scenario lead to changes in the meteorology. Many of the prior studies aimed at untangling the thermodynamic and dynamic processes involved in cloud microphysics and cloud macrostructure are idealized simulations (Morrison and Grabowski 2013; Grant and van den Heever 2015). While idealized simulations provide insight into how a single process might affect a convective system, they are limited in their applications as they often do not include surface heterogeneity and in many cases a constant CCN concentration (activated vs. non-activated) that is prescribed (van den Heever and Cotton 2007; Carrió et al. 2010). By using the coupled WRF-Chem model with online chemistry, we provide a direct link to dynamic aerosol concentrations that drive cloud microphysics, as well as closing the feedback loop shown in Figure 2.11 that allows the precipitation to alter aerosol concentrations themselves.

We do note several caveats in our simulations. The model does not include ice nucleation for any aerosol type, which may affect the formation of solid phase hydrometeors and the cold pool analysis. Additionally, we do not account for dust emitted from the surface

naturally, which would potentially have a large impact, as dust is an important ice forming nuclei. Because we are investigating severe weather and several studies show evidence for convective invigoration, it would be useful for future studies to include direct aerosol IN, especially in locations with potentially large amounts of dust such as the CGP. The nucleation of ice via dust might have significant radiative impacts as well as changing the cloud microphysics. Additionally, as noted in Section 2.4, there are lower than observed black carbon concentrations within our domain at the two sites with speciated aerosol observations. This could be a result of the omission of biomass-burning emissions within the domain or the underestimation of emissions within the MOZART simulations that drive the boundary conditions. These aerosols also may have important implications for the thermodynamic (semi-direct) response, and prior studies have shown that severe weather can be impacted by the presence of black carbon (Saide et al. 2015). While the analysis presented in this paper is focused on the second indirect effect, we recognize that the first direct effect is potentially impactful. The changes to the anvil as a result of scaling emissions would affect the radiation budget, influencing the stability of the atmosphere. These effects could be especially important in longer-term simulations (Fan et al. 2013). Finally, we note that we include chemical boundary conditions in these simulations to provide as much realism in the aerosol evolution as possible. However, our evaluation shows that we are likely simulating too much sulfate at the northern boundary of the model domain, triggering higher than observed concentrations of ammonium sulfate. Our three emissions scenarios would be impacted equally by the emissions and boundary conditions above, and we focus on processes in and around the urban area that are removed from the driving boundary conditions. Specifically, we have identified how the urban emissions at the domain center can affect the propagation of the large-scale meteorology.

Overall, we find that changing urban emissions magnitude has the potential to alter severe weather and rain patterns. During Phase I, increasing the urban emissions leads to a spatial shift in precipitation pattern while decreasing urban emissions leads to comparatively little change. The shift in total precipitation in the 2X ensemble can be attributed to slowed warm rain processes. Conversely, during Phase II the altered urban emissions has the opposite effect: decreasing urban emissions suppresses the squall line formation. We attribute the suppression to changes in cold pool strength and earlier precipitation, variables that are affected by microphysical processes and thus aerosol concentrations. Considering that the precipitation response to scaling emissions (and aerosol concentrations) is dependent on event, this type of analysis could be performed on several severe weather events, the results of which could be used to determine a threshold for how increasing or decreasing urban aerosols can influence regional precipitation. These changes in the precipitation patterns and locations of severe weather could impact urban planning and agriculture, as this study suggests that severe weather can be sensitive to urban emissions magnitude. The use of realistic, evolving aerosol concentrations within these simulations shows the effects that the concentrations have on different stages of the storm, and indicates the non-linearity of responses during the storm lifetime.

Acknowledgements
Funding for this research was provided by the NASA Interdisciplinary Science program through project # NNX12AM89G "Storms, forms, and complexity of the urban canopy: How land use, settlement patterns, and the shapes of cities influence severe weather". We thank David Stensrud at Pennsylvania State University and Larissa Reames at University of Oklahoma for assistance with model domain set up and Derek Posselt for suggestions on the analysis and manuscript.

References

Abdul‐Razzak, H., and S. J. Ghan, 2000: A parameterization of aerosol activation: 2. Multiple aerosol types. *Journal of Geophysical Research: Atmospheres*, **105,** 6837-6844.

Ahmadov, R., and Coauthors, 2012: A volatility basis set model for summertime secondary organic aerosols over the eastern United States in 2006. *Journal of Geophysical Research: Atmospheres (1984–2012)*, **117**.

Albrecht, B. A., 1989: Aerosols, cloud microphysics, and fractional cloudiness. *Science*, **245,** 1227-1230.

Alfaro, D. A., and M. Khairoutdinov, 2015: Thermodynamic Constraints on the Morphology of Simulated Midlatitude Squall Lines. *Journal of the Atmospheric Sciences*, **72,** 3116-3137.

Andreae, M. O., D. Rosenfeld, P. Artaxo, A. Costa, G. Frank, K. Longo, and M. Silva-Dias, 2004: Smoking rain clouds over the Amazon. *Science*, **303,** 1337-1342.

Ashley, W. S., T. L. Mote, P. G. Dixon, S. L. Trotter, E. J. Powell, J. D. Durkee, and A. J. Grundstein, 2003: Distribution of mesoscale convective complex rainfall in the United States. *Monthly Weather Review*, **131,** 3003-3017.

Bonner, W. D., 1968: Climatology of the low level jet. *Monthly Weather Review*, **96,** 833-850.

Boucher, O., and Coauthors, 2013: Clouds and aerosols. *Climate change 2013: the physical science basis. Contribution of Working Group I to the Fifth Assessment Report of the Intergovernmental Panel on Climate Change*, Cambridge University Press, 571-657.

Bryan, G. H., J. C. Wyngaard, and J. M. Fritsch, 2003: Resolution requirements for the simulation of deep moist convection. *Monthly Weather Review*, **131,** 2394-2416.

Carrió, G. G., W. R. Cotton, and W. Y. Y. Cheng, 2010: Urban growth and aerosol effects on convection over Houston. *Atmospheric Research*, **96,** 560-574.

Changnon Jr, S. A., 1981: METROMEX review and summary. *Meteor. Monogr.*, **40,** 181.

Cheng, C.-T., W.-C. Wang, and J.-P. Chen, 2010: Simulation of the effects of increasing cloud condensation nuclei on mixed-phase clouds and precipitation of a front system. *Atmospheric Research*, **96,** 461-476.

Christensen, M. W., and G. L. Stephens, 2012: Microphysical and macrophysical responses of marine stratocumulus polluted by underlying ships: 2. Impacts of haze on precipitating clouds. *Journal of Geophysical Research: Atmospheres*, **117**.

Corfidi, S. F., 2003: Cold pools and MCS propagation: Forecasting the motion of downwind-developing MCSs. *Weather and forecasting*, **18,** 997-1017.

Cziczo, D. J., K. D. Froyd, S. J. Gallavardin, O. Moehler, S. Benz, H. Saathoff, and D. M. Murphy, 2009: Deactivation of ice nuclei due to atmospherically relevant surface coatings. *Environmental Research Letters*, **4,** 044013.

Eidhammer, T., M. C. Barth, M. D. Petters, C. Wiedinmyer, and A. J. Prenni, 2014: Aerosol microphysical impact on summertime convective precipitation in the Rocky Mountain region. *Journal of Geophysical Research: Atmospheres*, **119,** 11,709-711,728.

Emmons, L., and Coauthors, 2010: Description and evaluation of the Model for Ozone and Related chemical Tracers, version 4 (MOZART-4). *Geoscientific Model Development*, **3,** 43-67.

Engerer, N. A., D. J. Stensrud, and M. C. Coniglio, 2008: Surface Characteristics of Observed Cold Pools. *Monthly Weather Review*, **136,** 4839-4849.

Fan, J., L. R. Leung, D. Rosenfeld, Q. Chen, Z. Li, J. Zhang, and H. Yan, 2013: Microphysical effects determine macrophysical response for aerosol impacts on deep convective clouds. *Proceedings of the National Academy of Sciences of the United States of America*, **110,** E4581-4590.

Grant, L. D., and S. C. van den Heever, 2015: Cold pool and precipitation responses to aerosol loading: Modulation by dry layers. *Journal of the Atmospheric Sciences*, **72,** 1398-1408.

Grell, G. A., S. E. Peckham, R. Schmitz, S. A. McKeen, G. Frost, W. C. Skamarock, and B. Eder, 2005: Fully coupled "online" chemistry within the WRF model. *Atmospheric Environment*, **39,** 6957-6975.

Guenther, A., T. Karl, P. Harley, C. Wiedinmyer, P. Palmer, and C. Geron, 2006: Estimates of global terrestrial isoprene emissions using MEGAN (Model of Emissions of Gases and Aerosols from Nature). *Atmospheric Chemistry and Physics Discussions*, **6,** 107-173.

Han, J.-Y., J.-J. Baik, and A. P. Khain, 2012: A numerical study of urban aerosol impacts on clouds and precipitation. *Journal of the Atmospheric Sciences*, **69,** 504-520.

Hand, J., B. Schichtel, W. Malm, and M. Pitchford, 2012: Particulate sulfate ion concentration and SO 2 emission trends in the United States from the early 1990s through 2010. *Atmospheric Chemistry and Physics*, **12,** 10353-10365.

Houze, R. A., 2004: Mesoscale convective systems. *Reviews of Geophysics*, **42**.

Jin, M., J. M. Shepherd, and M. D. King, 2005: Urban aerosols and their variations with clouds and rainfall: A case study for New York and Houston. *Journal of Geophysical Research: Atmospheres (1984–2012)*, **110**.

Kalina, E. A., K. Friedrich, H. Morrison, and G. H. Bryan, 2014: Aerosol Effects on Idealized Supercell Thunderstorms in Different Environments. *Journal of the Atmospheric Sciences*, **71,** 4558-4580.

Koren, I., G. Feingold, and L. A. Remer, 2010: The invigoration of deep convective clouds over the Atlantic: aerosol effect, meteorology or retrieval artifact? *Atmospheric Chemistry and Physics*, **10,** 8855-8872.

Lebo, Z. J., and J. H. Seinfeld, 2011: Theoretical basis for convective invigoration due to increased aerosol concentration. *Atmospheric Chemistry and Physics*, **11,** 5407-5429.

Lohmann, U., J. Feichter, C. C. Chuang, and J. E. Penner, 1999: Prediction of the number of cloud droplets in the ECHAM GCM. *Journal of Geophysical Research*, **104,** 9169.

Lu, Z., 2016, email correspondence ed., S. Kawecki, Ed.

Maddox, R. A., 1980: Meoscale convective complexes. *Bulletin of the American Meteorological Society*, **61,** 1374-1387.

Malm, W. C., J. F. Sisler, D. Huffman, R. A. Eldred, and T. A. Cahill, 1994: Spatial and seasonal trends in particle concentration and optical extinction in the United States. *Journal of Geophysical Research: Atmospheres*, **99,** 1347-1370.

Markowski, P., and Y. Richardson, 2011: *Mesoscale meteorology in midlatitudes.* Vol. 2, John Wiley & Sons.

Meier, J., I. Tegen, B. Heinold, and R. Wolke, 2012: Direct and semi‐direct radiative effects of absorbing aerosols in Europe: Results from a regional model. *Geophysical Research Letters*, **39**.

Min, Q. L., and Coauthors, 2014: Impacts of mineral dust on ice clouds in tropical deep convection systems. *Atmospheric Research*, **143,** 64-72.

Morrison, H., and W. W. Grabowski, 2013: Response of Tropical Deep Convection to Localized Heating Perturbations: Implications for Aerosol-Induced Convective Invigoration. *Journal of the Atmospheric Sciences*, **70,** 3533-3555.

Morrison, H., J. Curry, and V. Khvorostyanov, 2005: A new double-moment microphysics parameterization for application in cloud and climate models. Part I: Description. *Journal of the Atmospheric Sciences*, **62,** 1665-1677.

Niyogi, D., and Coauthors, 2011: Urban Modification of Thunderstorms: An Observational Storm Climatology and Model Case Study for the Indianapolis Urban Region*. *Journal of Applied Meteorology and Climatology*, **50,** 1129-1144.

NOAA, cited 2015: WRF Working Group 13: Ensemble Forecasting. [Available online at http://www.nssl.noaa.gov/users/stensrud/public_html/wg13/.]

Ntelekos, A. A., J. A. Smith, L. Donner, J. D. Fast, W. I. Gustafson, E. G. Chapman, and W. F. Krajewski, 2009: The effects of aerosols on intense convective precipitation in the northeastern United States. *Quarterly Journal of the Royal Meteorological Society*, **135,** 1367-1391.

Pereira, G., and Coauthors, 2016: Assessment of fire emissions inventories during the South American Biomass Burning Analysis (SAMBBA) experiment. *Atmos. Chem. Phys*, **16,** 6961 - 6975.

Peters, K., J. Quaas, P. Stier, and H. Graßl, 2014: Processes limiting the emergence of detectable aerosol indirect effects on tropical warm clouds in global aerosol-climate model and satellite data. *Tellus B*, **66**.

Rosenfeld, D., 2000: Suppression of rain and snow by urban and industrial air pollution. *Science*, **287,** 1793-1796.

Rosenfeld, D., and Coauthors, 2008: Flood or drought: how do aerosols affect precipitation? *Science*, **321,** 1309-1313.

Rosenfeld, D., and Coauthors, 2014: Global observations of aerosol‐cloud‐precipitation‐climate interactions. *Reviews of Geophysics*, **52,** 750-808.

Rotunno, R., J. B. Klemp, and M. L. Weisman, 1988: A theory for strong, long-lived squall lines. *Journal of the Atmospheric Sciences*, **45,** 463-485.

Saide, P. E., and Coauthors, 2015: Central American biomass burning smoke can increase tornado severity in the U.S. *Geophysical Research Letters*, **42,** 956-965.

Schell, B., I. J. Ackermann, H. Hass, F. S. Binkowski, and A. Ebel, 2001: Modeling the formation of secondary organic aerosol within a comprehensive air quality model system. *Journal of Geophysical Research: Atmospheres*, **106,** 28275-28293.

Schlemmer, L., and C. Hohenegger, 2014: The formation of wider and deeper clouds as a result of cold-pool dynamics. *Journal of the Atmospheric Sciences*, **71,** 2842-2858 %@ 0022-4928.

Schmid, P. E., and D. Niyogi, 2013: Impact of city size on precipitation-modifying potential. *Geophysical Research Letters*, **40,** 5263-5267.

Seifert, A., and K. Beheng, 2006: A two-moment cloud microphysics parameterization for mixed-phase clouds. Part 2: Maritime vs. continental deep convective storms. *Meteorology and Atmospheric Physics*, **92,** 67-82.

Seifert, A., C. Köhler, and K. Beheng, 2012: Aerosol-cloud-precipitation effects over Germany as simulated by a convective-scale numerical weather prediction model. *Atmos. Chem. Phys*, **12,** 709-725.

Shepherd, J. M., and S. J. Burian, 2003: Detection of urban-induced rainfall anomalies in a major coastal city. *Earth Interactions*, **7,** 1-17.

Stevens, B., and G. Feingold, 2009: Untangling aerosol effects on clouds and precipitation in a buffered system. *Nature*, **461,** 607-613.

Stockwell, W. R., P. Middleton, J. S. Chang, and X. Tang, 1990: The second generation regional acid deposition model chemical mechanism for regional air quality modeling. *Journal of Geophysical Research: Atmospheres (1984–2012)*, **95,** 16343-16367.

Storer, R., S. Heever, and T. L'Ecuyer, 2014: Observations of aerosol‐induced convective invigoration in the tropical east Atlantic. *Journal of Geophysical Research: Atmospheres*, **119,** 3963-3975.

Tao, W.-K., J.-P. Chen, Z. Li, C. Wang, and C. Zhang, 2012: Impact of aerosols on convective clouds and precipitation. *Reviews of Geophysics*, **50**.

Thompson, R. L., R. Edwards, J. A. Hart, K. L. Elmore, and P. Markowski, 2003: Close proximity soundings within supercell environments obtained from the Rapid Update Cycle. *Weather and forecasting*, **18,** 1243-1261.

Twomey, S., 1974: Pollution and the planetary albedo. *Atmospheric Environment (1967)*, **8,** 1251-1256.

Twomey, S., 1977: The influence of pollution on the shortwave albedo of clouds. *Journal of the atmospheric sciences*, **34,** 1149-1152.

UCAR: Image Archive : Meteorological case study selection kit.

van den Heever, S. C., and W. R. Cotton, 2007: Urban Aerosol Impacts on Downwind Convective Storms. *Journal of Applied Meteorology and Climatology*, **46,** 828-850.

Van den Heever, S. C., G. G. Carrió, W. R. Cotton, P. J. DeMott, and A. J. Prenni, 2006: Impacts of nucleating aerosol on Florida storms. Part I: Mesoscale simulations. *Journal of the atmospheric sciences*, **63,** 1752-1775.

Weisman, M. L., W. C. Skamarock, and J. B. Klemp, 1997: The resolution dependence of explicitly modeled convective systems. *Monthly Weather Review*, **125,** 527-548.

Yang, Q., and Coauthors, 2011: Assessing regional scale predictions of aerosols, marine stratocumulus, and their interactions during VOCALS-REx using WRF-Chem. *Atmospheric Chemistry and Physics*, **11,** 11951-11975.

Zhao, C., and Coauthors, 2010: The spatial distribution of mineral dust and its shortwave radiative forcing over North Africa: modeling sensitivities to dust emissions and aerosol size treatments. *Atmospheric Chemistry and Physics*, **10,** 8821-8838.

Table 2.1: WRF-Chem Model Physics and Chemistry Configuration

Physics Options		Chemistry Options	
Boundary Layer	YSU	*Gas-Phase*	RADM2
Microphysics	Morrison	*Aerosol Module*	MADE/SORGAM
LSM	NOAH	*Photolysis*	Fast-J
LW_Radiation	RRTMG	*Chemical BC*	MOZART-GEOS5
SW_Radiation	RRTMG	*Anthropogenic Emissions*	EPA NEI 2011
Surface Layer	Monin-Obukhov	*Meteorological BC*	NAM-Reanalysis (12km)
Urban Model	UCM		

Table 2.2: IMPROVE Aerosol and Modeled Aerosol (μg m^{-3})

	Ammonium Sulfate	Ammonium Nitrate	Soil-Antha	Elemental Carbon
EDS observed	1.43	0.29	0.35	0.35
EDS modeled	2.29	0.32	1.20	0.13
LAKE observed	1.24	0.74	0.19	0.34
LAKE modeled	9.82	1.45	0.53	0.09

Table 2.2: IMPROVE El Dorado Springs, MO (EDS, Figure 2.1) and Lake Seguma, IA (LAKE, Figure 2.1) aerosol composition as compared to model data (20km x 20 km averaging regions).

Figures

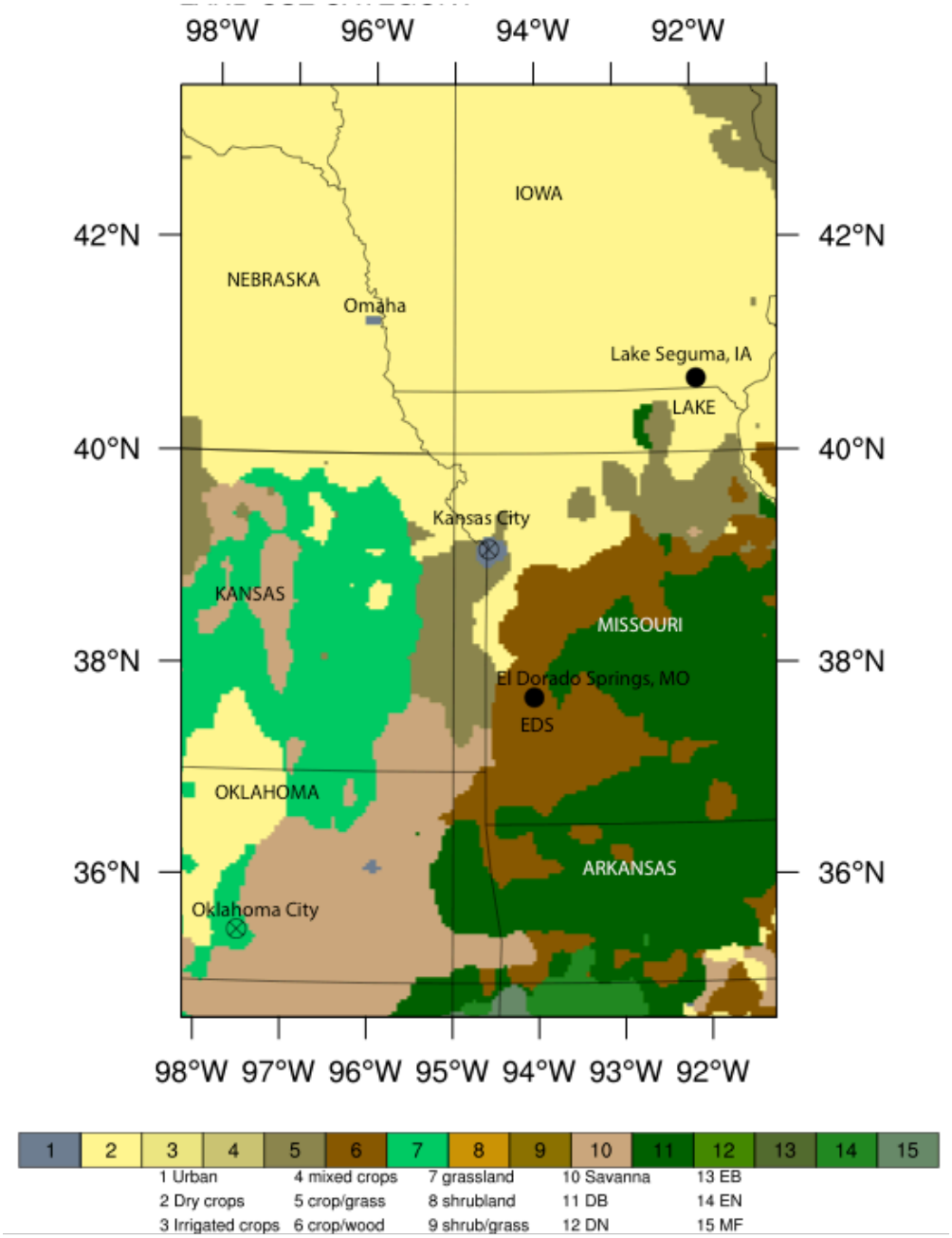

Figure 2.1: Domain landuse categories (color contours) and observation locations. Black circles are IMPROVE sites including Lake Seguma, IA (LAKE) and El Dorado Springs, MO (EDS). Large cities are also noted, including Kansas City, MO and Oklahoma City, OK.

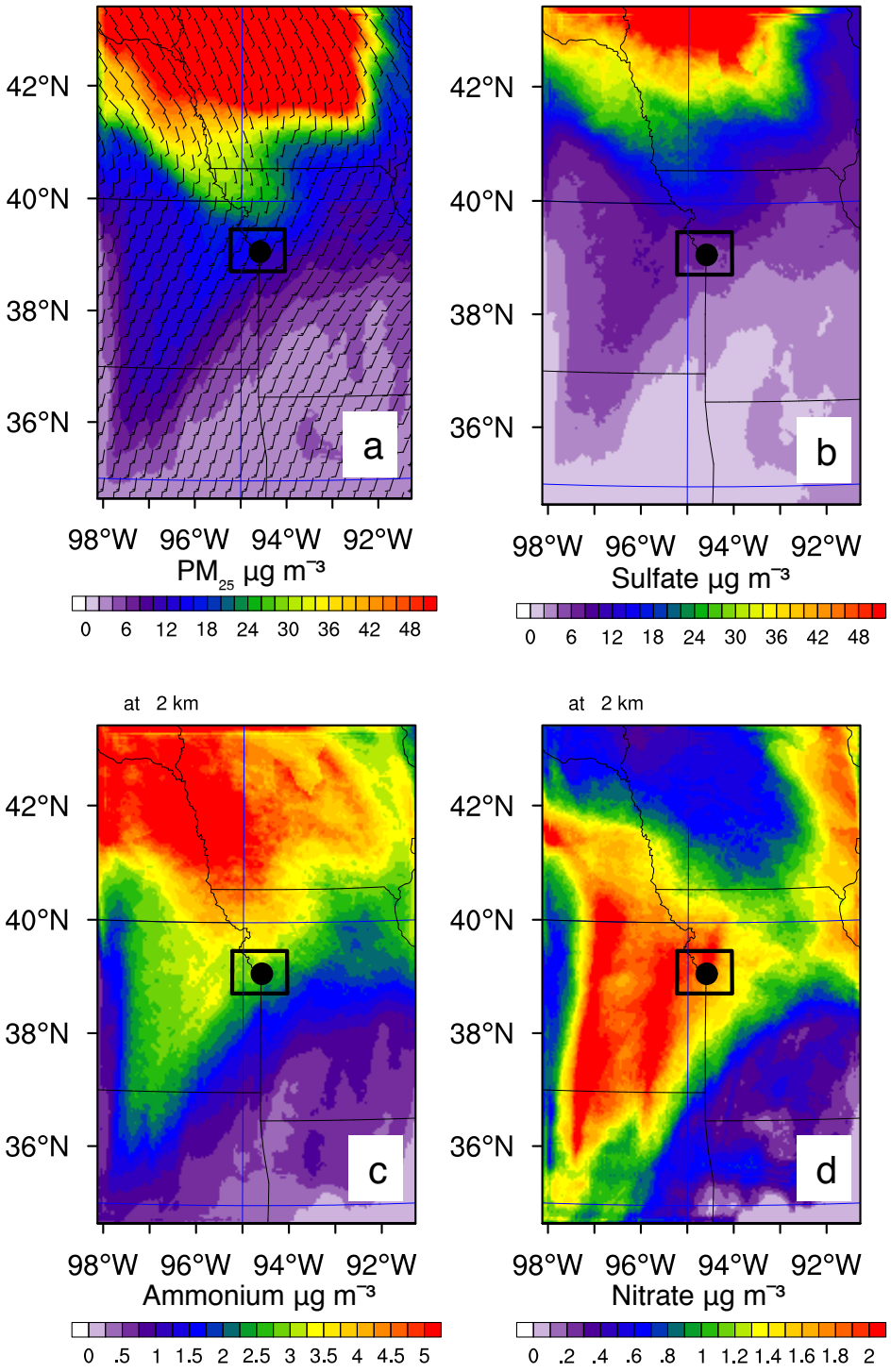

Figure 2.2: BASE case boundary layer (0-2 km), 24 hour averaged a) total PM 2.5 (µg m^{-3}), b) sulfate aerosol (µg m^{-3}) c) ammonium aerosol (µg m^{-3}), and d) nitrate aerosol (µg m^{-3}). The black box denotes the region where emissions scaling occurs in the 2X and HALF ensembles.

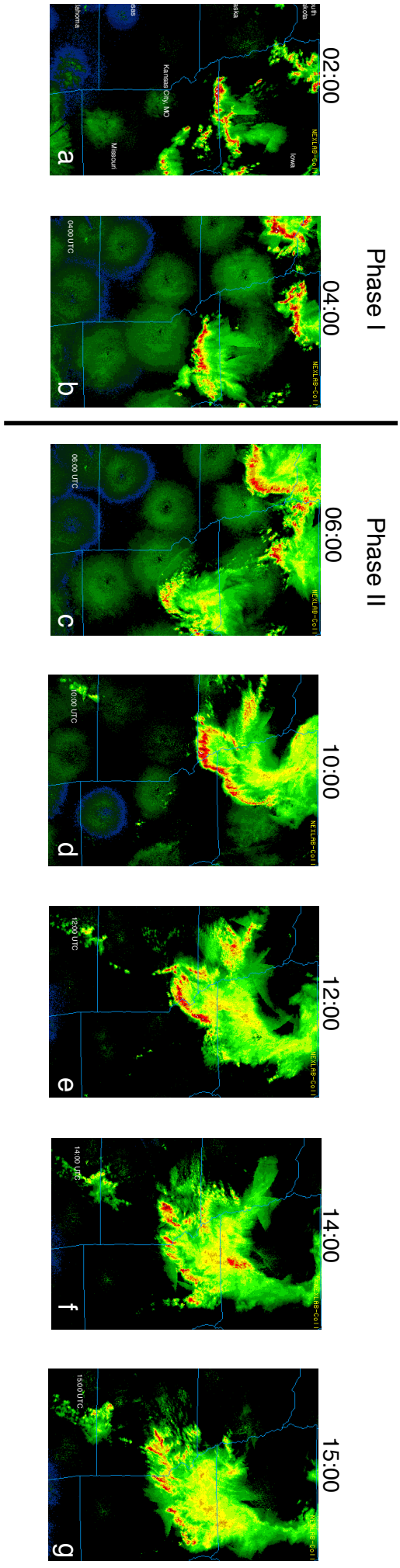

Figure 2.3: Observed radar reflectivity (dBz) over the Central Great Plains on May 27, 02:00 – 15:00 UTC. Retrieved from http://www2.mmm.ucar.edu/imagearchive/.

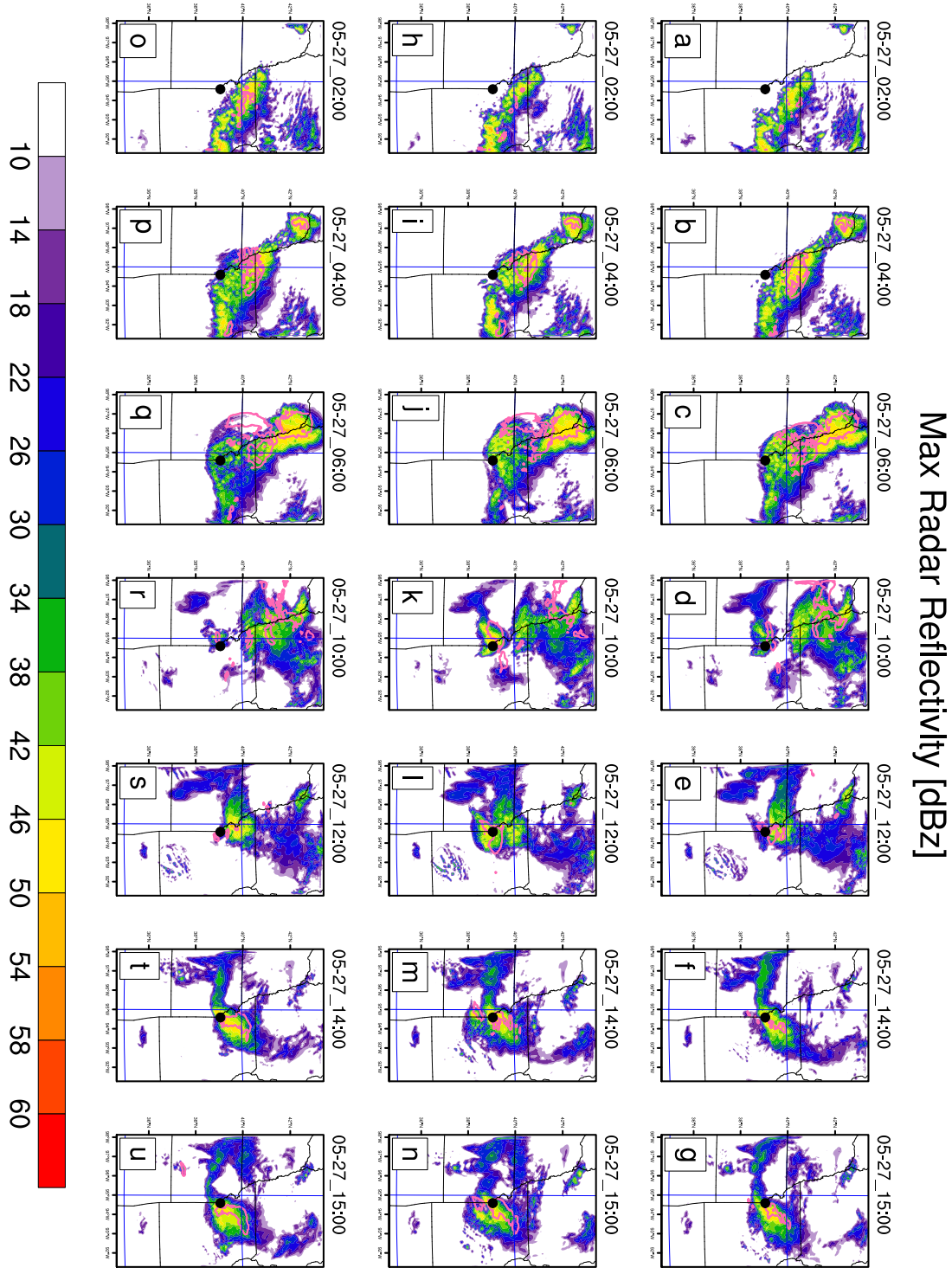

Figure 2.4: Simulated radar reflectivity (dBz) at selected time intervals over the duration of the simulation for the (a-g) BASE case,ensemble average (h-n) 2X case ensemble average, and (o-u) HALF case ensemble average. Time intervals based on convective events discussed in the text. Phase I (May 26 18:00 UTC – May 27 06:00 UTC) and Phase II (May 27 06:00 UTC – May 27

18:00 UTC) are delineated. Kansas City, MO is shown with a black marker. The pink line is the 12 m s^{-1}, 10-meter maximum wind speed contour.

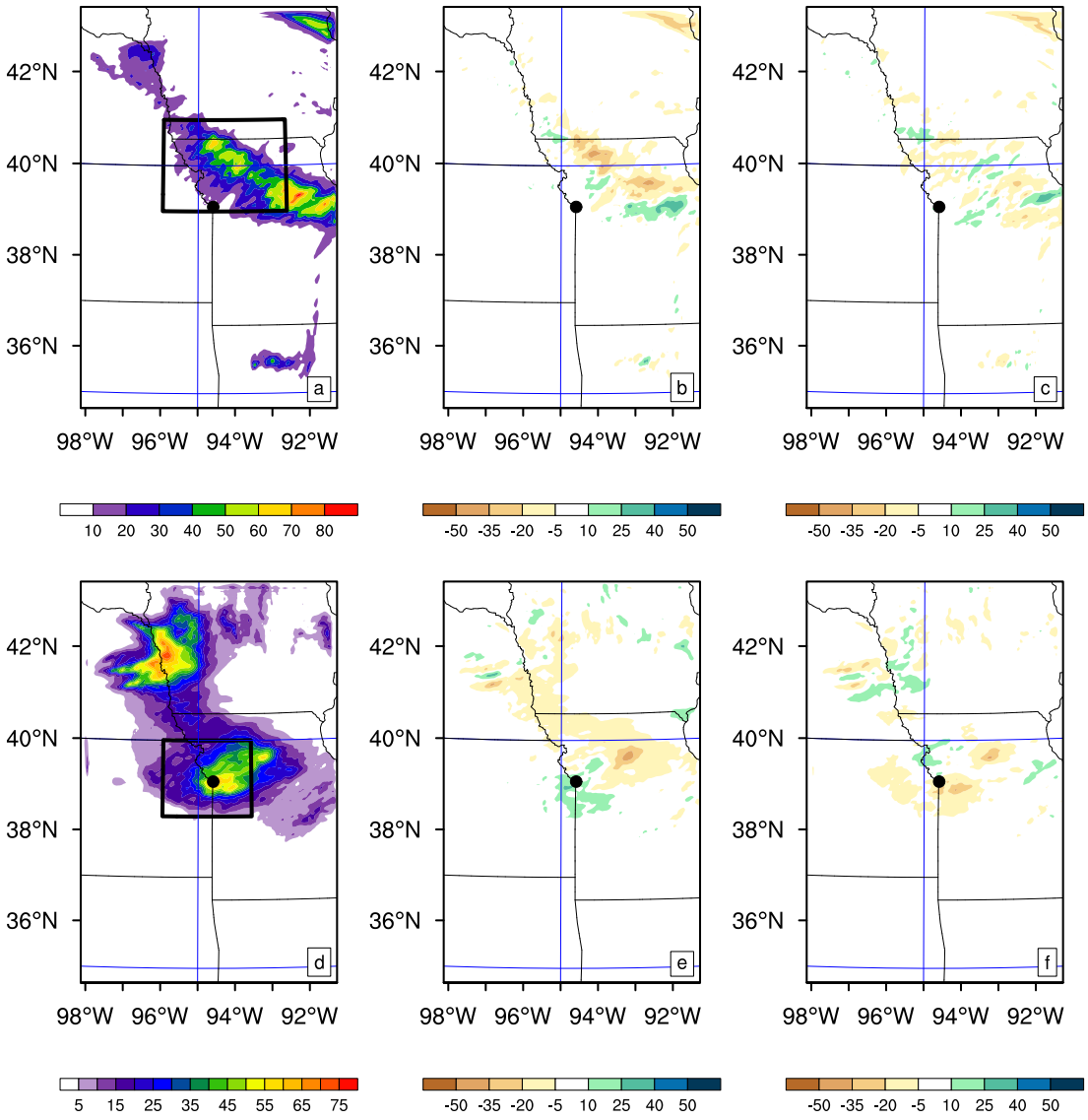

Figure 2.5: a) BASE case ensemble average accumulated precipitation (mm) over Phase I of the simulation (May 26 18:00 UTC – May 27 06:00 UTC), b) Phase I ensemble average 2X – BASE accumulated precipitation (mm), c) Phase I ensemble average HALF – BASE accumulated precipitation (mm). d) BASE case ensemble average accumulated precipitation (mm) over Phase II of the simulation (May 27 06:00 UTC – May 27 18:00 UTC), e) Phase II ensemble average 2X – BASE accumulated precipitation (mm), f) Phase II ensemble average HALF – BASE accumulated precipitation (mm). For difference plots, orange shades indicate a decrease in

precipitation due to the emissions change; blue shades indicate an increase in precipitation due to the emissions change. The black box in panel a indicates the averaging region used for a time series analysis of hydrometeors in Figure 2.7. The black box in panel d indicates the averaging region used for a time series analysis of hydrometeors in Figure 2.9.

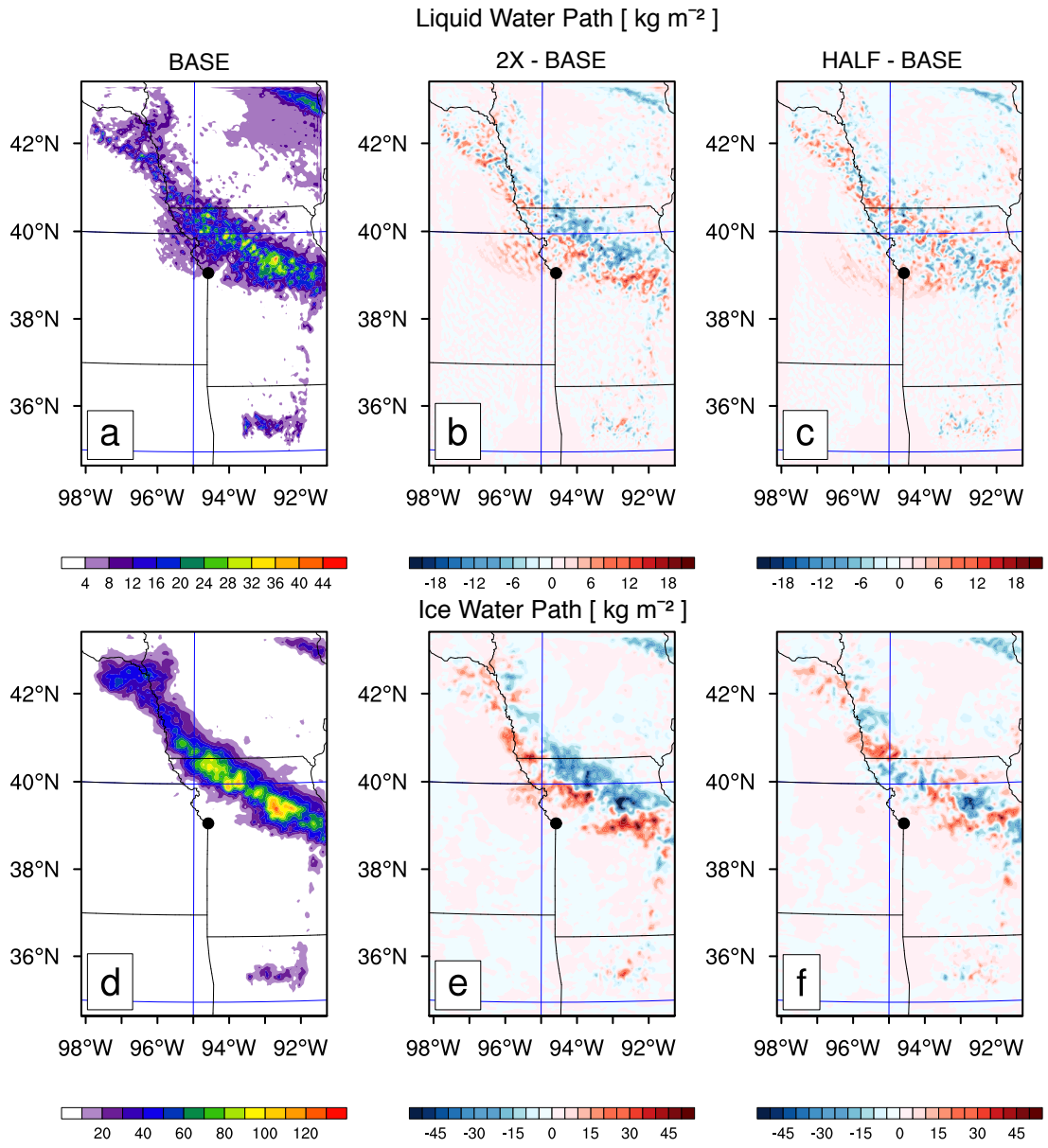

Figure 2.6: Phase I (May 26 18:00 – May 27 06:00 UTC) ensemble average temporally integrated (a,b,c) liquid and (d,e,f) ice water paths. a) BASE case LWP. b) 2X – BASE LWP. c) HALF – BASE LWP. d) BASE case IWP. e) 2X – BASE IWP. f) HALF – BASE IWP. For difference plots, red shades indicate an increase in LWP and IWP due to the emissions change; blue shades indicate a decrease in LWP and IWP due to the emissions change. The black dot indicates the location of Kansas City, MO.

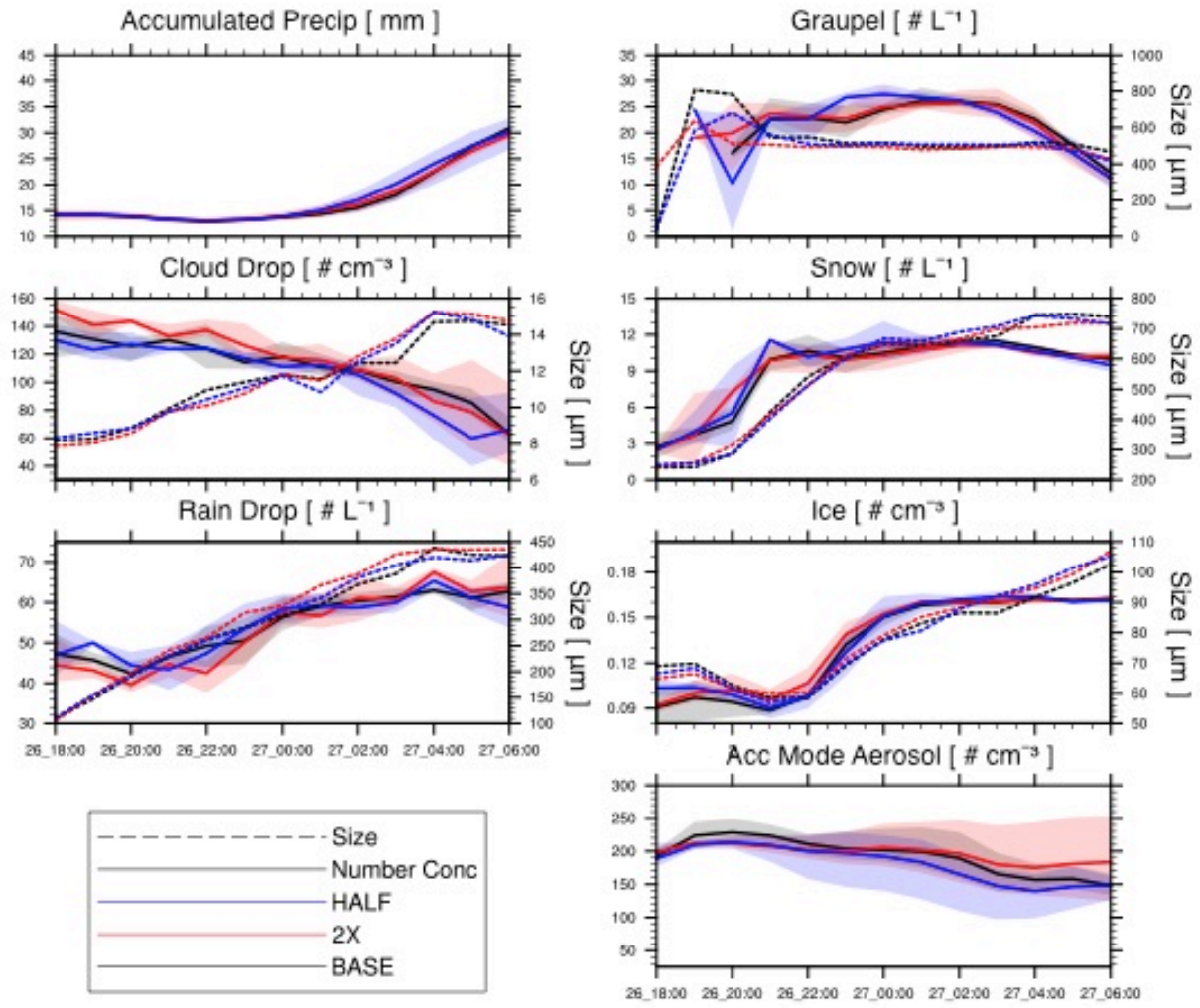

Figure 2.7: Phase I time series of spatially and vertically integrated hydrometeor number concentrations (solid lines, left Y-axes) and time series for the spatially and vertically averaged hydrometeor effective radius (dashed lines, right Y-axes; µm) for the BASE (black), 2X (red), and HALF (blue) cases. a) Accumulated precipitation (mm), b) Cloud drop number concentration (# cm-^{3}) and size c) Raindrop number concentration (# L^{-1}) and size. d) Graupel number concentration (# L^{-1}) and size. e) Snow number concentration (# L^{-1}) and size. f) Ice number concentration (# cm$^{-3)}$ and size. f) Accumulation mode interstitial aerosol number concentration (# cm^{-3}). Shading indicates minimum/maximum of ensemble members.

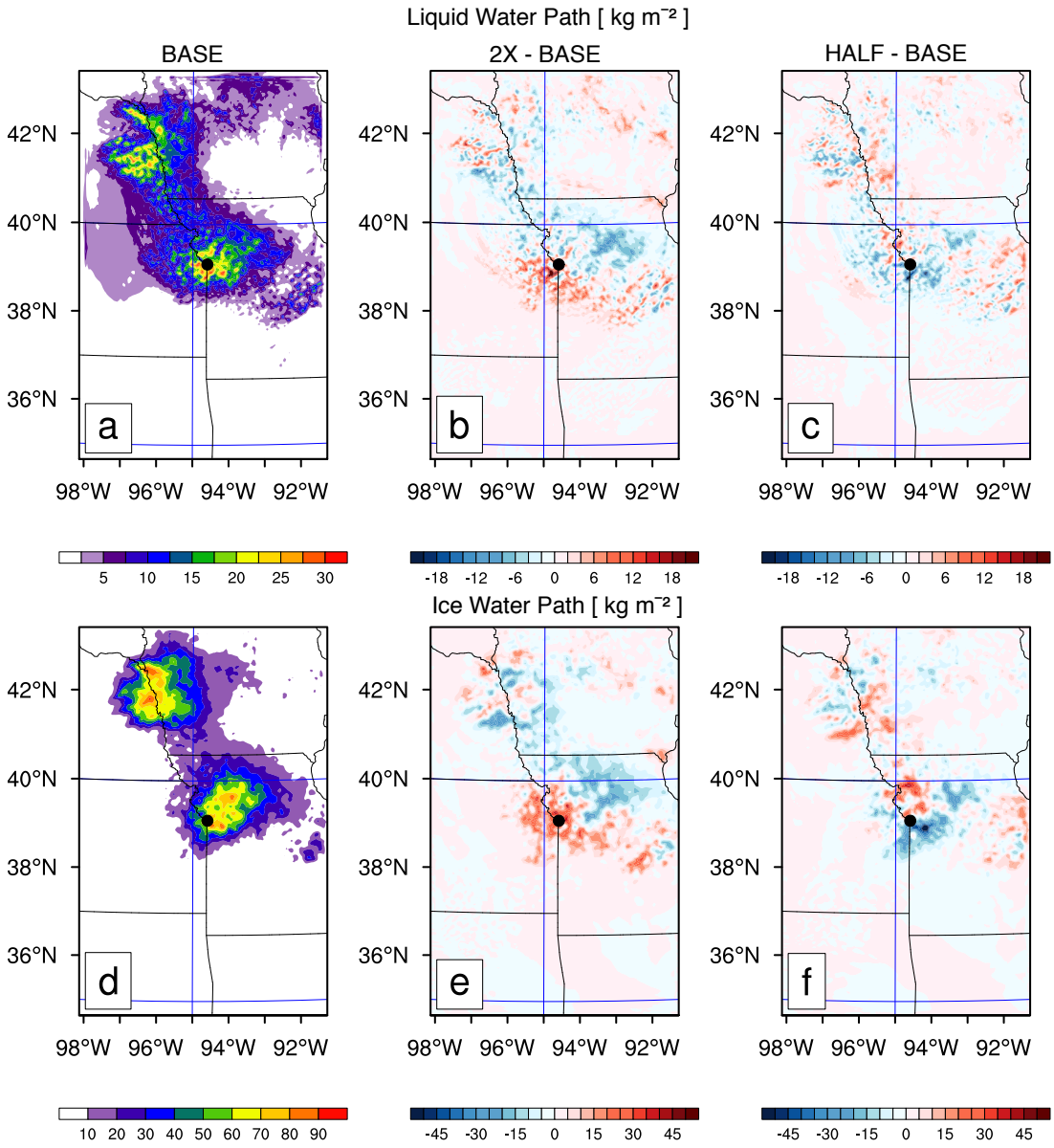

Figure 2.8: Same as Figure 6, but for Phase II (May 27 06:00 - 18:00 UTC).

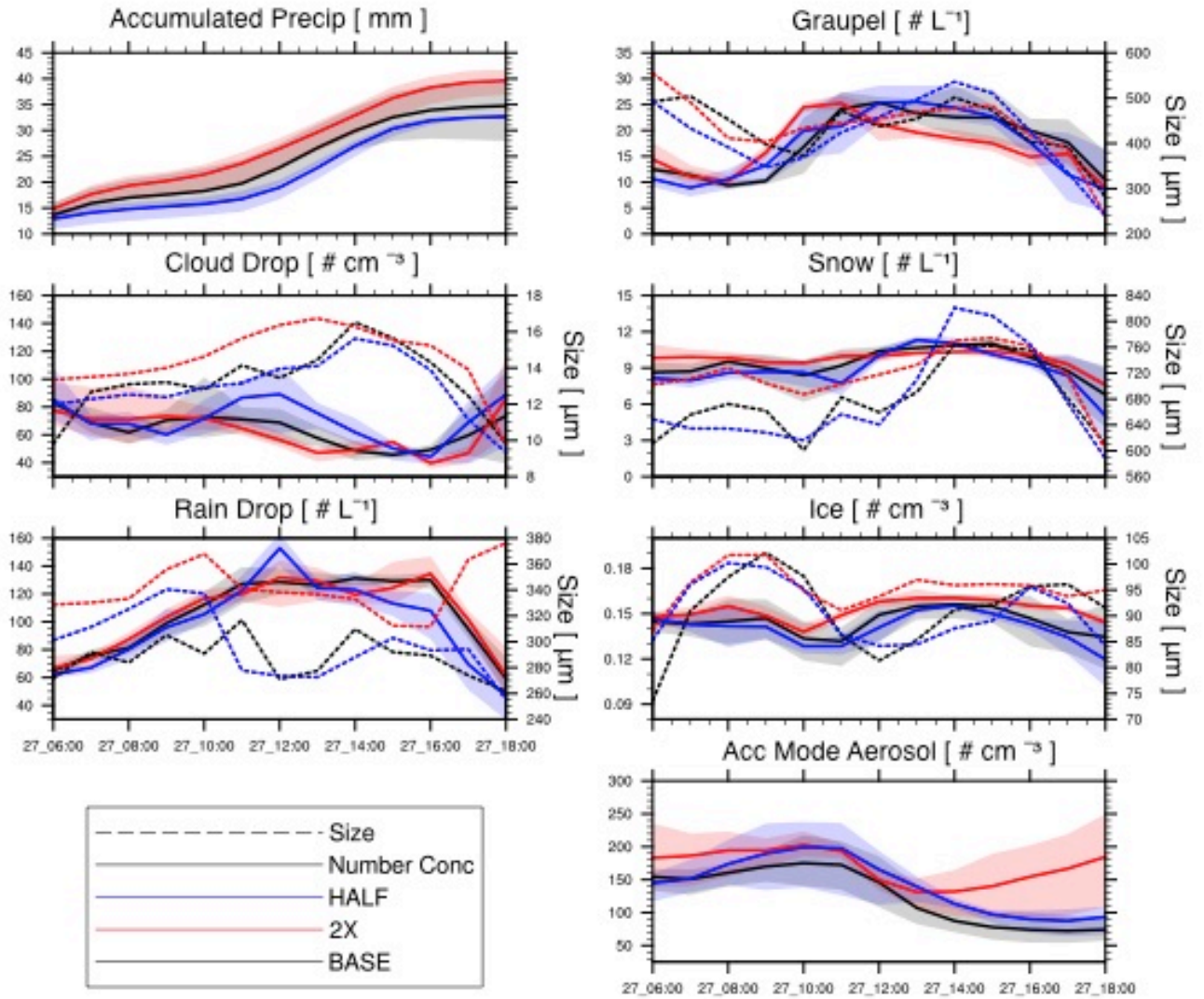

Figure 2.9: Same as Figure 7, but for Phase II (May 27 06:00 – 18:00 UTC).

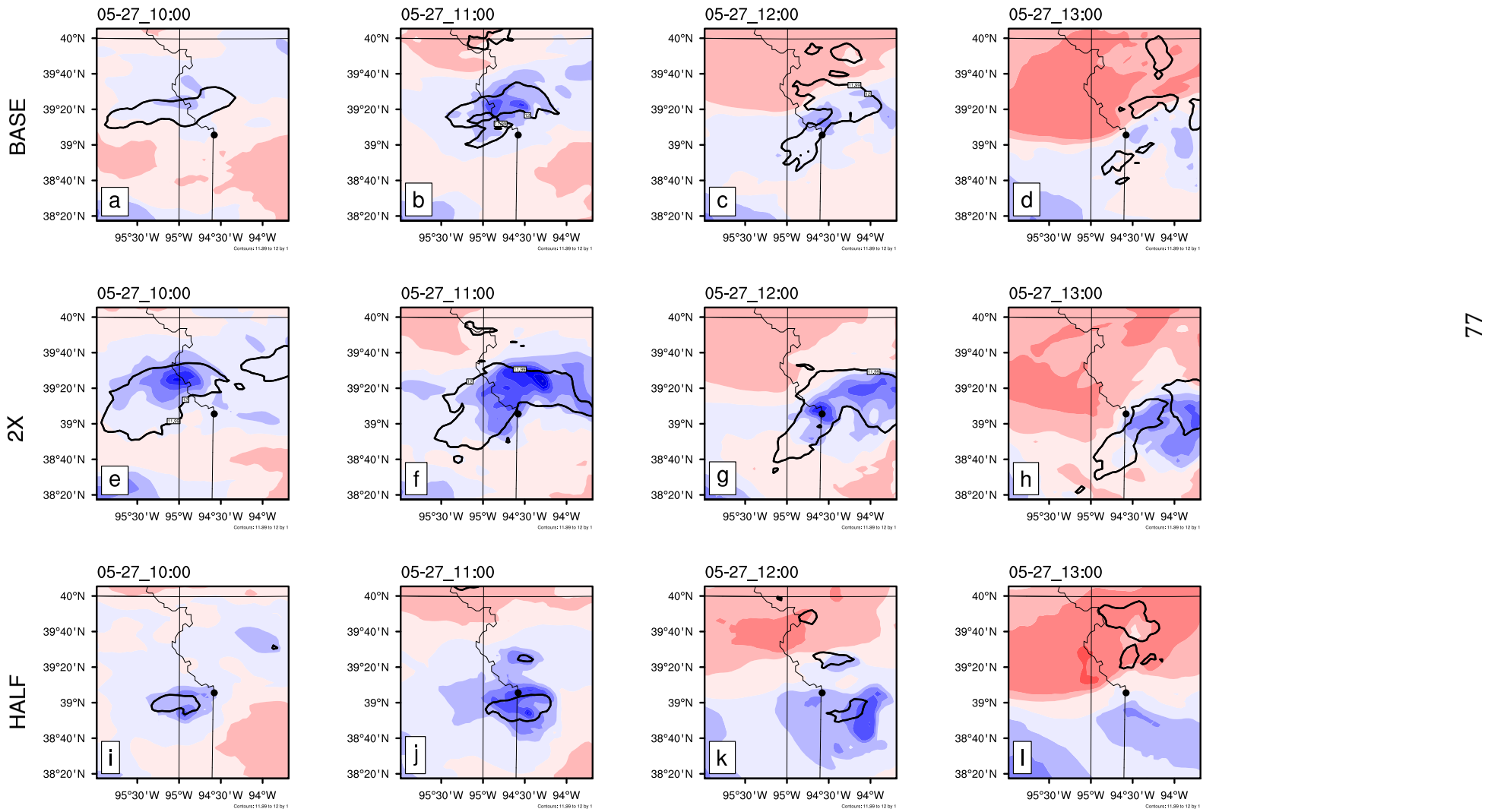
BASE
2X
HALF
05-27_10:00
05-27_11:00
05-27_12:00
05-27_13:00
a
b
c
d
e
f
g
h
i
j
k
l
40°N
39°40'N
39°20'N
39°N
38°40'N
38°20'N
95°30'W 95°W 94°30'W 94°W
-10 -9 -8 -7 -6 -5 -4 -3 -2 -1 0 1 2 3 4 5 6 7 8 9 10

Figure 2.10: 10- meter maximum wind speed (12 m s^{-1} contour; solid black line) and the lowest level perturbation temperature (K; blue (negative) and red (positive) contours) for BASE case (a-d), 2X case (e-h), and HALF case (i-l). The black dots indicate the location of Kansas City, MO.

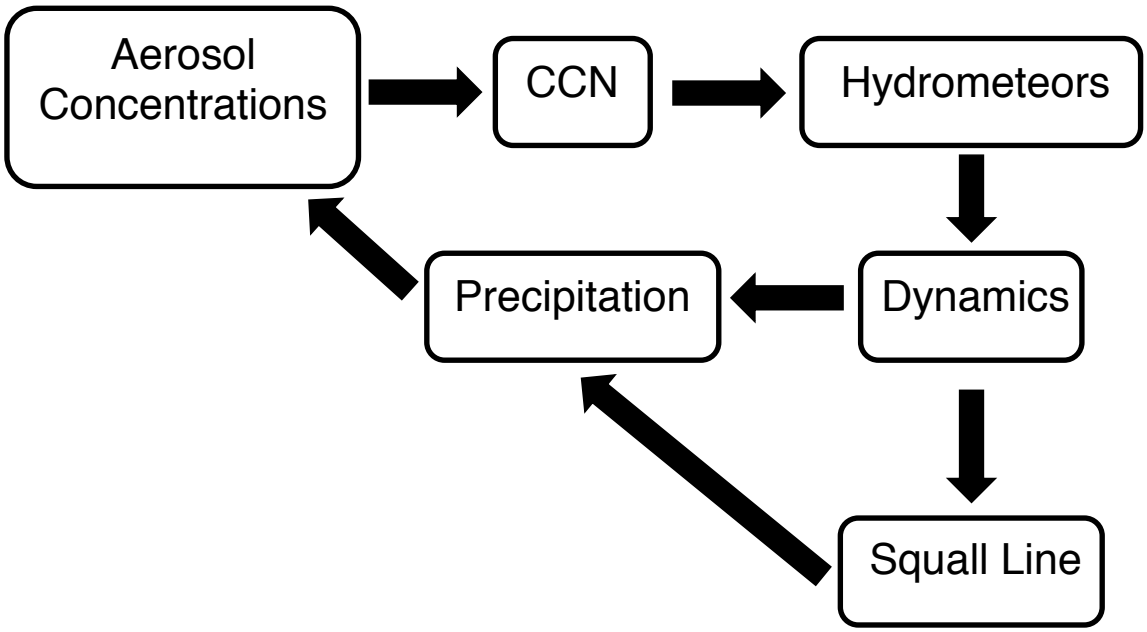

Figure 2.11: Schematic that describes the processes affected by changing urban emissions. Aerosol concentrations are directly affected by scaling urban emissions, which lead to changes in the number of CCN available and the growth and formation of hydrometeors. The growth and formation of hydrometeors affects the dynamics of the squall line via potential vorticity changes. The differences in the squall line propagation ultimately lead to a different precipitation spatial pattern and altered aerosol concentrations.

Chapter III

The influence of aerosol hygroscopicity on precipitation intensity during a mesoscale convective event

Stacey Kawecki, Department of Climate and Space Sciences and Engineering, University of Michigan, Ann Arbor, MI 48109

Allison L. Steiner, Department of Climate and Space Sciences and Engineering, University of Michigan, Ann Arbor, MI 48109

3.0 Abstract

We examine how aerosol composition affects precipitation intensity using the Weather and Research Forecasting Model with Chemistry (version 3.6). By changing the prescribed default hygroscopicity values to updated values from laboratory studies, we test model assumptions about individual component hygroscopicity values of ammonium, sulfate, nitrate, and organic species. We conduct five sensitivity simulations (BASE, using default hygroscopicity values; SULF, increasing the sulfate hygroscopicity; ORG, decreasing organic hygroscopicity; SWITCH, using a concentration-dependent hygroscopicity value for ammonium; and ALL, including all three changes) to understand the role of aerosol composition on precipitation during a mesoscale convective event. Changing the individual component

hygroscopicities leads to small bulk hygroscopicity changes excepting the ORG simulation, which shows a substantial decrease to lower hygroscopicity. Reducing bulk hygroscopicity (e.g., ORG simulation) causes fewer and larger cloud drops, which leads to increased precipitation due to enhanced collision and coalescence with larger raindrops. Increasing bulk hygroscopicity (e.g., SULF, SWITCH simulations) simulates more numerous and smaller cloud drops, which also leads to increased precipitation due to convective invigoration. In the ALL simulation, the changes in hygroscopicity lead to quicker rain out of water and early enhancement of precipitation, but later suppression due to less water available for microphysical processes. The combined changes in hygroscopicity (ALL) improve agreement with observed precipitation intensity, by reducing the over-prediction of intense events (>70 mm d^{-1}) and better capturing the range of moderate intensity (30-60 mm d^{-1}) events. This suggests that aerosol composition can play an important role in the simulation of high-intensity precipitation events.

3.1 Introduction

Atmospheric aerosols can affect clouds, weather and climate, yet their influence on cloud processes at varying spatial and temporal scales is highly uncertain (Stevens and Feingold 2009; Boucher et al. 2013; Fan et al. 2016). From the climate perspective, aerosols can alter the optical properties of the cloud (known as the first indirect effect; (Twomey 1977)) or change precipitation processes (known as the second indirect effect; (Albrecht 1989)). On shorter timescales, such as those governing deep convective clouds and severe weather, studies suggest that aerosols can affect weather events (Andreae et al. 2004; Tao et al. 2012; Saide et al. 2015). Within the meteorology community, it is widely accepted that cloud condensation nuclei (CCN) number and size distribution are dominant in determining aerosol indirect effects (Khain et al. 2000; Dusek et al. 2006). However, the chemical composition of aerosols also influences its

ability to act as CCN (Ekman et al. 2004; Fan et al. 2007). Specifically, some aerosol components are known to be extremely effective CCN (e.g., ammonium sulfate; (Easter and Hobbs 1974)), ice nuclei (IN; e.g., mineral dust; (DeMott et al. 2003)) or light absorbers (elemental carbon, soot, (Andreae and Gelencsér 2006)). While aerosol composition is studied in detail within the atmospheric chemistry community, composition effects are not traditionally included in meteorology models because of limited computing capabilities and the prioritization of efficiently representing microphysical processes (Ghan and Schwartz 2007; Khain et al. 2015). In many studies, CCN fields are prescribed using a fixed chemical composition of ammonium sulfate (Van den Heever et al. 2006; Carrió et al. 2010). In this manuscript, we examine the sensitivity of the simulation of a severe weather event to the representation of chemical composition of aerosols, with the goal to test the mechanistic understanding of the role of aerosol composition on mesoscale convective weather events.

Because of the favorable synoptic conditions, the United States Central Great Plains (CGP) frequently experiences convective weather in the form of mesocscale convective systems (MCSs). MCSs are defined as a complex of thunderstorms that organize on a scale larger than individual thunderstorms, persist for several hours or more, and develop a mesoscale circulation. MCSs have precipitation resulting from both convective and stratiform clouds and contribute to the formation of cirrus anvil clouds, making them radiatively relevant (Houze 2004; Fan et al. 2012). Additionally, MCSs are important because they produce intense precipitation that can damage crops and property as well as cause human injuries and fatalities. For example, from 1980 to 2011, severe local storms in the United States contributed to 94.6 billion dollars in damage (Smith and Katz 2013). Therefore it is imperative to understand the atmospheric processes that drive these systems. Within these thunderstorms, unstable air rises and cloud

drops form as the parcel of air reaches the lifted condensation level (LCL), releasing latent heat. This release of latent heat contributes to the instability of the air parcel, increasing the parcel's buoyancy and leading to stronger updraft velocities. Stronger updraft velocities enable greater vertical development, often reaching temperatures well below freezing, while the process of collision and coalescence aids in the formation of raindrops. Solid hydrometeors form during this transition into the mid and upper levels of the troposphere, including graupel (and/or hail), snow, and ice crystals (Dudhia 1996).

Aerosols play a complex role in deep convective clouds that constitute MCSs (Fan et al. 2016) because water may exist in all three phases, requiring an understanding of both warm and cold clouds. In warm, shallow, and precipitating clouds, increasing the number of hygroscopic aerosols increases the number of available cloud condensation nuclei (CCN), leading to smaller droplets and reduced precipitation rates (Rosenfeld 2000; Rosenfeld et al. 2008; Fan et al. 2013; Rosenfeld et al. 2014). These smaller droplets have been hypothesized to invigorate convection within deep convective systems as they can be lofted to higher altitudes, cause more mass to freeze, and release latent heat that further feeds the updraft (Van den Heever et al. 2006; van den Heever and Cotton 2007; Lebo and Seinfeld 2011). Further, changes in aerosol concentrations have been shown to affect the macrophysical properties of cloud systems and the subsequent precipitation patterns (Ntelekos et al. 2009; Cerully et al. 2015; Kawecki et al. 2016). In cold clouds, aerosols affect ice nucleation rates through heterogeneous freezing processes (e.g., immersion freezing, contact freezing). In mixed phase clouds, the interaction between warm and cold phases are important as ice crystals (snow) can grow at the expense of liquid water (cloud drops) as a result of the Wegener-Bergeron-Findeisen (WBF) process and influence cloud microphysical processes (Storelvmo and Tan 2015).

In warm clouds, aerosol activation as CCN is the first step in cloud and precipitation processes and is determined by several factors: the environmental supersaturation, the size of the aerosol, and the aerosol's composition (Köhler 1936). Aerosol hygroscopicity, a metric that describes the rate of water vapor uptake by an aerosol, can be measured in the laboratory and is determined by chemical speciation and dry diameter size. Petters and Kreidenweis (2007) developed the "kappa" parameterization that uses aerosol hygroscopicity, dry diameter and the environmental supersaturation to determine whether or not aerosols will activate. This type of parameterization has been implemented into meteorology-chemistry models such as the Regional Atmospheric Modeling System (RAMS; (Pielke et al. 1992)) and Weather and Research Forecasting Model with Chemistry (WRF-Chem; (Grell et al. 2005)). Because WRF-Chem has been shown to accurately simulate meteorological and chemical processes of aerosols, (Ward and Cotton 2011) used WRF-Chem simulations to provide cloud droplet number concentration and speciated aerosol information to RAMS simulations. Using the kappa parameterization, they evaluated differences between the hygroscopicity in the default WRF-Chem and those from lab-derived studies and found that organic hygroscopicities were overestimated and most inorganic species were underestimated with the default WRF-Chem parameterization. While this work evaluated the changes in hygroscopicity with the use of model-specified defaults, they did not evaluate the impact of these changes on meteorological processes and if these processes are sensitive to the spatial heterogeneity of aerosol mass and composition.

Several studies have investigated how aerosol composition can affect short-term weather on several severity scales. Many of these studies have focused on light absorbing carbon from biomass burning events, as emissions are large in magnitude and these aerosols have strong direct (Ackerman et al. 2000), indirect (Wang et al. 2009) and semi-direct effects (Fan et al.

2015). For example, Zhang et al. (2016) found that the presence of biomass burning aerosols can influence the accuracy of numerical weather prediction, where observed 2-meter temperatures are lower than simulated due to reduced surface radiation and altered boundary layer stability. Saide et al. (2015) showed that smoke from biomass burning in Central America increases the probability of tornadoes in the US Central Great Plains by lowering the LCL and affecting low-level wind shear. Other studies of light-absorbing aerosols from anthropogenic sources have been found to modify and even cause extreme precipitation events (Fan et al. 2015).

Here, we explore the role of aerosol hygroscopicity on severe weather events and expand this evaluation beyond light absorbing aerosols. We simulate a mesoscale convective system in the Central United States using the WRF-Chem to determine the sensitivity of precipitation intensity and spatial patterns to aerosol composition. Section 2 describes methods, model parameterizations, and the experimental setup to investigate the role of aerosol hygroscopicity through a series of sensitivity tests that alter the model-prescribed kappa values for sulfate, nitrate, and organic species. In section 3, we discuss the results and Section 4 follows with discussion and conclusions. These sensitivity tests show that accumulated precipitation patterns and the duration and intensity of precipitation are sensitive to the representation of aerosol hygroscopicity within the WRF-Chem model.

3.2.0 Methods

3.2.1 WRF-Chem description

To examine the effects of aerosol hygroscopicity on precipitation intensity during a severe weather event, we use the Weather and Research Forecast Model with online chemistry (WRF-Chem v 3.6; Grell, 2005). We simulate a mesoscale convective system that occurred on May 27, 2013 near Kansas City, MO, described in detail in Kawecki et al. (2016). This system

produced large amounts of rain and severe weather, including hail with diameters equal to or exceeding 1 inch (2.54 cm) and wind gusts exceeding 58 miles per hour (26 m s^{-1}). The model domain is centered on Kansas City, Missouri, a mid-sized city surrounded by agriculture (Figure 3.1). This region allows us to examine interactions of several types of aerosols, including organic aerosols derived from anthropogenic volatile organic compound (VOC) emissions, ammonium nitrate and ammonium sulfate formed as a result of agricultural ammonia emissions interacting with the nitrates and sulfates from urban areas and power generation.

The model is configured with a horizontal grid cell resolution of 4 km and 72 vertical levels. While the 4-km horizontal grid size is borderline for explicitly resolving this type of system, this squall line is driven by synoptic scale meteorology, and has been successfully simulated in previous work. Additionally, we were limited in computational resources. Meteorological boundary conditions are from the NAM-Reanalysis (12 km; (NCEI 2013)) and chemical boundary conditions are provided from MOZART-GEOS4 simulations (Emmons et al. 2010) and updated every 6 hours. We implement the Morrison microphysics parameterization (Morrison et al. 2005), which is a two-moment scheme that tracks five hydrometeors (cloud drop, raindrop, graupel, snow, ice and water vapor). Radiation is parameterized with the RRTMG for both long-wave and shortwave radiation schemes (Price et al. 2014). Boundary layer processes are parameterized using the Yonsei University scheme (Hong et al. 2006), surface layer parameters are resolved using the Monin-Obukhov scheme and the land surface is parameterized with the Noah land surface model (Ek et al. 2003) with the urban canopy model implementation. For chemistry, we use the RADM2 gas phase chemical mechanism (Stockwell et al. 1990) and MADE-SORGAM (Schell et al. 2001) aerosol model. Anthropogenic emissions are from the 2013 United States Environmental Protection Agency (EPA) National Emissions

Inventory (EPA 2011) gridded to the 4km model resolution. Biogenic isoprene emissions follow the MEGAN model (version 2; (Guenther et al. 2006)). Photolysis rates and reactions are calculated using the Fast-J photolysis scheme (Wild et al. 2000). Additional details on the meteorological event evaluation are described in Kawecki et al. (2016).

3.2.2 MADE/SORGAM Aerosol Parameterization

Aerosol size distributions are described by three internally mixed, lognormal modes (Aitken, accumulation and coarse) in the MADE/SORGAM aerosol mechanism (Schell et al. 2001). The Aitken and accumulation modes each have 16 chemical species, including primary un-speciated $PM_{2.5}$ ("p25"), sulfate, ammonium, nitrate, sodium, chlorine, elemental carbon, primary organic aerosol ("orgpa"), and eight categories of secondary organic aerosol (SOA). SOA categories include one from alkanes ("orgalk1"), one from olefins ("orgole1"), two formed from aromatics ("orgaro1" and "orgaro2"), and four from biogenic VOC ("orgba1", "orgba2", "orgba3", "orgba4"). The coarse mode comprises sea salt, soil-derived aerosol, and unspecified primary anthropogenic emissions, characterized as internally mixed continental aerosol.

There are three mechanisms for aerosols to enter one of the aerosol modes: primary emission, secondary formation, and new particle formation from sulfuric acid nucleation based on (Kulmala et al. 1998). Primary emissions include dust, anthropogenic emissions of inorganic and organic $PM_{2.5}$ in the Aitken and accumulation modes, sea salt and biomass burning. We note that in the simulations presented here, we do not include interactive dust (although some anthropogenic dust is emitted from urban areas in the US NEI), sea salt, or biomass burning emissions. Secondary formation of organic aerosol is simulated by the SORGAM mechanism, which allows condensation of organic mass based on estimated product yields (Schell et al. 2001).

The internally mixed aerosol modes are tracked as either clear air particles (interstitial) or cloud-borne (in-cloud) particles. Interstitial aerosols are activated as cloud drops based on the maximum supersaturation determined from a Gaussian spectrum of updraft velocities and internally mixed aerosol properties (i.e. hygroscopicity and density) within each mode (Chapman et al. 2009). These activated aerosols are then traced as "in-cloud" aerosol. Coarse and Aitken modes can become in-cloud aerosol via precipitation scavenging, and in-cloud aerosol can return to interstitial aerosols when cloud drops and raindrops evaporate. Currently, the MADE/SORGAM parameterization as implemented in WRF-Chem does not explicitly include the activation of aerosols as IN.

3.2.3 Hygroscopicity and implementation of the kappa parameterization

In the model configuration used in this study, each aerosol type is assigned a default hygroscopicity value by WRF-Chem (Table 3.1). For every grid cell at each time step, the volume-weighted bulk hygroscopicity is calculated for each of the three modes for interstitial aerosol. These bulk hygroscopicities are then used to activate a portion of the aerosols as CCN (or in-cloud aerosol) depending on the environmental supersaturation (Chapman, 2009). Because the aerosol modes are internally mixed, it is important to understand the hygroscopicities of all chemical species. Within the model domain sub-region downwind of Kansas City (Figure 3.1a), the most abundant aerosols are sulfate, ammonium, and nitrate (Figure 3.1), which are all assigned the same hygroscopicity value (0.5) in the default WRF-Chem (Table 3.1). Organic species have a relatively low hygroscopicity (default of 0.14; Table 1), and elemental carbon is prescribed an extremely low value (1.0×10^{-6}).

Because of the dominance of inorganic species in the region, the interactions between sulfate, nitrate and ammonium are key to determining the overall composition and

hygroscopicity of aerosol. Ammonia is an important neutralizing gas in the atmosphere (Behera et al. 2013), and tends to react quickly with either sulfuric or nitric acid in the atmosphere to form aerosols. Generally the formation of ammonium sulfate is favored, and due to its low vapor pressure, this process is essentially irreversible:

(R1) $NH_3 + H_2SO_4 \rightarrow NH_4HSO_{4s,aq}$

(R2) $2NH_3 + H_2SO_4 \rightarrow (NH_4)_2SO_{4s,aq}$

However, the ratio of ammonium to sulfate is important for determining whether ammonium will form either ammonium sulfate or ammonium nitrate. Values greater than two encourage reaction with nitrates (Ackermann et al. 1998), where ammonium nitrate can be formed via a reversible reaction:

(R3) $NH_3 + HNO_3 <--> NH_4NO_3$

Laboratory studies show that the hygroscopicity of ammonium depends on whether it is partitioned with sulfate or nitrate (Petters and Kreidenweis 2007). However, WRF-Chem default hygroscopicity values are all the same for these three components (Table 1).

Organic aerosol formed by the oxidation of aromatics have lab-derived hygroscopicity values of 0.051 and 0.094 respectively (Petters and Kreidenweis 2007), while aerosol derived from alkanes has a hygroscopicity value of 0.005 (Virkkula et al. 1999; Raymond and Pandis 2002; VanReken et al. 2005; Petters et al. 2009), a full order of magnitude lower than the default. Olefin-derived organic aerosol has been observed to have the highest organic hygroscopicity at 0.19 (Petters and Kreidenweis 2007). The current default settings in WRF-Chem include organics as one category of "organic carbon" with a single hygroscopicity that is applied to all SOA of 0.14, which is not representative of actual values (Ward and Cotton 2011).

The default hygroscopicities representing individual components in the standard version of WRF-Chem have not been explored or tested extensively. As shown above, several of the organics are misrepresented in the model with higher hygroscopicity than observed, while the default hygroscopicity of ammonium sulfate and nitrate are lower than observed and do not account for the partitioning of ammonium. The internal mixtures of the three aerosol modes depend on the spatial heterogeneity of the aerosols and their chemical process, and this internal mixture in turn determines the bulk hygroscopicity and the activating potential of the aerosols. Because the first step in cloud formation is the droplet activation, it is important to test the hygroscopicity assumptions that drive activation and subsequent precipitation processes through sensitivity simulations.

3.2.4: Experimental Design

To test the simulated precipitation duration and intensity sensitivity to aerosol hygroscopicity, we run five 60-hour simulations of a severe weather event on May 27, 2013 near Kansas City, MO. In the first simulation, we use the default hygroscopicity values provided in WRF-Chem (Table 1), hereinafter called the "BASE" case. We then conduct several sensitivity tests to examine the role of individual species' hygroscopicity by systematically changing hygroscopicity values in the MADE/SORGAM data module in WRF-Chem based on the suggested values in Ward and Cotton (2011) (Table 1). In the second simulation (SULF), we increase the sulfate hygroscopicity value from 0.5 to 0.71 (Petters and Kreidenweis 2007). For the third simulation (ORG), we change the values of the SOA formed from anthropogenic precursor VOC to laboratory-tested values (Table 1 for orgalk1, orgaro1, orgaro2, orgole1, orgpa) (Virkkula et al. 1999; VanReken et al. 2005; Petters et al. 2009), which overall reflects a decrease in the hygroscopicity of organic aerosol species. For the fourth simulation (SWITCH),

we incorporate a "switch" for ammonium. If the ratio of ammonium to sulfate is greater than 2.0, ammonia reacts with nitrates to form ammonium nitrate, and we assign ammonium a hygroscopicity of 0.67. If the ratio is less than two, the formation of ammonium sulfate is likely, resulting in the lower hygroscopicity of 0.5. Finally, we conduct a fifth simulation to provide an up-to-date representation of aerosol hygroscopicity from recent laboratory studies and incorporate all of the changes to the hygroscopicity values from Table 1 (ALL). The comparison of these simulations and their effects on a severe weather event is described in Section 3.0 below.

3.2.5 Aerosol Simulation Evaluation

The Central Great Plains simulation domain provides a unique blend of agriculture and industrial emissions (Kawecki et al. 2016). In the continental United States, ammonia emissions are increasing (Butler et al. 2016), while industrial emissions are declining (Hand et al. 2012). Additionally, sulfur dioxide (SO_2) emissions have substantially decreased since 2002 (Hand et al. 2012), reducing concentrations of sulfur dioxide (SO_2) and sulfuric acid (H_2SO_4) across the US. Prior model evaluation suggested that the sulfate concentrations at the model boundaries as provided by the MOZART chemical boundary conditions simulated too much sulfate as compared to ground-based observations (Kawecki et al. 2016), and here we remove incoming sulfate and sulfuric acid at all boundaries to improve our evaluation of simulated sulfate with ground-based observations from IMPROVE (Malm et al. 1994) observational network (Figure 3.1). We note that the IMPROVE site data is the average of May 22 and May 25 2013 samples, while the model data is the boundary layer average of a 3x3 grid cell average 144 km^2 region containing the location of the site from 5-26 06:00 UTC to 5-27 06:00 UTC,

Despite the elimination of model boundary sulfur compounds, the model still shows a positive bias for ammonium sulfate and ammonium nitrate at the two IMPROVE locations

within the model domain (El Dorado Springs, MO; and Lake Seguma, IA; Figure 3.1). At the Lake Seguma site, the modeled ammonium sulfate (2.15 μg m^{-3}) and ammonium nitrate (2.11 μg m^{-3}) are about 1.75 times and 2.85 times greater than observed, which are 1.24 μg $m^{-3}$and 0.74 μg m^{-3} respectively. The observed and modeled organic carbon is similar, with the model slightly lower than the observed value of 0.67 μg m^{-3}.

$PM_{2.5}$ is clearly associated with urban regions (Figure 3.1a), with plume concentrations of 5.5 μg m^{-3} originating from Oklahoma City and Tulsa in the southwestern portion of the domain, and a plume of $PM_{2.5}$ (5.5 μg m^{-3}) extending northward from Kansas City in the center of the domain. In comparison with the IMPROVE sites in the eastern portion of the domain, the model represents the speciated $PM_{2.5}$ fairly well at both locations. At the EDS site southeast of Kansas City, the model simulates similar amounts of ammonium sulfate and organic carbon, with more simulated than observed for ammonium nitrate (0.51 μg m^{-3} simulated versus 0.29 μg m^{-3} observed). The model underrepresents elemental carbon, where the observed is about 0.35 μg m^{-3}, approximately 2.5 times that simulated by the model which may be due to the lack of biomass burning emissions in the model. Though ammonium sulfate and nitrate is over-predicted in the northern portion of the simulations, the rain event that we focus on is to the west and south of this model bias, and will not likely affect the simulation of bulk aerosol hygroscopicity. Generally, the model evaluates well against the limited composition measurements available within the model domain.

3.3.0 Results

We evaluate the changes in precipitation patterns and intensity as simulated by WRF-Chem due to alterations of aerosol hygroscopicity values. We examine how changing the individual hygroscopicity values alters the bulk hygroscopicity in the accumulation mode, and

then demonstrate how these changes in hygroscopicity affect the cloud drop and rain drop number concentrations and sizes. Additionally, we examine the changes to the liquid water path as a result of changing hygroscopicities. Finally, we compare model results to observations of daily-accumulated precipitation from May 27, 2013 (Daymet; (Thornton et al. 2016)) to assess the realism of these sensitivity tests.

3.3.1 Meteorological Description and Precipitation Intensity Frequency

An intense rainfall event occurred near Kansas City, MO on May 27, 2015 (Figure 3.2a) as a mesoscale convective system crossed the region, spawning severe weather with large hail and strong winds. Previous work has shown the model represents this event by matching the placement and timing of the storm cells (Kawecki et al. 2016). Figure 3.2a shows the accumulated precipitation over the 24 hour period, reaching up to 100 mm in the region to the south of the city and extending eastward along the storm track. The four additional simulations with altered hygroscopicity (Figures 3.2b-e) show a similar pattern to the BASE simulation with a swath of precipitation starting at the junction of the Platt and Missouri Rivers and continuing southeast. However, the regions receiving the most precipitation differ between simulations. For example, in the SULF simulation, the maximum precipitation occurs to the east of Kansas City (Figure 3.2b), with high values (> 100 mm) covering a greater spatial extent than the BASE simulation. Another notable feature in the SULF case is the reduction of precipitation in the urban area of Kansas City, indicating that the increase in sulfate hygroscopicity is suppressing precipitation close to the high urban emissions. The ORG simulation, which overall reduced the hygroscopicity of organic aerosols, connects the Kansas City local precipitation maximum to regions of higher precipitation to the east (Figure 3.2c) with precipitation amounts exceeding 100 mm. In the SWITCH simulation, we allow for different hygroscopicity values of ammonium depending on the partitioning, and this simulation shows the greatest change from the BASE

simulation with greater precipitation accumulation (Figure 3.2d). The region with values exceeding 100 mm is to the north and east of Kansas City and is larger and more contiguous than in the other simulations. Finally, the ALL (Figure 3.2e) simulation, which incorporates all updated hygroscopicity changes, most resembles the BASE simulation with respect to both precipitation amounts and spatial patterns, suggesting that these sum total change between the default values and the lab-derived values may balance each other to provide a spatially similar result with slightly lower total precipitation.

Rainfall intensity is a measure of the amount of rain (depth, mm) that falls over a given amount of time (hour). While rainfall intensity does not determine whether a storm is classified as a severe threat or not, flooding and flash flooding are imminent dangers associated with high-intensity rainfall events. According to the American Meteorological Society (AMS), heavy rain accrues at a rate of more than 8 mm $hour^{-1}$. To examine how often heavy or high-intensity rainfall (HIR) occurs, we count the number of times each grid cell has greater than 10 mm $hour^{-1}$ during the final 24 hours of the simulations (Figure 3.2f-j). In the BASE simulation, there are two main regions where HIR occurs: (1) in the northwestern quadrant of the domain (40.5 - 41.0°N and 95.0-97.0°W), and (2) in the eastern portion of the domain around 39.5°N extending from Kansas City to the east. Like the accumulated precipitation, all four sensitivity simulations show a similar spatial pattern of HIR occurring along the storm track that moved from the northwest corner of the domain to the southeast. Generally, the largest HIR values occur concurrently with the largest values of accumulated precipitation. In the BASE case, there are only a few grid cells that have HIR exceeding 4 hours (Figure 3.2f). The SULF HIR overall pattern matches the BASE case, with more grid cells simulating higher HIR values especially on the southeastern edge of the system (Figure 3.2g). In the ORG simulation, the southeastern

portion of the rain event looks similar to the SULF simulation with reduced HIR. When including the switch for ammonium nitrate, the region east of Kansas City has maxima exceeding 8 hours of HIR (Figure 3.2i), which coincides with the large amounts of accumulated precipitation in this region (Figure 3.2d). Similar to precipitation accumulation, the ALL simulation HIR is similar to the BASE simulation, with the same pattern and magnitude of HIR (Figure 3.2j) (Figure 3.2e).

3.3.2 Changes in Aerosol Hygroscopicity and Microphysics

The region east of Kansas City shows the greatest differences between the BASE simulations and the hygroscopicity sensitivity simulations (red box; Figure 3.2a). Because of these differences, we investigate the hygroscopicity and microphysics before and during the intense rain event in this region. To understand how changes in simulated hygroscopicity can affect precipitation processes, we analyze two time periods: before the storm [0600 – 2300 UTC, 5-26-2013] and during the storm [0000 – 1800 UTC 5-27-2013]. The chemical composition of the aerosols east of Kansas City (Figure 3.1d) is well balanced between ammonium nitrate, ammonium sulfate and organics. Nitrates and sulfates dominate the mixture with averages of 1.7μg m^{-3} and 1.65, respectively, while the organics make up most of the remaining fraction (1.0 μg m^{-3}).

3.3.2.1 Before Intense Rain Event [0600 –2300 UTC, 5-26-2013]

Because most of aerosol will activate as cloud drops in the accumulation mode, we examine the accumulation mode bulk hygroscopicity. To understand the overall change in the simulated hygroscopicity, we show probability distribution functions (PDF) for each simulation that include all grid points within the highlighted box (Figure 3.2a) and all times from 0600 –

2300 UTC 5-26-2013, excluding grid cells with hygroscopicity values less than 0.001 (Figure 3.3). We define the "bulk hygroscopicity" as the volume-weighted average hygroscopicity of the internally mixed mode. In the BASE simulation, accumulation mode bulk hygroscopicity peaks at 0.165. Generally, the changes in the SWITCH and ALL case were not large enough to affect the bulk hygroscopicity and as a result the distribution is similar to the BASE simulation. While SULF has a slightly higher probability peak at 0.165 compared to the BASE case, the change is small. In contrast, the ORG simulation shows a shift towards lower hygroscopicity, with a probability peak at 0.10 and an increase in the probability of larger hygroscopicities (e.g., >0.35). Overall, this shows that the BASE, SULF, SWITCH, and ALL simulations have a higher probability of having a greater hygroscopicity than the ORG simulation. While organic aerosols are less abundant than the inorganic counterparts, implementing the lab-derived hygroscopicity values has a considerable effect in the pre-rain event accumulation mode bulk hygroscopicity (Figure 3.3a).

To understand how these changes in hygroscopicity affect precipitation processes we examine how number concentrations of cloud drops and raindrops are affected by these systematic changes in bulk hygroscopicity. Cloud drop number concentration (# cm^{-3}, Figure 3.3b) PDFs are calculated for every grid cell and time point within the selected box (Figure 3.2a) during the pre-rain event hours, excluding grid cells with less than 1 cloud drop cm^{-3}. Before the rain event, changes between simulations are small. Of note, however, is that the SULF simulation has higher probabilities of larger drop concentrations, correlating with the higher probability of smaller drop size (Figure 3d). Raindrop number concentration PDFs (# L^{-1}, Figure 3.3c) are calculated in the same manner but excluding grid cells with less than 0.1 raindrop L^{-1}. Changes in the raindrop PDFs become most evident for concentrations larger than 60 raindrops

L^{-1}, where the SWITCH and ALL simulations are most likely to have the greatest concentrations and the SULF and ORG simulations the lowest concentrations. The raindrop size PDF (Figure 3.3e) indicates that the BASE simulation would have the smallest probability of having rain drops of any size, except drops smaller than 40 microns. The other simulations are all similar in size probabilities. Overall, accounting only for the lab-derived organic aerosol hygroscopicity values leads to the largest changes in bulk hygroscopicity, shifting the peak probability to lower values. This shift has a larger effect on cloud and raindrop size than it does on number concentrations.

3.3.2.2 During Intense Rain Event [0000 –1800 UTC, 5-27-2013]

During the time period that encompasses the intense rain event (0000 – 1800 UTC 5-27-2013), the accumulation mode bulk hygroscopicity PDF is similar to that before the rain event (Figure 3.4a). However, differences between the BASE, SULF, ALL, and SWITCH simulations are more easily discerned. The BASE and SULF both have a peak probability (~30%) at 0.165 hygroscopicity, and the SWITCH and ALL simulations also peak at the same value with slightly lower probabilities. As hygroscopicity increases, the SULF and SWITCH simulations have a higher probability for greater hygroscopicity values, especially from 0.30 – 0.37. Within this range, both the SULF and SWITCH simulations have higher hygroscopicities than the BASE, ORG, and ALL simulations. Unsurprisingly, the ORG simulation has consistently the lowest hygroscopicity values.

These slight changes in hygroscopicity lead to more discernable microphysical changes than before the event. The BASE and ORG simulation cloud drop number concentration (# cm^{-3}, Figure 3.4b) have the highest probability (~13%) at less than 14 drops cm^{-3}, with decreasing probability as cloud drop number increases. While this pattern is the same for all simulations,

there are some notable differences. The SULF and SWITCH simulations are the least likely to have lower number concentrations (< 30 cm^{-3}) while the SULF simulation is the most likely to have higher number concentrations (> 35 cm^{-3}). The SWITCH simulation has the lowest probabilities from 10-40 cm^{-3} and the second lowest probability greater than 40-85 cm^{-3}, while the ALL simulation has the lowest probability in this range. The ORG simulation closely follows the BASE simulation.

These number concentrations translate to differently sized cloud drops (Figure 3.4d). All simulations have a peak probability at 10.5 microns followed by decreasing probability with increasing size, as in the cloud drop number concentrations. In the smallest range (5-12 microns), the BASE and SULF simulations are similar and exhibit the highest probabilities of these small radii. The ALL simulation is the least likely to have the smallest radii, while the SWITCH and ORG simulations fall between the two extremes. For cloud drops in the 14 – 21 micron range, the SULF simulation decreases in probability at the fastest rate, while the other simulations' probabilities decrease at a slower rate, with the ALL simulation probabilities decreasing at the slowest rate. Overall, the SWITCH and ALL simulations have the lowest probabilities in this size range but this changes at larger drop sizes. At 22 microns, the SWITCH simulation probability begins to increase with increasing size until 28 microns while all other simulations continue to decrease in probability. The SULF simulation is the least likely to have large drops (> 22 microns), the ORG, SWITCH, and ALL simulations are more likely to have large drops while the BASE simulation falls in between the sensitivity simulations.

The changes in cloud drop size and number concentrations lead to changes in the raindrop size and number concentrations. The probability of raindrop number concentrations less than 20 L^{-1} is similar for the BASE, SULF, and ORG simulations, (7.74%, 7.66%, and

7.44% respectively) and lower for both the SWITCH (6.73%) and ALL (6.26%) simulations (Figure 3.4c). As concentrations increase from 20 – 40 L^{-1}, this pattern remains the same. Once concentrations reach 53 raindrops L^{-1}, the ALL and BASE simulations become very similar, reflecting the similarity between the accumulated precipitation patterns (Figure 3.2a,e). The ORG simulation overall has the highest probability of having greater concentrations ranging from 60 – 80 raindrops L^{-1}, and above 80 raindrops L^{-1}, the SWITCH simulation has the highest probability of the greatest concentrations, followed by the ORG simulation, and the SULF aligns more closely with the BASE and ALL simulations. Changes to cloud and raindrop number concentration PDFs lead to changes in raindrop size PDFs. All simulations have a peak probability at raindrop effective radius of 47.5 microns (Figure 3.4e), monotonically decreasing in probability with increasing size. The BASE case raindrops are least likely to have radii ranging from 40.5-61.5 microns, the ALL and SULF simulations are very close to each other and have a slightly higher probability than the BASE case. The SWITCH simulation is the most likely to have raindrops of this size, followed by the ORG simulation. For larger raindrops (68.5-96.5 microns), the ORG simulation has the highest probability, followed by the SWITCH case. The ALL simulation has the lowest probability for raindrops with radii 60.5 – 96.5 microns. The SULF and BASE simulations are similar, and probabilities fall between the simulations.

Overall, changing the default hygroscopicity values to the lab-derived values leads to relatively small changes in bulk hygroscopicity, with the exception of the ORG simulation. In the ORG simulation, the entire distribution is shifted to lower hygroscopicities, resulting in fewer aerosols being activated as cloud drops. In the pre-rain event, these changes in bulk hygroscopicity have a greater effect on the sizes of cloud drops and raindrops than on the number concentrations. During the rain event the changes in hygroscopicity probability density functions

remain small, though they lead to important changes in the microphysical parameters. For example, increasing sulfate's hygroscopicity leads to more numerous and smaller cloud drops, and decreasing the hygroscopicity in the ORG simulations leads to a greater chance of larger cloud drops and raindrops. Because raindrop formation is dependent on the size and number of cloud drops, these differences in size and number concentrations have impacts on raindrop size and number concentrations. Therefore, small changes in cloud drop size and number concentrations would lead to comparatively larger changes in raindrop size and number concentrations. These impacts are further discussed in the following section.

3.3.3 Time evolution of hydrometeors, accumulated precipitation, and CAPE

To reconcile the small changes in microphysics with the corresponding larger changes in the accumulated precipitation, we examine the area-averaged accumulated precipitation (mm) (Figure 3.5a), the area-averaged maximum updraft velocity (m s^{-1}), and the time evolution of the hydrometeor mass mixing ratios (g kg^{-1}) with height for each simulation (Figures 3.5c-g). We combine the raindrop, snow and graupel mixing ratios because of their relative importance in the hydrometeor water budget and evaluate the area-averaged accumulated precipitation, vertical velocity and the combined mass mixing ratios before and during the intense precipitation event. This allows us to examine the time and height evolution of hydrometeors as a result of altering the aerosol hygroscopicity over the focus region (Figure 3.2a).

In the BASE simulation, there are two periods of intense rainfall (Figure 3.5a, black line) and three distinct time periods of strong updrafts (Figure 3.5b, black line) associated with cloud development (Figure 3.5c). The first cloud development time period corresponds with small amounts of rain, beginning at 08:00 UTC. The second (5-27-02:00 – 07:00 UTC) and third (5-27-12:00 – 17:00 UTC) times of cloud development occur during the intense precipitation event,

with the largest water content values (up to 1.7 g H_2O kg dry air $^{-1}$) during the final pulse of precipitation. The cloud development leads to a total area averaged precipitation of 59 mm over the 36-hour time period.

The sensitivity simulations have a similar cloud development pattern, which is expected due to the larger scale meteorological forcing of the squall line. However, the microphysical differences correspond to the changes in accumulated precipitation. In the previous section, the PDFs indicate that making aerosol more hygroscopic, as in the SULF simulation, leads to more numerous and smaller cloud drops and ultimately fewer and smaller raindrops. On the other hand, making aerosol less hygroscopic, as in the ORG simulation, leads to fewer and larger cloud drops and more numerous and larger rain drops. However, these processes ultimately result in similar precipitation responses. Because of the similarity between the SULF and ORG simulations, here we will discuss them together in comparison with the BASE simulation. In the SULF and ORG simulations, the first round of cloud development is delayed and then enhanced, leading to 10-20% more rainfall (1.9 mm and 0.9 mm in the SULF and ORG simulations, respectively). During the second pulse, more numerous cloud drops (Figure 3.4b) cause earlier cloud development in the SULF simulation (Figure 5d) and more numerous raindrops (Figure 3.4c) causing more rain to fall earlier with a similar intensity to the BASE case (20.2 mm of accumulated precipitation from 5-27-02:00 – 07:00 UTC). During this second pulse, the ORG simulation has weaker cloud development but more precipitation accumulation (Figure 3.5e; 4 mm more than the BASE simulation). Because there are more, larger raindrops (Figure 3.4c&e), more rain would fall as precipitation because the updrafts (Figure 3.5b) are weaker and are not be strong enough to carry these larger hydrometeors. Both the ORG and the SULF simulations have enhanced cloud development in the third pulse of activity, with maximum hydrometeor

mixing ratios exceeding 2 g kg^{-1} and 1.8 g kg^{-1} respectively. This results in larger rain rates for both simulations, with the ORG simulation reaching over 27 mm of rain during that time period and the SULF simulation reaching over 25 mm of rain. These more intense rain rates correspond to stronger updrafts in the third precipitation pulse (Figure 3.5b, green and red lines), suggesting convective invigoration.

In the SWITCH simulation (Figure 3.5f, Figure 3.5a&b blue line), the pre-event clouds gain more liquid and solid water mass and have stronger updrafts earlier resulting in more accumulated rainfall than the BASE during this time. The second pulse is delayed but enhanced, with a total accumulation of 42 mm versus 38 mm. The third pulse of cloud development and resulting precipitation are similar in both timing and intensity to the BASE simulation. However, the SWITCH simulation accumulates an additional 22 mm during the third pulse while the BASE accumulates only 18 mm. In the SWITCH case, most of the change in accumulated precipitation can be attributed to the intensified pulses. In the ALL simulation (Figure 3.5g, Figure 3.5a gray line), the cloud development prior to the intense rain event is stronger, with more mass in the hydrometeors than in the BASE simulation, leading to a 2.5 mm increase of accumulated precipitation over the BASE simulation by 5-26-16:00 UTC. This corresponds to the increase in raindrop number concentration probability for the ALL simulation in Figure 3.3c. The second ALL pulse is similar to the BASE second pulse, with the same maximum value hydrometeor mixing ratio value (1.1 g kg^{-1}) occurring at approximately the same time. The similarity in cloud development leads to a 2 mm difference of accumulated precipitation (21 mm vs 19 mm). However, in the BASE simulation, there is a break in the precipitation between the second and third pulses (07:00 – 12:00 UTC). The final pulse at 12:00 UTC in the ALL simulation is weakened compared to the BASE simulation, with maximum mixing ratios of 1.1g

kg^{-1}. This is reflected in the accumulated precipitation, where the third pulse of the ALL simulation has a reduced rate of precipitation compared to the BASE simulation.

In all three simulations that altered the hygroscopicity of individual species (SWITCH, ORG, and SULF), delayed cloud development leads to enhanced precipitation. This is especially true in the ORG simulation, where the final pulse yields the largest hydrometeor mixing ratios. This suggests that several factors are affected by the changes in hygroscopicities. Initial suppression followed by convective invigoration (SULF, ORG, SWITCH) or quicker rainout due to larger drops (Figure 3.3e) being able to form more quickly (ALL), are both causes for these differences. While large-scale meteorological forcing and local thermodynamic factors are clearly the drivers of this precipitation event, it is clear that chemical composition can affect the intensity of hydrometeor formation and rain rates.

The thermodynamic environment influences storm development, so here we examine the convective available potential energy (CAPE) averaged over the region east of Kansas City (Figure 3.6). The pre-storm environment CAPE follows a diurnal pattern, beginning at 800 J and increasing to 2400 J, with little difference between the simulations until May 27, 02:00 UTC. At 02:00, The SULF, ORGO, and SWITCH CAPE values all increase at the same rate until through 07:00 UTC, which corresponds to the increase in precipitation and the decrease in vertical velocity. The ALL simulation, which has the most accumulated precipitation during this time, also has the least amount of CAPE, suggesting the earlier rainout depletes the environment of water, altering the stability. During the last pulse of convective activity (12:00 – 17:00 UTC), the CAPE values increase for each simulation and the highest CAPE values correspond to the highest maximum updrafts and largest hydrometeor mixing ratios. Aerosols have been shown to affect mesoscale storms and the resulting precipitation within this CAPE range (Storer et al,

2010). Based on the similarity of the CAPE during the pre-storm environment between all five of the simulations, it is reasonable to conclude that changing the aerosol hygroscopicities affects CAPE, which in turn affects precipitation and vertical velocities.

3.3.4 Evaluation against observed precipitation intensity

To understand the realism of these hygroscopicity sensitivity tests, we compare the PDF of the observed accumulated precipitation values to simulated precipitation in the selected box (Figure 3.6). We use the 1-km Daymet gridded daily precipitation product (Thornton et al. 2016), which is a high-resolution daily product of precipitation, and re-grid to our domain to compare with accumulated precipitation from the five model simulations. The observed precipitation intensity shows a peak probability at 30 mm, with low probabilities at the lower accumulated values (< 20 mm, 10%) and high accumulated values (< 80 mm, <3%) with several different characteristics than observed. Like all gridded datasets, the Daymet dataset has biases. Within the model domain region, the Daymet dataset captures average precipitation quite well, with a positive bias of less than 0.25 mm. However, for events with greater than 100 mm of accumulated precipitation, the Daymet dataset has a negative bias of about 40 mm. While this is actually on the order of 50%, this amount of bias is common with gridded datasets. Generally, all cases simulate an increased probability of low intensity (<15 mm) and high intensity (>60 mm) events, and lower frequencies at the center of the precipitation distribution. Of the five simulations, the ALL simulation most closely matches observations, primarily by reducing amount of both low (<15 mm) and high (> 60 mm) precipitation intensities and improving the tail ends of the PDF. While the ALL simulation shifts the observed peak at 35 mm to higher values (50 mm), it reproduces the overall shape of the observed distribution better than the other simulations. The BASE simulation also generally matches the pattern of the observed PDF, yet

misses the observed 35 mm peak accumulation and simulates greater values at the distribution tails. The ORG simulation diverges from the observed PDF, with a large probability of low-intensity rain events and an increased probability of high-intensity rain events, with the lowest probability of mid-range events. The SULF and SWITCH simulation PDFs are similar, with increases in both low and high-intensity events compared to the observed PDF, and much lower probability of the mid-range events. In the ORG, SWITCH and SULF simulations especially, this pattern indicates that the model is simulating too much rainfall in some grid cells and too little rainfall in others in all simulations. The ALL simulation provides the best evaluation with observations by improving the number of grid cells with the mid-range rain accumulations compared to the other simulations. While the microphysical changes shown in Figure 3.4 are relatively small between simulations, the sensitivity of accumulated precipitation to changes in hygroscopicity is quite large. By incorporating lower organic hygroscopicity values and higher hygroscopicity values for sulfate, ammonium and nitrate that depend on the portioning of ammonium, the ALL simulation not only more closely matches the BASE simulation, it also improves the model's ability to represent observed accumulated precipitation.

This improved representation of mid-range intensity precipitation (30 – 60 mm d^{-1}) is a result of how the ALL simulation represents each of the final two pulses of precipitation (May 26 21:00 – May 27 07:00 UTC; May 27 12:00 – 18:00 UTC). By the end of the second pulse, the probability of 45 mm accumulated exceeds all the other simulations, which is reflected in Figure 3.5a when the area-averaged accumulated precipitation is greatest for the ALL simulation at ~ 50 mm. Consistently, the combined hydrometeor mass mixing ratios increase to 0.91 g kg^{-1} two hours earlier than in the other simulations (Figure 3.5g), suggesting an increase in rates of hydrometeor growth precipitation during this time period. During the third pulse, the likelihood

of grid cells in the ALL simulation having accumulated less than 35 mm is larger than the other simulations, as evidenced by the slower accumulation of precipitation (Figure 3.5a) and the smaller hydrometeor mixing ratios (1.21 g kg^{-1} maximum; Figure 3.5g). Accordingly, the other four simulations show an increase in the probabilities of accumulated precipitation amounts exceeding 35 mm, corresponding to the increased slopes (Figure 3.5a) and greater hydrometeor mass mixing ratio maxima (1.5 – 2.0 g kg^{-1}; Figure 3.5c,d,e,f).

3.4.0 Discussion and Conclusions

We test the default hygroscopicity values in WRF-Chem during a mesoscale event to understand the role of the hygroscopicity parameterization on the simulation of high intensity rainfall. We find that updating the model parameters to laboratory-derived values and including a switch to account for changes in ammonium hygroscopicity based on partitioning produces accumulated precipitation values closest to the observed values of precipitation intensity. Changing hygroscopicity for individual aerosol species alters the accumulation and accumulation mode bulk hygroscopicity distributions, and these distribution differences drive changes in microphysical characteristics (rain and cloud drop numbers and sizes) that alter rainfall duration and intensity. The largest contiguous area of rainfall amounts greater than 100 mm exists in the SWITCH case, which implies that including the larger hygroscopicity values for ammonium and nitrate could impact the simulation of storm severity and flooding. Compared to the observations of daily-accumulated precipitation, the model evaluation improves when all lab-derived hygroscopicities are included, with the caveat that the gridded dataset has a large negative bias, and likely misses the most extreme precipitation events.

While including more complex representations of aerosol activation as CCN aims to more closely represent real-world environments, there are limitations in our model simulations.

First, the activation of aerosols as CCN does not account for interactions on the aerosol surface. While the modal and bin representations of aerosol size assume internally mixed modes and bins, individual aerosols are highly complex, and cannot accurately account for aging processes in the atmosphere. Even though the hygroscopicity is a good metric for activating aerosols that are mostly inorganic (e.g., ammonium sulfate, ammonium nitrate, salts), it has trouble representing activation of aerosols that are mixtures of organic and inorganic species (Good et al. 2010). Often the kappa method will activate these mixtures at smaller diameters than actually observed, potentially due to heterogeneous surface interactions where surface tension increases linearly with decreasing surface concentration (Ruehl et al. 2016). Secondly, the responses of bulk hygroscopicity and microphysical parameters to the aerosol hygroscopicity changes are small, but lead to relatively large precipitation changes. Because we do not incorporate ensembles in this study, there is no baseline for how these hygroscopicity changes compare with initial conditions differences. Even with these limitations, moving towards a more realistic modeling approach is necessary in understanding potential changes in precipitation patterns as a result of current and future heterogeneity of aerosol sources. For example, Saide et al. (2016) found that using a bulk hygroscopicity value of 0.4 for all aerosols potentially changes the significant tornado parameter, which is a measure of how likely the environment is to produce a strong tornado. These changes have implications for severe weather. Additionally, the implemented switch is based solely on the ratio of ammonium to sulfate. In regions with relatively large amounts of nitrate and sulfate, such as urban regions, this may misrepresent ammonium hygroscopicity and therefore lead to unrealistic changes in the microphysics and precipitation patterns. Additionally, the current microphysics implementation does not include aerosols as ice nuclei, which can impact the radiative balance within deep convection (Fan et al. 2013). We note

this is important, especially for dust, which is documented as efficient ice nuclei (DeMott et al. 2003). While this study focused primarily on the liquid phase, the solid phase has been shown to affect precipitation processes and total rainfall amounts (Cheng et al. 2010).

Overall, these results suggest that the model treatment of aerosol composition via the hygroscopicity parameter can affect short-term weather and the simulation of high intensity events. Including updated hygroscopicity values overall leads to an improved simulation of high intensity precipitation events, and suggests that this be evaluated more closely in future model studies in regions with varying aerosol compositions.

Acknowledgements
Funding for this research was provided by the NASA Interdisciplinary Science program through Project NNX12AM89G: "Storms, forms, and complexity of the urban canopy: How land use, settlement patterns, and the shapes of cities influence severe weather," the National Science Foundation grant 1313897, and the Elizabeth Caroline Crosby Grant.

References

Abdul‐Razzak, H., and S. J. Ghan, 2000: A parameterization of aerosol activation: 2. Multiple aerosol types. *Journal of Geophysical Research: Atmospheres*, **105,** 6837-6844.

Ackerman, A. S., O. Toon, D. Stevens, A. Heymsfield, V. Ramanathan, and E. Welton, 2000: Reduction of tropical cloudiness by soot. *Science*, **288,** 1042-1047.

Ackermann, I. J., H. Hass, M. Memmesheimer, A. Ebel, F. S. Binkowski, and U. Shankar, 1998: Modal aerosol dynamics model for Europe: Development and first applications. *Atmospheric environment*, **32,** 2981-2999 %@ 1352-2310.

Albrecht, B. A., 1989: Aerosols, cloud microphysics, and fractional cloudiness. *Science*, **245,** 1227-1230.

Andreae, M., and A. Gelencsér, 2006: Black carbon or brown carbon? The nature of light-absorbing carbonaceous aerosols. *Atmospheric Chemistry and Physics*, **6,** 3131-3148.

Andreae, M. O., D. Rosenfeld, P. Artaxo, A. Costa, G. Frank, K. Longo, and M. Silva-Dias, 2004: Smoking rain clouds over the Amazon. *science*, **303,** 1337-1342.

Behera, S. N., M. Sharma, V. P. Aneja, and R. Balasubramanian, 2013: Ammonia in the atmosphere: a review on emission sources, atmospheric chemistry and deposition on terrestrial bodies. *Environmental Science and Pollution Research*, **20,** 8092-8131 %@ 0944-1344.

Boucher, O., and Coauthors, 2013: Clouds and aerosols. *Climate change 2013: the physical science basis. Contribution of Working Group I to the Fifth Assessment Report of the Intergovernmental Panel on Climate Change*, Cambridge University Press, 571-657.

Butler, T., F. Vermeylen, C. M. Lehmann, G. E. Likens, and M. Puchalski, 2016: Increasing ammonia concentration trends in large regions of the USA derived from the NADP/AMoN network. *Atmospheric Environment %@ 1352-2310*.

Carrió, G. G., W. R. Cotton, and W. Y. Y. Cheng, 2010: Urban growth and aerosol effects on convection over Houston. *Atmospheric Research*, **96,** 560-574.

Cerully, K. M., and Coauthors, 2015: On the link between hygroscopicity, volatility, and oxidation state of ambient and water-soluble aerosols in the southeastern United States. *Atmospheric Chemistry and Physics*, **15,** 8679-8694.

Chapman, E. G., W. Gustafson Jr, R. C. Easter, J. C. Barnard, S. J. Ghan, M. S. Pekour, and J. D. Fast, 2009: Coupling aerosol-cloud-radiative processes in the WRF-Chem model: Investigating the radiative impact of elevated point sources. *Atmospheric Chemistry and Physics*, **9,** 945-964.

Cheng, C.-T., W.-C. Wang, and J.-P. Chen, 2010: Simulation of the effects of increasing cloud condensation nuclei on mixed-phase clouds and precipitation of a front system. *Atmospheric Research*, **96,** 461-476.

DeMott, P. J., and Coauthors, 2003: African dust aerosols as atmospheric ice nuclei. *Geophysical Research Letters*, **30**.

Dudhia, J., 1996: Back to basics: thunderstorms: Part 1. *Weather*, **51,** 371-376.

Dusek, U., and Coauthors, 2006: Size matters more than chemistry for cloud-nucleating ability of aerosol particles. *Science*, **312,** 1375-1378 %@ 0036-8075.

Easter, R. C., and P. V. Hobbs, 1974: The formation of sulfates and the enhancement of cloud condensation nuclei in clouds. *Journal of the Atmospheric Sciences*, **31,** 1586-1594 %@ 1520-0469.

Ek, M., and Coauthors, 2003: Implementation of Noah land surface model advances in the National Centers for Environmental Prediction operational mesoscale Eta model. *Journal of Geophysical Research: Atmospheres*, **108**.

Ekman, A., C. Wang, J. Wilson, and J. Ström, 2004: Explicit simulations of aerosol physics in a cloud-resolving model: a sensitivity study based on an observed convective cloud. *Atmospheric Chemistry and Physics*, **4,** 773-791.

Emmons, L., and Coauthors, 2010: Description and evaluation of the Model for Ozone and Related chemical Tracers, version 4 (MOZART-4). *Geoscientific Model Development*, **3,** 43-67.

EPA, 2011: National Emissions Inventory.

Fan, J., Y. Wang, D. Rosenfeld, and X. Liu, 2016: Review of Aerosol–Cloud Interactions: Mechanisms, Significance, and Challenges. *Journal of the Atmospheric Sciences*, **73,** 4221-4252.

Fan, J., R. Zhang, G. Li, W. K. Tao, and X. Li, 2007: Simulations of cumulus clouds using a spectral microphysics cloud‐resolving model. *Journal of Geophysical Research: Atmospheres*, **112**.

Fan, J., D. Rosenfeld, Y. Ding, L. R. Leung, and Z. Li, 2012: Potential aerosol indirect effects on atmospheric circulation and radiative forcing through deep convection. *Geophysical Research Letters*, **39**.

Fan, J., D. Rosenfeld, Y. Yang, C. Zhao, L. R. Leung, and Z. Li, 2015: Substantial contribution of anthropogenic air pollution to catastrophic floods in Southwest China. *Geophysical Research Letters*, **42,** 6066-6075.

Fan, J., L. R. Leung, D. Rosenfeld, Q. Chen, Z. Li, J. Zhang, and H. Yan, 2013: Microphysical effects determine macrophysical response for aerosol impacts on deep convective clouds. *Proc Natl Acad Sci U S A*, **110,** E4581-4590.

Ghan, S. J., and S. E. Schwartz, 2007: Aerosol properties and processes. *Bulletin of the American Meteorological Society*, **88,** 1059.

Good, N., and Coauthors, 2010: Consistency between parameterisations of aerosol hygroscopicity and CCN activity during the RHaMBLe discovery cruise. *Atmospheric Chemistry and Physics*, **10,** 3189-3203.

Grell, G. A., S. E. Peckham, R. Schmitz, S. A. McKeen, G. Frost, W. C. Skamarock, and B. Eder, 2005: Fully coupled "online" chemistry within the WRF model. *Atmospheric Environment*, **39,** 6957-6975.

Guenther, A., T. Karl, P. Harley, C. Wiedinmyer, P. Palmer, and C. Geron, 2006: Estimates of global terrestrial isoprene emissions using MEGAN (Model of Emissions of Gases and Aerosols from Nature). *Atmospheric Chemistry and Physics Discussions*, **6,** 107-173.

Hand, J., B. Schichtel, W. Malm, and M. Pitchford, 2012: Particulate sulfate ion concentration and SO 2 emission trends in the United States from the early 1990s through 2010. *Atmospheric Chemistry and Physics*, **12,** 10353-10365.

Hong, S.-Y., Y. Noh, and J. Dudhia, 2006: A new vertical diffusion package with an explicit treatment of entrainment processes. *Monthly Weather Review*, **134,** 2318-2341.

Houze, R. A., 2004: Mesoscale convective systems. *Reviews of Geophysics*, **42**.

Kawecki, S., G. M. Henebry, and A. L. Steiner, 2016: Effects of Urban Plume Aerosols on a Mesoscale Convective System. *Journal of the Atmospheric Sciences*, **73,** 4641-4660 %@ 0022-4928.

Khain, A., M. Ovtchinnikov, M. Pinsky, A. Pokrovsky, and H. Krugliak, 2000: Notes on the state-of-the-art numerical modeling of cloud microphysics. *Atmospheric Research*, **55,** 159-224.

Khain, A., and Coauthors, 2015: Representation of microphysical processes in cloud‐resolving models: Spectral (bin) microphysics versus bulk parameterization. *Reviews of Geophysics*, **53,** 247-322.

Köhler, H., 1936: The nucleus in and the growth of hygroscopic droplets. *Transactions of the Faraday Society*, **32,** 1152-1161.

Kulmala, M., A. Laaksonen, and L. Pirjola, 1998: Parameterizations for sulfuric acid/water nucleation rates. *Journal of Geophysical Research: Atmospheres*, **103,** 8301-8307 %@ 2156-2202.

Lebo, Z. J., and J. H. Seinfeld, 2011: Theoretical basis for convective invigoration due to increased aerosol concentration. *Atmospheric Chemistry and Physics*, **11,** 5407-5429.

Malm, W. C., J. F. Sisler, D. Huffman, R. A. Eldred, and T. A. Cahill, 1994: Spatial and seasonal trends in particle concentration and optical extinction in the United States. *Journal of Geophysical Research: Atmospheres*, **99,** 1347-1370.

Morrison, H., J. Curry, and V. Khvorostyanov, 2005: A new double-moment microphysics parameterization for application in cloud and climate models. Part I: Description. *Journal of the Atmospheric Sciences*, **62,** 1665-1677.

NCEI, 2013: North American Model-Reanalysis, 6-hourly dataset. NCEI, Ed., http://nomads.ncdc.noaa.gov/data/namanl/201305/.

Ntelekos, A. A., J. A. Smith, L. Donner, J. D. Fast, W. I. Gustafson, E. G. Chapman, and W. F. Krajewski, 2009: The effects of aerosols on intense convective precipitation in the northeastern United States. *Quarterly Journal of the Royal Meteorological Society*, **135,** 1367-1391.

Petters, M. D., and S. M. Kreidenweis, 2007: A single parameter representation of hygroscopic growth and cloud condensation nucleus activity. *Atmospheric Chemistry and Physics*, **7,** 1961-1971 %@ 1680-7316.

Petters, M. D., and Coauthors, 2009: Towards closing the gap between hygroscopic growth and activation for secondary organic aerosol–Part 2: Theoretical approaches. *Atmospheric Chemistry and Physics*, **9,** 3999-4009 %@ 1680-7316.

Pielke, R. A., and Coauthors, 1992: A comprehensive meteorological modeling system—RAMS. *Meteorology and Atmospheric Physics*, **49,** 69-91 %@ 0177-7971.

Price, E., J. Mielikainen, M. Huang, B. Huang, H.-L. A. Huang, and T. Lee, 2014: GPU-accelerated longwave radiation scheme of the Rapid Radiative Transfer Model for General Circulation Models (RRTMG). *IEEE Journal of Selected Topics in Applied Earth Observations and Remote Sensing*, **7,** 3660-3667 %@ 1939-1404.

Raymond, T. M., and S. N. Pandis, 2002: Cloud activation of single‐component organic aerosol particles. *Journal of Geophysical Research: Atmospheres*, **107**.

Rosenfeld, D., 2000: Suppression of rain and snow by urban and industrial air pollution. *Science*, **287,** 1793-1796.

Rosenfeld, D., and Coauthors, 2008: Flood or drought: how do aerosols affect precipitation? *science*, **321,** 1309-1313.

Rosenfeld, D., and Coauthors, 2014: Global observations of aerosol‐cloud‐precipitation‐climate interactions. *Reviews of Geophysics*, **52,** 750-808.

Ruehl, C. R., J. F. Davies, and K. R. Wilson, 2016: An interfacial mechanism for cloud droplet formation on organic aerosols. *Science*, **351,** 1447-1450 %@ 0036-8075.

Saide, P. E., G. Thompson, T. Eidhammer, A. M. Silva, R. B. Pierce, and G. R. Carmichael, 2016: Assessment of biomass burning smoke influence on environmental conditions for multiyear tornado outbreaks by combining aerosol‐aware microphysics and fire emission constraints. *Journal of Geophysical Research: Atmospheres*, **121**.

Saide, P. E., and Coauthors, 2015: Central American biomass burning smoke can increase tornado severity in the U.S. *Geophysical Research Letters*, **42,** 956-965.

Schell, B., I. J. Ackermann, H. Hass, F. S. Binkowski, and A. Ebel, 2001: Modeling the formation of secondary organic aerosol within a comprehensive air quality model system. *Journal of Geophysical Research: Atmospheres*, **106,** 28275-28293.

Smith, A. B., and R. W. Katz, 2013: US billion-dollar weather and climate disasters: data sources, trends, accuracy and biases. *Natural hazards*, **67,** 387-410 %@ 0921-0030X.

Stevens, B., and G. Feingold, 2009: Untangling aerosol effects on clouds and precipitation in a buffered system. *Nature*, **461,** 607-613.

Stockwell, W. R., P. Middleton, J. S. Chang, and X. Tang, 1990: The second generation regional acid deposition model chemical mechanism for regional air quality modeling. *Journal of Geophysical Research: Atmospheres (1984–2012)*, **95,** 16343-16367.

Storelvmo, T., and I. Tan, 2015: The Wegener-Bergeron-Findeisen process–Its discovery and vital importance for weather and climate. *Meteor. Z*, **24,** 455-461.

Tao, W.-K., J.-P. Chen, Z. Li, C. Wang, and C. Zhang, 2012: Impact of aerosols on convective clouds and precipitation. *Reviews of Geophysics*, **50**.

Thornton, P. E., M. M. Thornton, and R. S. Vose, 2016: Daymet V3: Annual Tile Summary Cross-Validation Statistics for North America, Hawaii. ORNL DAAC, Oak Ridge, Tennessee, USA.

Twomey, S., 1977: The influence of pollution on the shortwave albedo of clouds. *Journal of the atmospheric sciences*, **34,** 1149-1152.

van den Heever, S. C., and W. R. Cotton, 2007: Urban Aerosol Impacts on Downwind Convective Storms. *Journal of Applied Meteorology and Climatology*, **46,** 828-850.

Van den Heever, S. C., G. G. Carrió, W. R. Cotton, P. J. DeMott, and A. J. Prenni, 2006: Impacts of nucleating aerosol on Florida storms. Part I: Mesoscale simulations. *Journal of the atmospheric sciences*, **63,** 1752-1775.

VanReken, T. M., N. L. Ng, R. C. Flagan, and J. H. Seinfeld, 2005: Cloud condensation nucleus activation properties of biogenic secondary organic aerosol. *Journal of Geophysical Research: Atmospheres*, **110**.

Virkkula, A., R. Van Dingenen, F. Raes, and J. Hjorth, 1999: Hygroscopic properties of aerosol formed by oxidation of limonene, α‐pinene, and β‐pinene. *Journal of Geophysical Research: Atmospheres*, **104,** 3569-3579 %@ 2156-2202.

Wang, J., S. C. van den Heever, and J. S. Reid, 2009: A conceptual model for the link between Central American biomass burning aerosols and severe weather over the south central United States. *Environmental Research Letters*, **4,** 015003.

Ward, D., and W. Cotton, 2011: A Method for Forecasting Cloud Condensation Nuclei Using Predictions of Aerosol Physical and Chemical Properties from WRF/Chem. *Journal of Applied Meteorology and Climatology*, **50,** 1601-1615.

Wild, O., X. Zhu, and M. J. Prather, 2000: Fast-J: Accurate simulation of in-and below-cloud photolysis in tropospheric chemical models. *Journal of Atmospheric Chemistry*, **37,** 245-282.

Zhang, J., J. S. Reid, M. Christensen, and A. Benedetti, 2016: An evaluation of the impact of aerosol particles on weather forecasts from a biomass burning aerosol event over the Midwestern United States: observational-based analysis of surface temperature. *Atmospheric Chemistry and Physics*, **16,** 6475-6494.

Aerosol Species	WRF-Chem Value	Ward & Cotton
SO_4^{-2}	0.5	0.71
NO_3^-	0.5	0.51
NH_4^+ (SO_4)	0.5	0.61
NH_4^+ (NO_3)	0.5	0.67
Antha	0.14	0.3
OIN	0.14	N/A
orgaro1	0.14	0.051
orgaro2	0.14	0.094
orgalk	0.14	0.005
orgole	0.14	0.19
orgba1	0.14	0.10
orgba2	0.14	0.10
orgba3	0.14	0.08
orgba4	0.14	0.08
orgpa (orgoin)	0.14	0.073
ec	1.0 x 10-6	0.02
seasalt	1.16	1.28
soila	0.1	0.04

Table 3.1: Hygroscopicity values assigned for aerosol types in the MADE/SORGAM WRF-Chem version 3.6 and the values assigned in Ward and Cotton (2011).

Figures

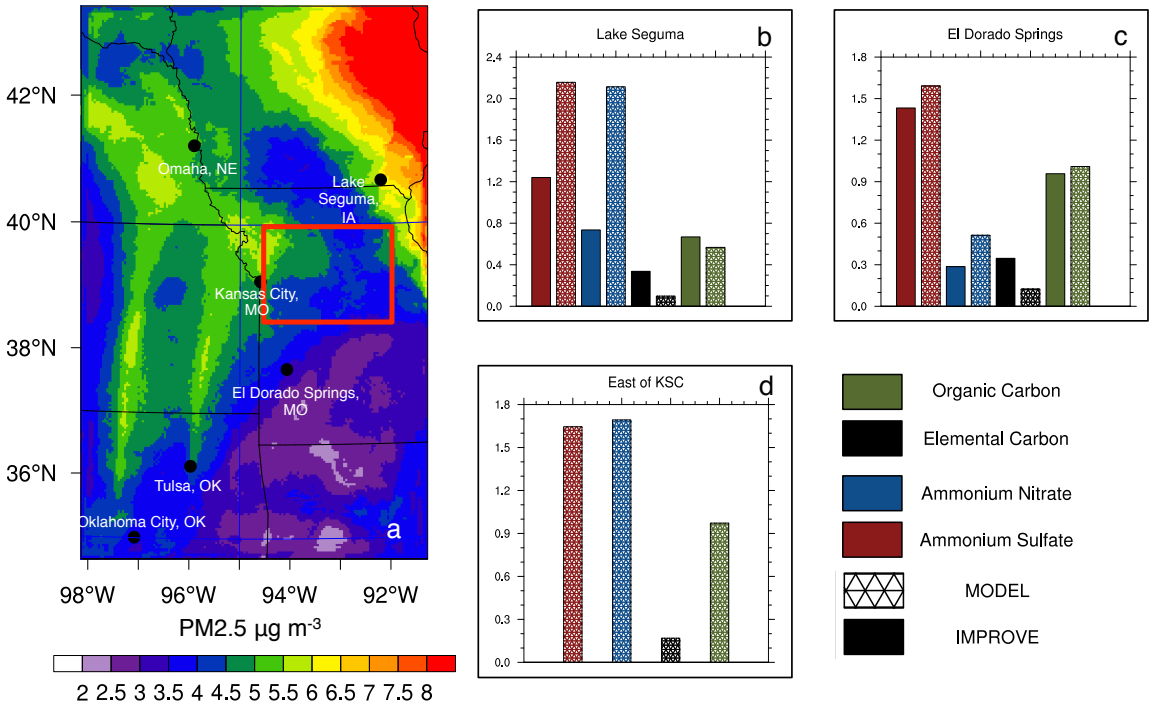

Figure 3.1: a) BASE case boundary layer (0-2 km), 24 hour averaged (5-26 06:00 UTC to 5-27 06:00 UTC) total PM 2.5 (µg m^{-3}). IMPROVE (solid) and modeled (hatched) speciated aerosol for b) Lake Seguma, IA (LAKE) and c) El Dorado Springs, MO (EDS). IMPROVE data is the average of May 22 and 25 2013 samples and modeled data is the boundary layer average of a 3x3 grid cell average of 144 km^2 region containing the location of the site. d) Modeled speciated aerosol east of Kansas City in the region of high precipitation (denoted by the red box in Figure 3.1a).

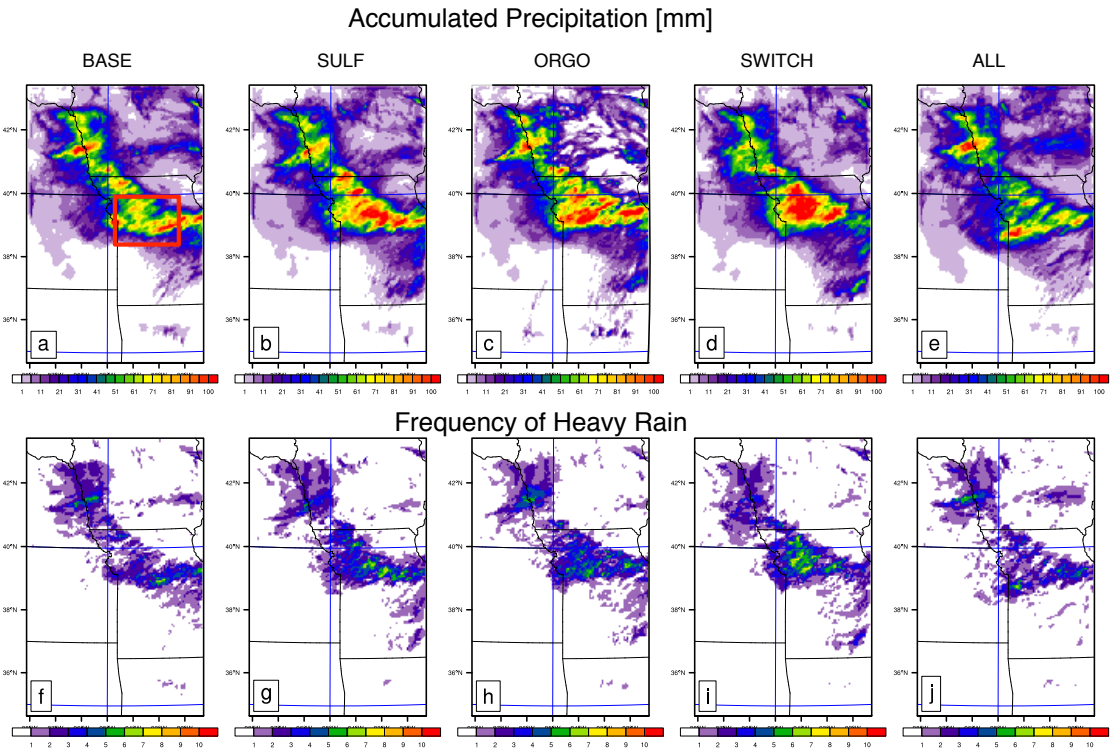

Figure 3.2: Accumulated precipitation for the 24 hour period ending on 5-27 at 18:00 UTC for the a) BASE, b) SULF, c) ORG, d) SWITCH and e) ALL simulations. Frequency of heavy rain (< 10 mm/hour) occurring over the same 24 hour period for the f) BASE, g) SULF, h) ORG, i) SWITCH, and j) ALL simulations. The red box in Figure 1a indicates the analysis region in Figures 3.3-3.5.

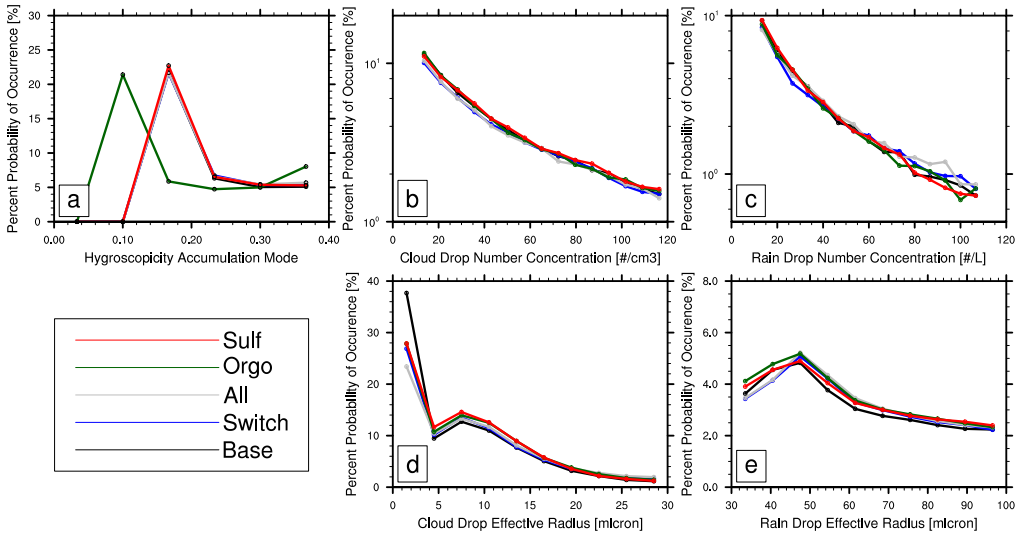

Figure 3.3: Probability distribution functions (PDFs) for the five simulations (BASE, SULF, ORGO, SWITCH, ALL) for a) Accumulation mode bulk hygroscopicity, b) cloud drop number concentration (# cm^{-3}), c) rain drop number concentration (# L^{-1}), d) cloud drop effective radius (microns), and e) raindrop effective radius (microns). PDFs are computed based on the time period ranging from 0600 –2300 UTC, 5-26-2013 in the red box denoted in Figure 3.2a.

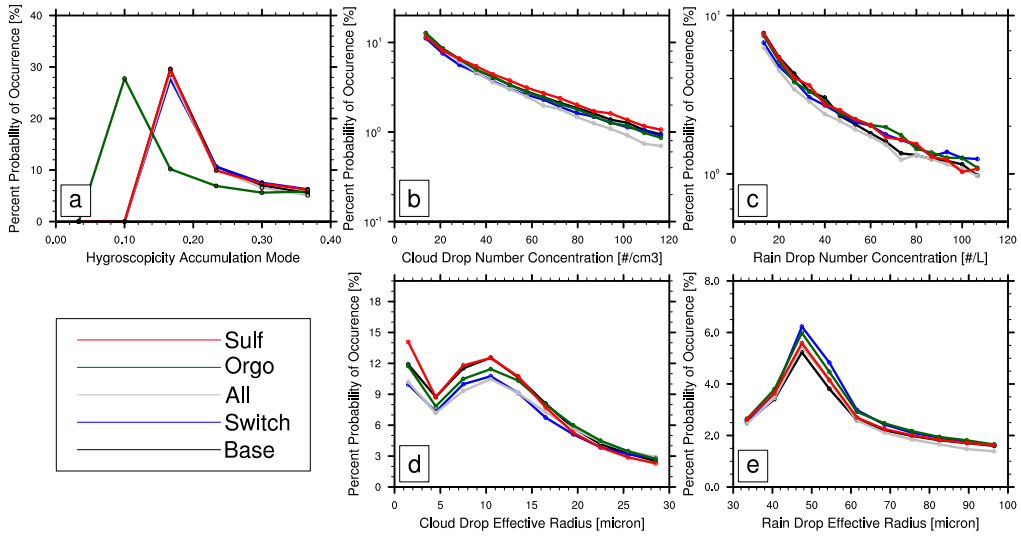

Figure 3.4: The same as Figure 3 but during the intense rain event (0000 –1800 UTC, 5-27-2013).

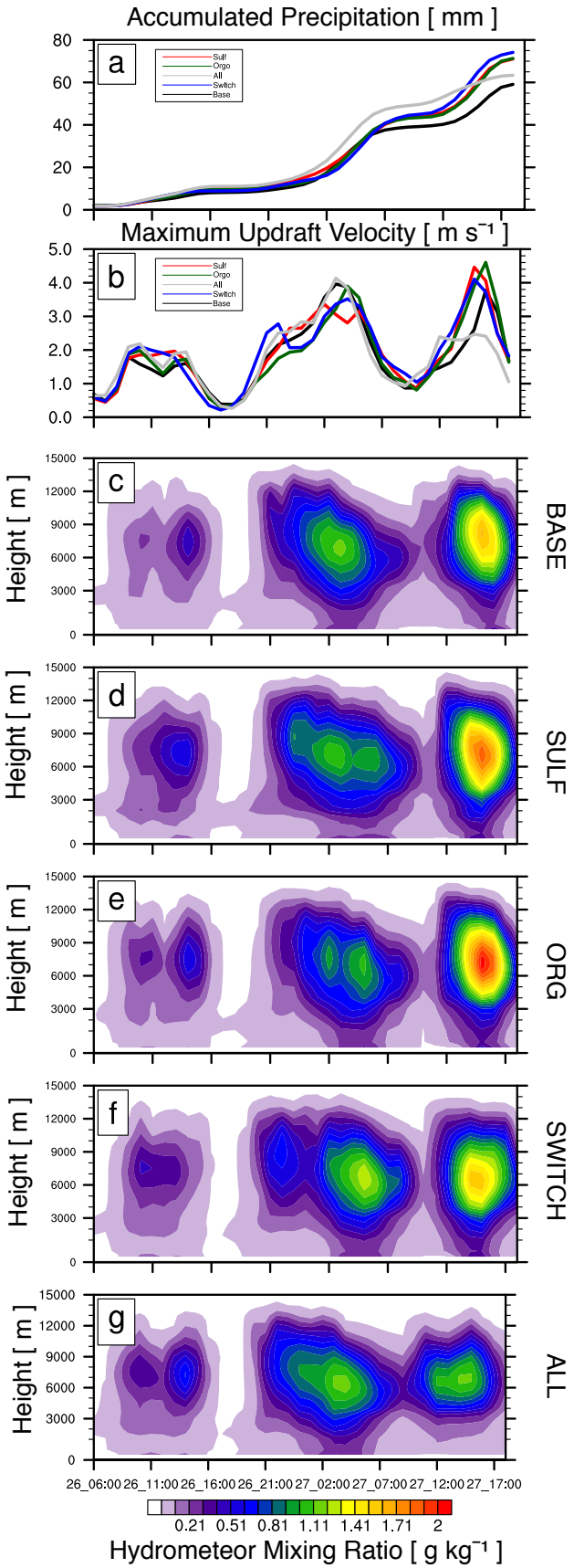
Accumulated Precipitation [mm]
a
Sulf
Orgo
All
Switch
Base
Maximum Updraft Velocity [m s⁻¹]
b
Height [m]
c
BASE
d
SULF
e
ORG
f
SWITCH
g
ALL
26_06:00 26_11:00 26_16:00 26_21:00 27_02:00 27_07:00 27_12:00 27_17:00
0.21 0.51 0.81 1.11 1.41 1.71 2
Hydrometeor Mixing Ratio [g kg⁻¹]

Figure 3.5: Area averaged (red box; Figure 3.2a) time series of a) accumulated precipitation and b) maximum updraft velocity for BASE (black line), SWITCH (blue line), ALL (gray line), ORG (green line), and SULF (red line) simulations. Area averaged (Figure 3.2a) time versus height of combined hydrometeor mass mixing ratios (rain, snow, and graupel; g kg^{-1}) for the c) BASE, d) SULF, e) ORG, f) SWITCH, and g) ALL simulations. Contours indicate mass mixing ratios (g kg^{-1}).

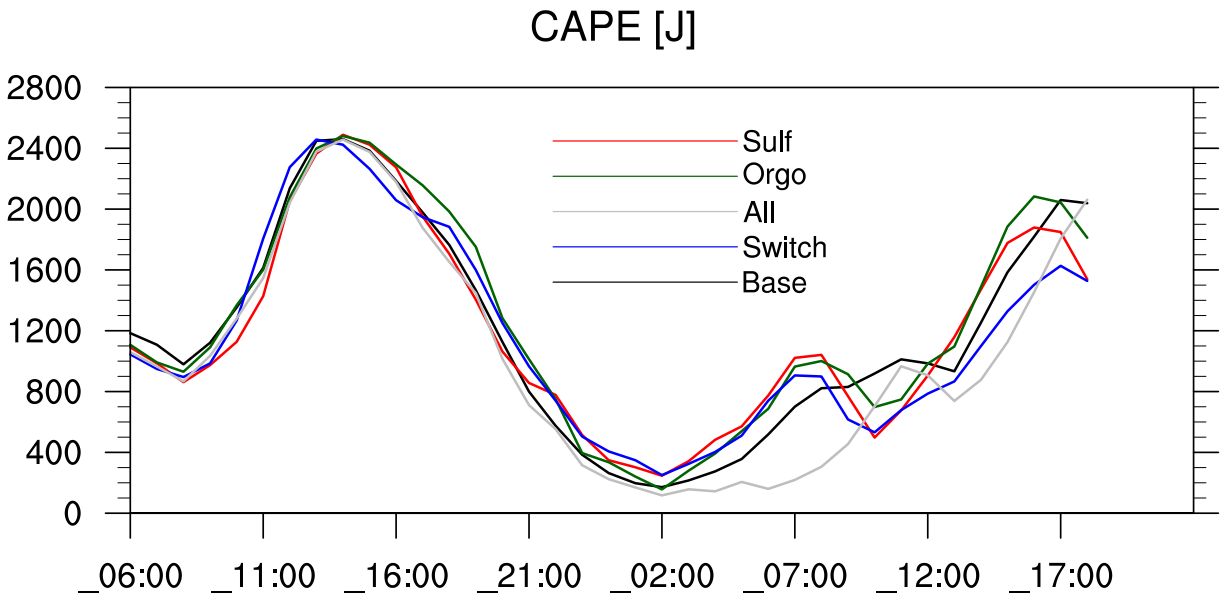

Figure 3.6: Area averaged (red box; Figure 3.2a) time series of convective available potential energy (CAPE; Joules) for BASE (black line), SWITCH (blue line), ALL (gray line), ORG (green line), and SULF (red line) simulations.

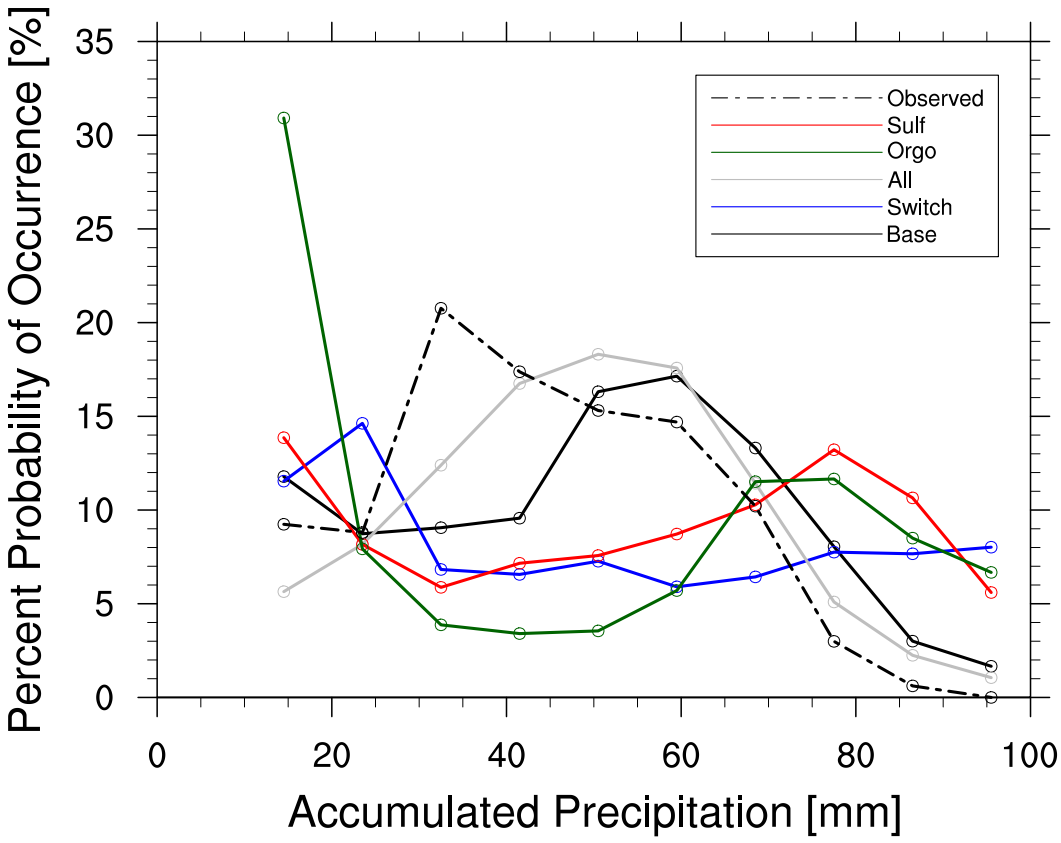

Figure 3.7: Probability density function (PDF) of observed (grey) and modeled (BASE-black, SULF-red, ORG-green, SWITCH-blue, ALL – black dashed) 24-hour accumulated precipitation calculated over the red box denoted in Figure 3.2a.

Chapter IV

Dust as ice nuclei: Implications for a mesoscale convective system in the Central Great Plains.

Stacey Kawecki, Department of Climate and Space Sciences and Engineering, University of Michigan, Ann Arbor, MI 48109

Allison L. Steiner, Department of Climate and Space Sciences and Engineering, University of Michigan, Ann Arbor, MI 48109

Hugh Morrison, National Center for Atmospheric Research Boulder, CO

4.0 Abstract

Dust is an important aerosol component in the Central Great Plains region due to the large amount of agriculture. Frequent severe weather occurs in this region, such as squall lines and supercell formation, whose mesoscale dynamics include the formation, maintenance and dissipation of mixed phase and cold clouds. Because dust is an important ice nucleating particle, these aerosols may play an important role in the development and maintenance of supercell systems. The current Morrison microphysics ice nucleation rate (Morrison et al. 2005) within the WRF-Chem framework depends only on temperature and ice supersaturation. The role of interactive dust as ice-nucleating particles is not included. In this study we develop a new

parameterization that uses the simulated and dynamic dust concentrations from the chemistry portion of the code in the microphysics portion of the code. Using previously described relationships for deposition nucleation and condensation/immersion freezing, we include dust as INPs. To determine the impacts of this INP change on a mesoscale convective event, we simulate a supercell that occurred on May 29-30, 2012 north of Oklahoma City, OK. Including dust as INPs leads to decreases in ice and snow number concentrations, and also shifts the cold-phase hydrometeors to larger effective radii. Interestingly, these differences do not demonstrate a significant impact on storm severity or precipitation. However, there is a notable increase in outgoing long-wave radiation with the new implementation, as a result of the decrease in the solid phase hydrometeor number concentrations. While including dust as INPs does not affect the overall severity of convection in this specific system, the significant changes in outgoing long-wave radiation could have important climate feedbacks for these severe weather systems.

4.1 Introduction

The effects of clouds on climate are highly uncertain (Boucher et al. 2013), and much of this uncertainty is due to the poorly constrained interactions between clouds and aerosols (Stevens and Feingold 2009). Aerosols affect the climate directly, by absorbing or scattering incoming radiation (Twomey 1974; Twomey 1977), which provides a direct feedback to the Earth's radiation budget. Aerosols also affect the climate indirectly via their interactions with clouds. The first indirect effect describes how aerosols increase the number of CCN, and with a fixed liquid water content, this decreases the drop size and increases scattering (Twomey 1977), and the second indirect effect quantifies how aerosols change cloud lifetime and subsequent precipitation (Albrecht 1989). For example, in low-altitude marine clouds, increasing the number of CCN increases the clouds' albedo, which decreases the amount of solar radiation reaching the

Earth's surface. In warm clouds, the addition of hygroscopic aerosols can delay precipitation resulting in longer cloud lifetimes (Rosenfeld 2000; Andreae et al. 2004; Rosenfeld et al. 2008; Fan et al. 2015). Adding aerosols can also invigorate convection in deep convective clouds leading to higher anvil clouds with larger spatial extent, thereby influencing the radiation budget (Fan et al. 2013). Therefore, understanding the impacts that aerosols have on the ice clouds formed from deep convection is imperative to mitigating the uncertainties that the cloud and aerosol interactions have on the climate system.

Anvil clouds are made up of ice crystals, which can form either homogeneously or heterogeneously in the atmosphere. Homogeneous freezing occurs when drops spontaneously freeze without the presence of ice-nucleating particles (INP), at temperatures near -40°C with high supersaturation with respect to ice (Heymsfield and Sabin 1989). This process is well understood and is incorporated into meteorology models. Heterogeneous freezing processes require the presence of INP and can proceed by several physical mechanisms including deposition freezing, contact freezing, immersion freezing, and condensation freezing (Hoose and Möhler 2012). Deposition freezing is defined as water vapor depositing onto an INP, and occurs when the environment is supersaturated with respect to ice and sub-saturated with respect to water at temperatures ranging from -30°C to -40°C, In contact freezing, which occurs at water supersaturation between 0 to -15°C, super-cooled water droplets come into contact with an INP and freeze on contact. Immersion freezing occurs in an environment close to water supersaturation with temperatures ranging from -15°C to – 30°C, and an INP becomes immersed in a drop of water and freezes. Finally, condensation freezing occurs at water saturation between -25°C to -30°C, where water condenses onto an INP and then freezes (Cantrell and Heymsfield 2005).

Dust is an efficient INP and plays an important role in heterogeneous ice nucleation (Cziczo et al. 2013) and has the potential to play an important role in climate (Lohmann and Diehl 2006; Boucher et al. 2013). As an atmospheric aerosol, dust is a highly varying and abundant, representing the second largest natural aerosol primary emission after sea spray (Mahowald et al. 2014). On a global scale, large deserts act as sources, where dust can be lofted into the free troposphere and transported to other regions. For example dust from the Sahara desert can be transported to the eastern United States via the easterly trade winds (Schütz et al. 1981). Local sources of dust and soil also provide significant contributions to aerosol composition, and can make up 15-25% of the aerosol mass in the Central Great Plains throughout the year (Hand et al. 2012).

Quantifying the effects of dust on weather and climate requires being able to accurately simulate the emissions, transport, and fate of dust in the atmosphere (Mahowald et al. 2014). The Weather Research and Forecasting model coupled with chemistry (WRF-Chem, (Grell et al. 2005)) incorporates the emissions, transport and the direct effects of dust aerosols on climate (Zhao et al. 2010). Aerosol indirect effects are also included via activation of aerosols as cloud condensation nuclei (Chapman et al. 2009), although dust alone is not very hygroscopic and does not act as a good cloud condensation nuclei (CCN) for warm cloud formation (Koehler et al. 2009). However, the role of dust in heterogeneous freezing processes is currently not included in the microphysics parameterizations coupled with online chemistry (e.g., the Lin (Hong et al. 2004) and Morrison (Morrison et al. 2005) microphysics schemes), and therefore it does not include the indirect effects resulting from dust. In the current implementation of the model, heterogeneous freezing processes are represented using a temperature-only dependent empirical, experimentally derived parameterization (Cooper 1986; Meyers et al. 1992). Temperature-only

dependent schemes do not capture the ice number particle concentration, and including dust in an empirical parameterization has been shown to improve the predicted number of ice particles (DeMott et al. 2010). An improved ice particle number prediction means potentially an improved representation of ice clouds and the radiative impacts of these clouds.

In this work, we replace the current ice nucleation parameterization in the Morrison microphysics scheme with a parameterization that includes deposition nucleation (Phillips et al. 2008) and immersion freezing (DeMott et al. 2010; Thompson and Eidhammer 2014) as a function of dust number concentrations and temperature. We simulate a mesoscale super-cell event that produced severe weather on May 29, 2012 and large hail north of Oklahoma City, OK. This event was observed as part of the Deep Convective Clouds and Chemistry (DC3) campaign (Barth et al. 2015b) and is therefore provides a unique opportunity to compare the new parameterization with a detailed set of observations of aerosols and clouds. To place the relative importance of these ice nucleation changes into the context of the internal model variability, we perform a sensitivity study using an ensemble of simulations . We examine how including dust concentrations in the ice nucleation parameterization affects a super-cell storm and its anvil cloud, and thus its radiative impacts. In section 2, we describe the model configuration and experimental design. We compare the meteorology of the event to the simulations and examine the results of the experiments in section 3. Finally, in section 4 we discuss the effects of the addition of the new ice nucleation parameterization changes and their potential impacts on the simulation of severe weather events.

4.2.0 Methods

4.2.1 Model configuration

To better understand the effects of dust as ice nucleating particles on a severe storm, we use the Weather Research and Forecasting model coupled with chemistry, (WRF-Chem version 3.6; (Grell et al. 2005))with modifications to the microphysics parameterization discussed in Section 2.2 below. We simulate a severe weather event with large hail reported (> 2 inch diameter (Center 2012)) that occurred on May 29-30, 2012 in Oklahoma. Because supercell thunderstorms are governed primarily by mesoscale processes, we simulate a nested domain to capture the fine horizontal resolution needed to represent the event, where the outer domain has a horizontal grid spacing of 4 km and the inner domain has a horizontal grid spacing of 1.33 km (Figure 4.1), with 72 vertical levels in all simulations. In the outer domain, we use a dynamical timestep of 15 seconds and a chemical timestep of 1 minute, and a dynamical timestep of 10 seconds and a chemical timestep of 30 seconds in the inner domain. To simulate planetary boundary layer processes we use the Yonsei-University scheme (Hong et al. 2006), with surface physics represented by the Monin-Obukov scheme. Cloud physics are resolved by the Morrison microphysics scheme with modifications (Morrison et al. 2005). Because we are explicitly resolving convection, no cumulus parameterization is used in the inner or outer domains. Long and short wave radiation is represented by the RRTMG (Price et al. 2014) parameterization, which is coupled with aerosols to represent the direct effects and coupled to the microphysics to represent the indirect effects. Meteorological boundary conditions are derived from the NAM-Reanlysis (12km, (NCEI 2013)) and are updated every 6 hours.

Gas-phase chemistry is represented by the Regional Acid Deposition Model v2 (RADM2, (Stockwell et al. 1990)) mechanism and aerosol chemistry is represented by the MADE-SORGAM model (Ackermann et al. 1998; Schell et al. 2001). Chemical emissions are provided

for anthropogenic emissions by the 2011 US EPA National Emissions Inventory (NEI) (EPA 2011) and biogenic emissions are simulated by the MEGAN v2 model (Guenther et al. 2006). MOZART-GOES4 chemical boundary conditions are applied to the outer 4 km domain only, and include dust (Emmons et al. 2010). Additionally, we scale dust by 2.5 from these boundary conditions to match surface observations (see discussion in Section 2.5).

4.2.2 Aerosol Representation

Several chemical and physical parameterizations can be combined to represent aerosol-cloud interactions in the WRF-Chem framework. In this experiment, we use RADM2-MADE/SORGAM with aqueous chemistry. The MADE/SORGAM mechanism represents aerosols by three log normal, internally mixed modes: the Aitken (10 nm – 100 nm) mode, the accumulation mode (100 nm – 2.5 microns), and the coarse mode (> 2.5 microns). The Aitken and accumulation modes includes up to sixteen chemical species: ammonium, nitrate, sulfate, sodium, chloride, elemental carbon, primary organic aerosol, and nine types of secondary organic aerosols simulated by SORGAM. The coarse mode includes up of three chemical constituents: sea salt, un-speciated anthropogenic aerosol, and mineral dust. In this work, we focus on the dust coarse mode aerosol.

4.2.3 Description of microphysics and model development

The Morrison microphysics is a two-moment bulk parameterization that tracks the number concentrations and mass mixing ratios for five hydrometeor species (cloud drop, raindrop, snow, ice, graupel/hail) and the water vapor mixing ratio (Morrison, 2005). The growth and decay of these hydrometeor species is determined by the environmental supersaturation, interactions between hydrometeors and the environment, and hydrometeors with

other hydrometeors. A full description of this microphysics scheme that includes ice and liquid processes can be found in Morrison et al (2009). Of particular importance in this study are the ice nucleating processes. In the original parameterization, the total number of ice nuclei (n_{IN}; # cm^{-3}) is calculated as a function of the total probability of a particle with radius *D* freezing (P_{tot}):

$$n_{IN} = 1/\Delta t \int f_a(r_D) P_{tot}\, dr_D. \quad (1)$$

where P_{tot} is a function of the combined probabilities of a particle freezing either heterogeneously (P_{CF}) or homogeneously (P_{HF}):

$$P_{tot} = P_{CF} + P_{HF} - P_{CF}P_{HF}. \quad (2)$$

Heterogeneous freezing (P_{HF}) is assumed to only include condensation freezing of deliquesced aerosol containing an insoluble nucleus surrounded by soluble material and occurs as a function of temperature and ice supersaturation (Cooper, 1986), and is defined as:

$$P_{CF} = 1 - \exp(-J_{CF}(r_N))\Delta t, \quad (3)$$

where J_{CF} is the rate of freezing from condensation. Equation 4 represents the probability of a drop freezing homogeneously (P_{HF}):

$$P_{HF} = 1 - \exp(-J_{HF}(r_w)(4\pi/3)(r_w^3 - r_N^3)\Delta t), \quad (4)$$

where J_{HF} is the rate of homogeneous freezing. Deposition of vapor onto aerosol is not considered. While these equations were configured with aerosols at a constant value, they are represented in the model as functions of only temperature and supersaturation with respect to ice and water. In this work, we replace this total ice nucleation rate with a parameterization that depends on coarse-mode dust number concentrations.

One prior study with WRF tested the influence of INP on weather events. Thompson and Eidhammer (2014) show that including ice-nucleating particles improves meteorological evaluation of a mid-latitude cyclone by incorporating an aerosol aware framework into the Thompson microphysics scheme. In regimes where the environment is supersaturated with respect to ice and sub-saturated with respect to water, they assume deposition nucleation is the primary process and incorporate heterogeneous freezing by deposition nucleation following the methodology from Phillips et al (2008). In this parameterization, the number of activated ice nucleating particles (n_{IN}) is a function of μ, which is dependent on the aerosol size distribution (D_X), temperature (T) and ice supersaturation (S_i):

$$n_{IN,X} = \int \{ 1 - \exp[-\mu_X(D_X,S_i,T)]\} \times dn_X/d \log D_X \quad (5)$$

where μ_X is a function of the total surface area (Ω_x) of all coarse mode aerosols:

$$\mu_X = H_X(S_i, T)\, \xi(T) \left(\alpha_X n_{IN}/\Omega_X\right) \times d\Omega_X/dn_X \quad (6)$$

In this expression, H_x refers to an empirically derived fraction that describes heterogeneous nucleation in sub-saturated conditions, α_X is the fractional contribution of aerosol to n_{IN} from the aerosol group X. $\xi(T)$ is assigned a value of zero for temperatures warmer than -2°C or a value of one for temperatures colder than -5°C, using a cubic interpolation between these values. Immersion freezing at near water saturation is implemented via the DeMott et al (2010) ice nucleation parameterization:

$$n_{IN,T^k} = a(273.16 - T_k)^b (n_{aer,0.5})^{(c(273.16-T_k)+d)} \quad (7)$$

where $n_{aer,0.5}$ refers to the number of coarse mode aerosols and T_k is the atmospheric temperature in Kelvin. Homogeneous freezing at very cold temperatures is included, as is the freezing of cloud and raindrops. In the Thompson and Eidhammer (2014) study, vertical profiles of hygroscopic, or "cloud-friendly", aerosol concentrations and ice nucleating, or "ice-friendly," aerosol concentrations that can activate as cloud drops or act as INP for ice crystal formation were prescribed. Our study differs from this work because in our configuration, aerosols are not prescribed; they are emitted, transformed, advected and removed with the chemistry component of the model. Additionally, these aerosols are allowed to interact with meteorology, where their presence can influence meteorology and their concentrations can be altered by meteorology, either through radiative or cloud and precipitation feedbacks.

Here, we modify the Morrison microphysics to relate environmental factors of temperature, ice supersaturation, water supersaturation, and aerosol number concentrations to an ice nucleation rate. Then, we replace the original ice nucleation rate by providing dynamic coarse mode aerosol concentrations to the Morrison microphysics parameterization via the Phillips (2008) (Equations 5 and 6) and DeMott et al (2010) ice nucleation scheme (Equation 7). The total ice nucleation rate is based on the dust concentration as the coarse number concentration, which is calculated as part of the emissions/tracer scheme. The number concentration of dust (coarse soil) is passed into the microphysics module and together with environmental factors, determines the total ice nucleation rate. Because this event is characterized by hail, we enable the switch within the WRF-Chem that changes the graupel density to hail density (Morrison et al. 2009).

4.2.4 Experimental Design

We employ a nested grid with a 4km horizontal resolution representing a outer domain and a 1.3 km resolution inner domain to understand the role of the new INP on the simulation of microphysics and the supercell event. In all following analysis, we focus on the results of the fine resolution inner domain. To address the model's sensitivity to including dust as ice nuclei, we incorporate an ensemble approach to the sensitivity simulations for the fine (1.3 km) resolution domain as described below and in Table 4.1.

We conduct three coarse resolution simulations at 4-km horizontal grid cell size for the outer domain (Figure 4.1). The first simulation uses the original Morrison microphysics scheme (MMP) and scales dust emissions to match surface aerosol observations (described in Section 2.5). The second simulation uses the modified microphysics scheme and also scales boundary layer dust to match surface observations (MMP+IN). The third simulation also uses the modified microphysics scheme but scales boundary dust to one tenth of the MMP+IN simulation (MMP+0.1IN) to understand the sensitivity of microphysics to the amount of dust present in the atmosphere. These coarse resolution simulations provide the boundary conditions for the ensemble of inner domain simulations with 1.33 km grid cell size.

We then performed five inner-domain simulations using the original microphysics scheme (MMP; 5 members), and three simulations using the newly incorporated dust as IN microphysics scheme (MMP+IN; 3 members). Because running multiple ensemble members is computationally expensive, we use five members to explore the internal variability in the standard simulation (i.e., MMP) and fewer members for the sensitivity tests. To test the model sensitivity to dust concentrations, we complete three additional members using the newly incorporated dust as IN microphysics scheme with one tenth of the original dust (MMP+0.1IN; 3 members). Ensemble members are created by perturbing the initial conditions in the wrfinput

data file where the perturbation temperature is modified by a statistically generated value that is derived by the ensemble member number and a given variance (NOAA 2007). This method was initially developed by the WRF Working Group 13: Ensemble Forecasting group, and is modified for this study.

4.2.5 Surface Concentration of Soil: Dust characterization 4km MMP

To test the sensitivity of the microphysics to the aerosol-cloud interactions, a static dust emission is preferable, as online dust emissions would evolve with changing microphysics and precipitation. For this reason, we use the MOZART boundary conditions to provide dust concentrations to the outer 4km domain (Emmons et al, 2010). Dust emissions at the boundaries are relatively low (~1.5 μg m^{-3} at the surface), increasing with altitude to 18.5 μg m^{-3} at 4.5 km, and then decrease back to close to 1 μg m^{-3}at 15 km.

To simulate a realistic surface concentration of dust, we increased the incoming coarse mode soil from MOZART boundary conditions by a factor of 2.5 on the 4-km domain. We then average over the region encompassing the 1.33 km inner domain boundary layer over 24 hours (12Z-12Z) and compare to observed surface PM_{10} concentrations from the three **I**MPROVE sites (Malm et al. 1994) located within the experimental domain. These sites include Tallgrass, KS, Cedar Bluff, KS, and Stilwell, OK (Figure 4.1). The average IMPROVE PM10 concentration for May 29 is 17 mg m^{-3} (Figure 4.2a, solid gray), and the 4km MMP simulated soil concentration of 14 mg m^{-3} (Figure 4.2a, horizontal lines gray) compares well with the observed values of PM_{10}. We use a scaling factor of 2.5 to drive the MMP and MMP+IN ensemble members' boundary conditions for dust. This results in the inner domain having lower concentrations than the 4km domains, e.g., the inner domain (1.33 km resolution) soil concentration is 10 mg m^{-3} (Figure 4.2a, slanted gray lines). When using a scaling factor of 0.25,

the 4-km domain (Figure 4.2a, gray hashing) simulated surface soil concentration is 6 mg m^{-3}, resulting in the inner domain surface concentration of 7 mg m^{-3} (Figure 4.2a, gray dots).

The modeled inner-domain average vertical profile of dust shows that much of this occurs in the mid-troposphere, with the local maxima occurring at 4.5 km (~20 mg m^{-3}) (Figure 4.2b). The MMP1-5 and MMP+IN1-3 members all have indistinguishable soil concentration differences, showing that the soil concentration is consistent between members and is therefore strongly dependent on initial boundary conditions. The MMP+0.1IN1-3 members simulate values near 2 mg m^{-3}at 4.5 km, reflecting the initial ten percent scaling factor. This consistency between ensemble members indicates that changes between the MMP and MMP+IN simulations are due primarily to the changes in the microphysics parameterization and not the dust concentrations.

4.3.0 Results

4.3.1 Meteorology

In this study, we investigate the formation of a supercell over north-central Oklahoma on May 29, 2012, as this storm system was sampled by the DC3 campaign from May 29 1950 UTC to May 30 0125 UTC (Barth et al. 2015a). In the observed radar reflectivity (Figure 4.3), the storm of interest begins at 2100 UTC on May 29, 2012 (Figure 4.3a) just south of the Kansas state line near Enid, Oklahoma. This cell develops and moves eastward as another region to the south begins to develop at 2130 UTC (Figure 4.3b). By 2300 (Figure 4.3e), the cells have intensified and some have merged. Thirty minutes later at 2330 UTC (Figure 4.3f), smaller cells quickly pop up north of Oklahoma City, while the larger cells slowly move eastward to form a NW to SE axis of convection. By 0000 UTC (Figure 4.3g), the region of active convection has

grown, extending both east and west of Enid, OK, with several cells of intense rain observed with radar reflectivity values exceeding 65 dbz, indicating the presence of hail. The largest cell slowly moves to the southeast and begins to dissipate and forms a squall line (00:30 UTC; Figure 4.3h) as it merges with the outflow from the smaller cells. This squall line then continues to move southeast into Arkansas and Texas from 01:00 UTC to 06:00 UTC (not shown). North of the region of main convection, storms initiate as the outflow boundary from the super-cell propagates north.

Qualitatively, the model simulates the super-cell, though the convective initiation is displaced to the south of the Kansas-Oklahoma state line and initiates an hour before observed, at 20:00 UTC instead of 21:00 UTC (Figure 4.4). Additionally, the model produces more convective cells both to the south and north of the super-cell than observed. For brevity, we examine a single 1 km MMP member (MMP4), where the radar reflectivity is calculated within the microphysics. At 20:00 UTC (Figure 4.4a) a simulated cell of convection initiates at 98W and 36N, roughly an hour earlier than observed. This cell grows and moves east like the observed cells, however, the model also simulates the growth of cells to the north, which is not observed (Figure 4.4b-d). At 2200 UTC, the modeled cells are further east and closer to Oklahoma City, OK than the observed cells at 23:00 (Figure 4.4e), and then the simulated cells merge and move southeast. By 2300 UTC, the number of individual cells increases on the tail end of the storm (Figure 4.4g), which is similar the observed radar. The northern and central cells merge and then move eastward more quickly than observed. Overall, intense convection occurs in approximately the right place at the right time, despite the fact that smaller-scale features show some discrepancies.

4.3.2. Precipitation: Rain

To understand the effects of altering the ice nucleation microphysics parameterization on precipitation patterns, we examine the rain accumulated over the hours from May 29, 1800 UTC – May 30 0900 UTC. The MMP(1-5) ensemble mean has two regions with intense precipitation (> 60 mm; Figure 4.5a), and here we focus on one of these regions defined by the swath straddling the Kansas – Oklahoma state line denote it as "Region 1" (R1, red box Figure 4.5a). Individual members (not shown) demonstrate larger maxima (> 75 mm) and smaller minima locally, but overall produce a similar precipitation pattern. We can qualitatively describe the differences between the MMP ensemble mean and the MMP+IN ensemble mean in this region. In R1, there is a shift northward of accumulated precipitation. Compared to the MMP ensemble, precipitation in the MMP+IN ensemble is enhanced on the northern end of the accumulated precipitation and suppressed to the south (Figure 4.5b), with similar magnitudes for both suppression and enhancement (30-40 mm). A similar spatial difference pattern repeats in the MMP+0.1IN (Figure 4.5c) ensemble mean with weaker magnitudes (~20-30 mm) in R1.

To compare the overall magnitude of precipitation change for this region, the R1-spatially averaged (Figure 4.5a, red box) accumulated rain exhibits less variation than the spatial representation (Figure 4.5d). Rain begins to accumulate in all eleven members beginning at 2200 UTC on 5-29, and continues until 0900 UTC on 5-30. It is difficult to distinguish between members until the rain rate subsides at around 0200 UTC. While the spatial differences of accumulated rain between both ensemble members and ensemble means are on the order of 50%, the MMP and MMP+0.1IN ensemble member accumulated rain values overlap each other. By the end of the rain period, the ensemble members all range within 1 mm of each other (22 mm < X < 23 mm), but the MMP+IN's slight increase indicates a potential shift towards enhanced rain amounts. Overall, this suggests that the impacts of the new INP on accumulated precipitation

are relatively small. The shift in the spatial patterns of intense precipitation and the small change in the domain-averaged precipitation indicate the system may be water limited. Additionally, the mesoscale environment may have a larger influence on precipitation amounts than including dust as INP.

4.3.3 Storm Intensity

As there is little variability in the accumulated rain, we take another approach to understand how the inclusion of dust as IN may affect storm intensity via the ensemble members' probability density functions (PDF) for accumulated precipitation, maximum 10-meter wind speed, and maximum updraft velocity. While rainfall amounts are not used to assess whether or not a storm is severe, rainfall intensity is a metric used for forecasting flooding threats. Including dust as IN leads to a slight shift in the accumulated precipitation PDF, where the largest probability of the MMP+IN ensemble occurs at 4 mm of accumulated precipitation (Figure 4.6a). Decreasing dust concentrations (MMP+0.1IN) leads to a slight increase in the probability of greater accumulated precipitation amounts compared to the MMP+IN ensemble mean. The shift in the distribution of the MMP+IN ensemble towards less rain indicates that including dust as IN might lead to more low-intensity rainfall events and fewer high-intensity rainfall events. Decreasing the dust concentration (e.g., the MMP+0.1IN) somewhat mitigates this effect, indicating competing processes that determine rainfall intensity. However, these changes in the distribution are small and generally fall within the variability of the MMP ensemble spread (Figure 4.7a).

In addition to rainfall, both horizontal and vertical wind speeds are useful metrics in determining storm intensity. The probability of occurrence for 10-m maximum wind speeds has a normal distribution for the MMP ensemble. The largest probability (30.5%) occurrs at a wind

speed of 12.5 m s^{-1} (Figure 4.6b). Including dust as IN (MMP+IN) decreases the probability of weaker horizontal winds and increases mid-range intensity wind speeds. However, no change in probability occurs for stronger winds (> 16 m s^{-1}). Decreasing the dust concentrations (MMP+0.1IN) leads to an overall shift towards weaker winds, highlighting the complexity of disentangling the microphysics feedbacks into mesoscale systems. These weaker winds do not necessarily mean that the storm is less intense, as it could also indicate a larger area of convection occurring with changes to the microphysics. These changes in the ensemble means come from a large variability between ensemble members (Figure 4.7b), thus there is a large degree of uncertainty associated with these differences.

Finally, we examine the maximum updraft velocities. The MMP ensemble mean (Figure 4.6c) has a U-shaped distribution, with largest probabilities occurring for strong and weak updrafts. Including dust as IN (MMP+IN) changes the distribution by decreasing the probability for weaker updraft velocities and increasing the probability for mid-range updrafts. Decreasing dust concentrations (MMP+0.1IN) leads to a slight probability increase in weak updraft range, when compared to the MMP+IN ensemble, and an increase in the probability of a stronger updraft velocity occurring at 22.5 m s^{-1}. However, no change occurs in the tail end of this distribution, as the probability of updraft velocities exceeding 27 m s^{-1} is 9.5% for all three ensemble means. Like the 10-meter maximum wind speed, the updraft velocity individual ensemble members are noisy, with a wide range of variability, especially with increasing updraft strength (Figure 4.7c). Therefore, the differences between the ensemble's means come with the caveat of relatively large uncertainty.

Including dust as IN has little effect on the highest values, suggesting that the inclusion of an interactive dust-microphysics scheme does not affect the strongest intensity systems.

However, there is a general shift towards the mid-range intensities of updrafts, indicating mid-range intensities might be more readily influenced by these changes.

4.3.4 Precipitation: Hail

As with rain, we examine the amount of hail accumulated during the time period from May 29 1800 UTC – May 30, 0900 UTC over the inner domain. Spatially, the five-member MMP ensemble mean is similar to the accumulated rain, with maximum accumulations occurring within region R1 (Figure 4.8a; ~1.5 mm). Individual ensemble members have higher maxima, exceeding 4 mm (not shown). The difference between the MMP and the MMP+IN accumulated hail ensemble means also have a similar spatial pattern to the difference of accumulated rain ensemble means, which is expected as hail and rain are likely to be co-located. The R1 differences between the MMP ensemble means and the sensitivity ensemble means are noisier than the accumulated rain differences, with differences are on the order of 50% (1-2 mm) for both the MMP+IN (Figure 4.8b) and the MMP+0.1IN (Figure 4.8c) ensemble means.

The spatially averaged time series of accumulated hail, like accumulated rain, is less variable than the corresponding spatial representations. The MMP ensemble spread ranges from 0.31-0.36 mm (0.05 mm; Figure 4.8d). The MMP+IN spread ranges from 0.33 to 0.40 (0.07 mm), and the MMP+0.1IN spread falls in the middle of the two from 0.31 to .35 (0.04 mm). While these differences are small, the increase in MMP+IN follows that of the increase in rain totals and does not overlap with the MMP ensemble variability on the upper limit, and therefore may be statistically significant. Hydrometeor differences may be driving these changes, and we discuss this in the following section.

Overall, the amount of precipitation falling in the domain does not change significantly with changes to both the microphysics parameterization and the dust concentration. Despite the

small differences in the regionally averaged accumulated precipitation or rain and hail, the spatial changes in the accumulated precipitation fields of rain and hail are large and on the order of 50% or greater in magnitude. The lack of variability within the spatial averages indicates that the system is water limited and the regions of precipitation are affected more than the total precipitation amounts.

4.3.5 Hydrometeors

Changes in precipitation rates are driven by hydrometeor changes, and in this section we examine the vertical structure of modeled hydrometeors (including ice crystals, snow, hail, raindrops, and cloud drops) to understand how the microphysical changes driven by the INP parameterization affect precipitation rates. Each vertical profile is constructed by averaging spatially over R1 (Figure 4.1) and temporally from May 29, 18:00 UTC – May 30, 09:00 UTC. For each hydrometeor, we discuss the general structure of the MMP ensemble mean number concentration and the variability of the ensemble members, and compare with the MMP+IN and MMP+0.1IN ensembles. Finally, we examine probability density functions (PDFs) of hydrometeor effective radii over all altitudes to understand the role of changing size distributions.

4.3.5.1 Ice

Because the DeMott and Phillips parameterizations affect ice nucleation rates within the microphysics system, the hydrometeor most likely to be affected is the ice hydrometeor. Maximum ice hydrometeor number concentrations (# L^{-1}, Figure 4.9a) occur at 10.5 km, where the MMP ensemble mean number concentration is 760 L^{-1}. The members' variability at 10.5 km ranges from 752 to 789 L^{-1} and there is clear distinction between the three ensembles (MMP, MMP+IN and MMP+0.1IN) at this altitude, suggesting a significant change to the ice

hydrometeor number concentrations when we include dust as IN. The MMP+IN ensemble mean number concentration maximum still occurs at 10.5 km but its magnitude is a factor of five smaller than the MMP ensemble mean (142 L-^{1}) (Figure 4.9a). Like the MMP members, the MMP+IN member variability is also small, with maximum values ranging from 126 to 153 L^{-1}. Decreasing the dust concentration to 10% (MMP+0.1IN) leads to only a small change in ice number concentration when compared to the MMP+IN ensemble (132 L^{-1} at 10.5km) with low variability between members (from 119 to 145 L^{-1}). These changes indicate that the physical representation of ice nucleation within the microphysics has a larger and more significant effect on ice number concentrations than the concentrations of dust. These changes are directly related to the ice nucleation rate (not shown), which decreases with the inclusion of interactive dust as INP.

Hydrometeor size, also referred to as the effective radius, is an important feature of the hydrometeor because it determines fall speed and radiation impact. The probability density function of the ice effective radius (Figure 4.9e) demonstrates a shift in ice hydrometeor size when changing the microphysics parameterization. The MMP members have a normal distribution, where an effective radii of 80 microns have the largest probability of occurrence. The variability between the MMP members is indistinguishable. However, there is a clear shift in the effective radius distribution when considering dust as IN where the MMP+IN and MMP+0.1IN ensembles have a lower probability of being smaller (< 100 microns) and a greater probability of being larger (> 100 microns). This clear shift towards larger hydrometeors corresponds with the reduced number concentrations.

4.3.5.2 Snow

The maximum snow number concentrations occur between an altitude of 9.5 and 10 km for all ensemble members (Figure 4.9b). The MMP ensemble mean snow number concentration maximum value is 55 L^{-1}, with an ensemble range from 54 to 56 L^{-1}. These differences between members are small when compared with the differences between ensembles. The MMP+IN ensemble mean snow number concentration maximum value at 9.5km altitude is 35 L^{-1}, and this 20 L^{-1} change represents a 36% reduction in number concentration. The MMP+IN members do not overlap with the MMP ensemble members at 9.5 km and have a similar spread, ranging from 34 L^{-1} to 37 L^{-1}. Finally, the MMP+0.1IN ensemble mean maximum snow number concentration is 35 L^{-1}, with slightly less variability in ensemble members with maximum concentrations ranging from 35 L^{-1} to 36 L^{-1}. As with the ice number concentrations, the change in microphysics ice nucleation parameterization has a significant effect on snow number concentrations while the dust concentration does not.

The probability density function of snow hydrometeor size demonstrates that snow effective radius size also changes with the ice nucleation change (Figure 4.9f). MMP ensemble members increase in probability from 139 microns to 190 microns (maximum probability), and then probability decreases slightly as size increases (> 190 microns). The distribution is shifted for both the MMP+IN and the MMP+0.1IN ensemble members. Like the MMP ensemble members, the probability increases with increasing size for the MMP+IN and MMP+0.1IN members. However, the probability of snow radii sized 139 – 224 microns is much lower than the MMP ensemble members. MMP+IN and MMP+0.1IN probability increases until 241 microns, then remains steady. This shift in distribution is similar yet not as strong a that simulated for the ice number, as there is less of an increase in the probability of snow size at larger sizes.

4.3.5.3 Hail

The differences between ensemble means for hail are more subtle than the differences for snow and ice. The maximum values for all ensemble members occur at an altitude of 9 km. The MMP ensemble mean maximum hail number concentration is 28 L^{-1}, with the spread ranging from 27 to 29 L^{-1} (Figure 4.9c). The MMP+IN ensemble mean's maximum hail number concentration is the same, at 28 L^{-1}, with the members' values also ranging from 27 to 29 L^{-1}. The MMP+IN ensemble members overlap with the MMP ensemble members, suggesting no significant change. Reducing the dust concentration leads to a slight increase in hail number concentrations, where the MMP+0.1IN ensemble mean maximum value is 29 L^{-1} (individual members vary from 28 L^{-1} to 30 L^{-1}), overlapping with both the MMP and MMP+IN ensemble members at smaller concentrations. The slight increase in hail number concentrations with the decreased dust concentration suggests that with hail, other processes besides ice nucleation are important in determining the number concentrations. Interestingly, the PDF of hail size (Figure 4.9g) indicates that there could be a significant change in hail size by including dust as IN. The most probable hail size occurrence for all members is hail smaller than 36 microns. For sizes larger than 47 microns, the MMP+IN and MMP+0.1IN members all have a greater probability, indicating that in the unaltered simulations, hail is likely to be smaller than when including dust as IN. The differences between the MMP+IN and MMP+0.1IN members are indistinguishable. Therefore, hail number concentrations are more sensitive to dust concentrations than the change in ice nucleation rates, while the hail size is more sensitive to the change in ice nucleation rate than the dust concentrations. Hail accumulation was more sensitive to the change in ice nucleation rate (Figure 4.9d), indicating that the change in size could drive the change in accumulation.

4.3.5.4 Raindrops

The MMP ensemble mean rain drop number concentration has a bimodal vertical distribution, with an overall maximum of 63 L^{-1} at 6 km and another local maximum of 56 L^{-1} at 4 km (Figure 4.9d). The MMP ensemble members exhibit the greatest variability of all three ensembles, ranging from 53 L^{-1} to 66 L^{-1}. Including dust as IN (MMP+IN) leads to a larger maximum raindrop number concentration at 6 km (64 L^{-1}), and the local maximum at 4km is not simulated. Finally, the MMP+0.1IN ensemble mean raindrop number concentrations are less than the MMP and MMP+IN from altitudes from 3.5 km to 7 km. The maximum value at 6 km (56 L^{-1}) is significantly less than raindrop number concentrations from the MMP and MMP+IN ensembles, with a similar variability (53-58 L^{-1}). There is a distinct difference between the MMP+0.1IN and the other two ensembles, which suggests that like hail, rain hydrometeors are more sensitive to the dust concentration than to the change in ice nucleation rate.

Raindrop effective radii distributions are generally noisy and including dust as IN and decreasing the dust concentration lead to raindrop size distributions that fall within the variability of the MMP ensemble members (Figure 4.9h). The increase in MMP+IN raindrop number concentrations at higher altitudes corresponds with the decrease in hail number concentrations, while the decrease in MMP+0.1IN raindrop number concentrations corresponds with an increase in the hail number concentrations. This sensitivity could be a result of the greater hail number concentrations in the MMP+0.1IN ensemble, and representing the complex role ice hydrometeors play in the formation of raindrops, especially in mixed phase clouds.

Cloud drop number concentrations are not significantly affected by including dust as IN or by decreasing the dust concentrations (not shown). Because aerosol activation happens within

the accumulation mode, we would not expect that including dust as IN and changing dust emissions would have a large effect on cloud drop formation.

4.3.6 Liquid Water Path, Ice Water Path, and Radiation

To link precipitation and hydrometeor changes, we examine the R1-averaged time series of the liquid and ice water paths (LWP and IWP, respectively; kg m^{-2}). The LWP and IWP are useful metrics because they represent the total column amount and phase of water residing in the atmosphere. LWP, which includes raindrops and cloud drops, increases slightly with the initiation of convection at 20:00 UTC (Figure 4.10a). As the storm system builds, hydrometeor mass increases rapidly, peaking at 00:00 UCT, with a value of 0.53 kg m^{-2} for all three ensembles. The differences between the ensemble means are indistinguishable, with similar variability, suggesting that the changes in ice nucleation rate and dust concentration do not significantly affect convection in the early stages. LWP remains consistent between the three ensembles through 02:00 UTC, similar to the accumulated rain (Figure 4.5d). After 02:00 UTC, the MMP ensemble has lower values of LWP than both the MMP+IN and MMP+0.1IN, though the means are within ensemble variability. As the system moves out of R1, LWP continues to decrease and by 06:00 UTC, the differences between ensembles become indistinguishable again.

The R1-averaged IWP (calculated from ice and snow, Figure 4.10b) has a one hour lag from the LWP path maxima, reaching its maximum value at 01:00 UTC instead of 00:00 UTC. Differences between the ensembles become apparent earlier (00:00 UTC), where the MMP+IN leads to lower IWP values. This trend continues from 00:00 UTC until 04:00 UTC, as the IWP decreases. At 04:00 UTC, the MMP IWP continues to decrease. The MMP+IN and MMP+0.1IN ensembles also decrease but at a slower rate, indicating there are more clouds comprised of snow and ice in the region at this time. The hail water path (HWP) is not shown because hail is not

included in the radiation calculation for outgoing longwave radiation. The HWP peaks at 00:00 UTC (like the LWP) and decreases more quickly than either the LWP or IWP, which is indicative of the faster fall speeds associated with the more dense hail hydrometeor.

One of the main climatic implications of deep convection is the effect of resulting ice clouds on Earth's radiation budget. Outgoing longwave radiation (OLR) allows a relationship between the radiation budget and the microphysics. At the beginning of the simulation (May 29 18:00 UTC), there is little cloud development and all the ensembles have the similar values, of 306-307 W m^{-2} (Figure 4.10c). Ensemble differences is difficult to discern until 00:00 UTC on May 30, after convection has initiated in the model and becomes widespread. From 01:00 – 05:00 UTC, the MMP ensemble OLR is distinctly lower than both the MMP+IN and MMP+0.1IN ensembles. The largest difference at 03:00 UTC coincides with the timing of lower IWP values in the MMP+IN and MMP+0.1IN ensembles (Figure 4.9b). The MMP+IN ensemble mean is 18 W m^{-2} greater than the MMP ensemble, and the MMP+0.1IN is 16 W m^{-2} greater than the MMP ensemble. From 01:00 – 04:00 UTC, the differences between the MMP+IN and MMP+0.1IN ensembles are less than the differences between MMP and either of these ensembles. This separation suggests including dust as IN leads to a significant increase in OLR during deep convection, consistent with known theory about the role of INP (Tang et al. 2016). The associated pattern in the IWP indicates that these changes are related to the differences in the ice and snow hydrometeors.

4.3 Discussion and Conclusions

In this work, we implement an ice nucleation parameterization in WRF-Chem that uses interactive dust concentrations. Currently, WRF-Chem does not have a dynamic method to allow dust concentrations to affect the formation of cold clouds, and ice nucleation is based on a

temperature-dependent process only. The new parameterization replaces the existing ice nucleation rate within the Morrison microphysics with an ice nucleation rate that accounts for dust aerosols via deposition freezing based on Phillips et al. (2008), and immersion condensation freezing following DeMott et al. (2010). With the updated model, we simulate a supercell thunderstorm with large hail that occurred on May 29-30, 2012 near the Oklahoma – Kansas state line and incorporate the use of ensembles to address internal model variability.

We find that including interactive dust in the microphysics does not significantly affect the domain total accumulated precipitation amounts. The spatial variability of accumulated rain is large between ensemble means and also between individual ensemble members, suggesting that there is quite of bit of model internal variability that are driving these differences. However, the small differences between the members of domain-averaged accumulated rain totals indicate that including dust as IN does not alter the regional rain amounts and liquid precipitation associated with the simulated storm is not sensitive to changes in the ice nucleation rate. Hail accumulation is also largely insensitive to the ice nucleation rate changes. The vertical profiles of cloud drops, and raindrops are largely unaltered with the change in ice nucleation rate (Figure 4.8). The largest and potentially significant change in raindrop vertical distribution occurs with a change in dust concentration, where the decrease in dust leads to fewer raindrops from altitudes of 3 – 7 km. However, this difference does not lead to a significant change in total accumulated precipitation.

The change in ice nucleation scheme has a considerable effect on two of the three ice hydrometeors (snow and ice). While these changes do not lead to significant changes in precipitation or the intensity of the storms, they do lead to changes in radiation. The outgoing longwave radiation is not sensitive to the change in dust concentration, but it does increase with

representation of ice nucleation. This increase in OLR is a result of the change in ice and snow number concentrations and effective radii sizes, which greatly influence the radiative properties of the cloud. Understanding how ice nucleation representation affects the radiation budget is essential for understanding the cloud and aerosol interactions and mitigating the uncertainty surrounding these quantifications.

While this work represents an advance in the treatment of ice nucleation, we do note a few limitations. While we simulate the supercell using a relatively fine resolution, the 1.33 km grid cell size is not fine enough to capture the process of dust entrainment into the cloud (Craig and Dörnbrack 2015). Not including this process could potentially affect the amount of dust ingested into the storm system and could affect the overall impacts of dust on the storm system. Our simulations use consistent dust concentrations from the boundaries to avoid the potential precipitation-aerosol feedbacks that can occur in these systems. Additionally, while WRF-Chem simulates strong convection during this event, its timing is slightly misplaced and it also simulates more convection than observed by radar reflectivity. However, because all simulations show a similar pattern of convection, our conclusions based on the sensitivity and ensemble simulations capture the impact of the inclusion of a new dust implementation and would likely be consistent regardless of the specific meteorological shortcomings. While this study assesses the inclusion of dust as INP within one particular system, a more complete understanding of how the water limitation in this system influences the microphysics would be useful. Evaluating the amount of supercooled water within the system, and testing the sensitivity of the microphysical parameters and rainfall amounts to an increase in water vapor could accomplish this. However, these additional tests are beyond the scope of this work, but provide useful questions for further research.

In this work, we show that the accumulation of precipitation is not significantly affected by including dust as INP. This supercell system may be water limited. However, the significant differences in snow and ice hydrometeors lead to radiative impacts via changes to the IWP and resulting OLR flux. This study has taken steps taken to account for the first and second indirect effects of dust within WRF-Chem, and this will improve the evaluation of radiation impacts of ice forming nuclei and the potential impacts on storm severity.

Acknowledgements
The Elizabeth Caroline Crosby Grant provided funding for this research.

References

Ackermann, I. J., H. Hass, M. Memmesheimer, A. Ebel, F. S. Binkowski, and U. Shankar, 1998: Modal aerosol dynamics model for Europe: Development and first applications. *Atmospheric environment*, **32,** 2981-2999 %@ 1352-2310.

Albrecht, B. A., 1989: Aerosols, cloud microphysics, and fractional cloudiness. *Science*, **245,** 1227-1230.

Andreae, M. O., D. Rosenfeld, P. Artaxo, A. Costa, G. Frank, K. Longo, and M. Silva-Dias, 2004: Smoking rain clouds over the Amazon. *science*, **303,** 1337-1342.

Barth, M. C., and Coauthors, 2015a: The deep convective clouds and chemistry (DC3) field campaign. *Bulletin of the American Meteorological Society*, **96,** 1281-1309.

Barth, M. C., and Coauthors, 2015b: The Deep Convective Clouds and Chemistry (DC3) Field Campaign. *Bulletin of the American Meteorological Society*, **96,** 1281-1309.

Boucher, O., and Coauthors, 2013: Clouds and aerosols. *Climate change 2013: the physical science basis. Contribution of Working Group I to the Fifth Assessment Report of the Intergovernmental Panel on Climate Change*, Cambridge University Press, 571-657.

Cantrell, W., and A. Heymsfield, 2005: Production of Ice in Tropospheric Clouds: A Review. *Bulletin of the American Meteorological Society*, **86,** 795-807.

Center, S. P., cited 2017. [Available online at http://www.spc.noaa.gov/exper/archive/event.php?date=20120529.]

Chapman, E. G., W. Gustafson Jr, R. C. Easter, J. C. Barnard, S. J. Ghan, M. S. Pekour, and J. D. Fast, 2009: Coupling aerosol-cloud-radiative processes in the WRF-Chem model: Investigating the radiative impact of elevated point sources. *Atmospheric Chemistry and Physics*, **9,** 945-964.

Cooper, W. A., 1986: Ice initiation in natural clouds. *Precipitation Enhancement—A Scientific Challenge*, Springer, 29-32.

Craig, G. C., and A. Dörnbrack, 2015: Entrainment in cumulus clouds: What resolution is cloud-resolving? *Journal of the Atmospheric Sciences*, **72**.

Cziczo, D. J., and Coauthors, 2013: Clarifying the dominant sources and mechanisms of cirrus cloud formation. *Science*, **340,** 1320-1324.

DeMott, P. J., and Coauthors, 2010: Predicting global atmospheric ice nuclei distributions and their impacts on climate. *Proceedings of the National Academy of Sciences*, **107,** 11217-11222.

Emmons, L., and Coauthors, 2010: Description and evaluation of the Model for Ozone and Related chemical Tracers, version 4 (MOZART-4). *Geoscientific Model Development*, **3,** 43-67.

EPA, 2011: National Emissions Inventory.

Fan, J., D. Rosenfeld, Y. Yang, C. Zhao, L. R. Leung, and Z. Li, 2015: Substantial contribution of anthropogenic air pollution to catastrophic floods in Southwest China. *Geophysical Research Letters*, **42,** 6066-6075.

Fan, J., L. R. Leung, D. Rosenfeld, Q. Chen, Z. Li, J. Zhang, and H. Yan, 2013: Microphysical effects determine macrophysical response for aerosol impacts on deep convective clouds. *Proc Natl Acad Sci U S A*, **110,** E4581-4590.

Grell, G. A., S. E. Peckham, R. Schmitz, S. A. McKeen, G. Frost, W. C. Skamarock, and B. Eder, 2005: Fully coupled "online" chemistry within the WRF model. *Atmospheric Environment*, **39,** 6957-6975.

Guenther, A., T. Karl, P. Harley, C. Wiedinmyer, P. Palmer, and C. Geron, 2006: Estimates of global terrestrial isoprene emissions using MEGAN (Model of Emissions of Gases and Aerosols from Nature). *Atmospheric Chemistry and Physics Discussions*, **6,** 107-173.

Hand, J. L., B. A. Schichtel, M. Pitchford, W. C. Malm, and N. H. Frank, 2012: Seasonal composition of remote and urban fine particulate matter in the United States. *Journal of Geophysical Research*, **117**.

Heymsfield, A. J., and R. M. Sabin, 1989: Cirrus crystal nucleation by homogeneous freezing of solution droplets. *Journal of the Atmospheric Sciences*, **46,** 2252-2264.

Hong, S.-Y., J. Dudhia, and S.-H. Chen, 2004: A revised approach to ice microphysical processes for the bulk parameterization of clouds and precipitation. *Monthly Weather Review*, **132,** 103-120.

Hong, S.-Y., Y. Noh, and J. Dudhia, 2006: A new vertical diffusion package with an explicit treatment of entrainment processes. *Monthly Weather Review*, **134,** 2318-2341.

Hoose, C., and O. Möhler, 2012: Heterogeneous ice nucleation on atmospheric aerosols: a review of results from laboratory experiments. *Atmospheric Chemistry and Physics*, **12,** 9817.

Koehler, K. A., S. M. Kreidenweis, P. J. DeMott, M. D. Petters, A. J. Prenni, and C. M. Carrico, 2009: Hygroscopicity and cloud droplet activation of mineral dust aerosol. *Geophysical Research Letters*, **36**.

Lohmann, U., and K. Diehl, 2006: Sensitivity studies of the importance of dust ice nuclei for the indirect aerosol effect on stratiform mixed-phase clouds. *Journal of the Atmospheric Sciences*, **63,** 968-982.

Mahowald, N., S. Albani, J. F. Kok, S. Engelstaeder, R. Scanza, D. S. Ward, and M. G. Flanner, 2014: The size distribution of desert dust aerosols and its impact on the Earth system. *Aeolian Research*, **15,** 53-71.

Malm, W. C., J. F. Sisler, D. Huffman, R. A. Eldred, and T. A. Cahill, 1994: Spatial and seasonal trends in particle concentration and optical extinction in the United States. *Journal of Geophysical Research: Atmospheres*, **99,** 1347-1370.

Meyers, M. P., P. J. DeMott, and W. R. Cotton, 1992: New primary ice-nucleation parameterizations in an explicit cloud model. *Journal of Applied Meteorology*, **31,** 708-721.

Morrison, H., J. Curry, and V. Khvorostyanov, 2005: A new double-moment microphysics parameterization for application in cloud and climate models. Part I: Description. *Journal of the Atmospheric Sciences*, **62,** 1665-1677.

Morrison, H., G. Thompson, and V. Tatarskii, 2009: Impact of Cloud Microphysics on the Development of Trailing Stratiform Precipitation in a Simulated Squall Line: Comparison of One- and Two-Moment Schemes. *Monthly Weather Review*, **137,** 991-1007.

NCEI, 2013: North American Model-Reanalysis, 6-hourly dataset. NCEI, Ed., http://nomads.ncdc.noaa.gov/data/namanl/201305/.

NOAA, cited 2015: WRF Working Group 13: Ensemble Forecasting. [Available online at http://www.nssl.noaa.gov/users/stensrud/public_html/wg13/.]

Phillips, V. T. J., P. J. DeMott, and C. Andronache, 2008: An Empirical Parameterization of Heterogeneous Ice Nucleation for Multiple Chemical Species of Aerosol. *Journal of the Atmospheric Sciences*, **65,** 2757-2783.

Price, E., J. Mielikainen, M. Huang, B. Huang, H.-L. A. Huang, and T. Lee, 2014: GPU-accelerated longwave radiation scheme of the Rapid Radiative Transfer Model for General Circulation Models (RRTMG). *IEEE Journal of Selected Topics in Applied Earth Observations and Remote Sensing*, **7,** 3660-3667 %@ 1939-1404.

Rosenfeld, D., 2000: Suppression of rain and snow by urban and industrial air pollution. *Science*, **287,** 1793-1796.

Rosenfeld, D., and Coauthors, 2008: Flood or drought: how do aerosols affect precipitation? *science*, **321,** 1309-1313.

Schell, B., I. J. Ackermann, H. Hass, F. S. Binkowski, and A. Ebel, 2001: Modeling the formation of secondary organic aerosol within a comprehensive air quality model system. *Journal of Geophysical Research: Atmospheres*, **106,** 28275-28293.

SCHÜTZ, L., R. JAENICKE, and H. PIETREK, 1981: Saharan dust transport over the North Atlantic Ocean. *Geological Society of America Special Papers*, **186,** 87-100.

Stevens, B., and G. Feingold, 2009: Untangling aerosol effects on clouds and precipitation in a buffered system. *Nature*, **461,** 607-613.

Stockwell, W. R., P. Middleton, J. S. Chang, and X. Tang, 1990: The second generation regional acid deposition model chemical mechanism for regional air quality modeling. *Journal of Geophysical Research: Atmospheres (1984–2012)*, **95,** 16343-16367.

Tang, M., D. J. Cziczo, and V. H. Grassian, 2016: Interactions of Water with Mineral Dust Aerosol: Water Adsorption, Hygroscopicity, Cloud Condensation, and Ice Nucleation. *Chem Rev*, **116,** 4205-4259.

Thompson, G., and T. Eidhammer, 2014: A Study of Aerosol Impacts on Clouds and Precipitation Development in a Large Winter Cyclone. *Journal of the Atmospheric Sciences*, **71,** 3636-3658.

Twomey, S., 1974: Pollution and the planetary albedo. *Atmospheric Environment (1967)*, **8,** 1251-1256.

Twomey, S., 1977: The influence of pollution on the shortwave albedo of clouds. *Journal of the atmospheric sciences*, **34,** 1149-1152.

Zhao, C., and Coauthors, 2010: The spatial distribution of mineral dust and its shortwave radiative forcing over North Africa: modeling sensitivities to dust emissions and aerosol size treatments. *Atmospheric Chemistry and Physics*, **10,** 8821-8838.

Figures

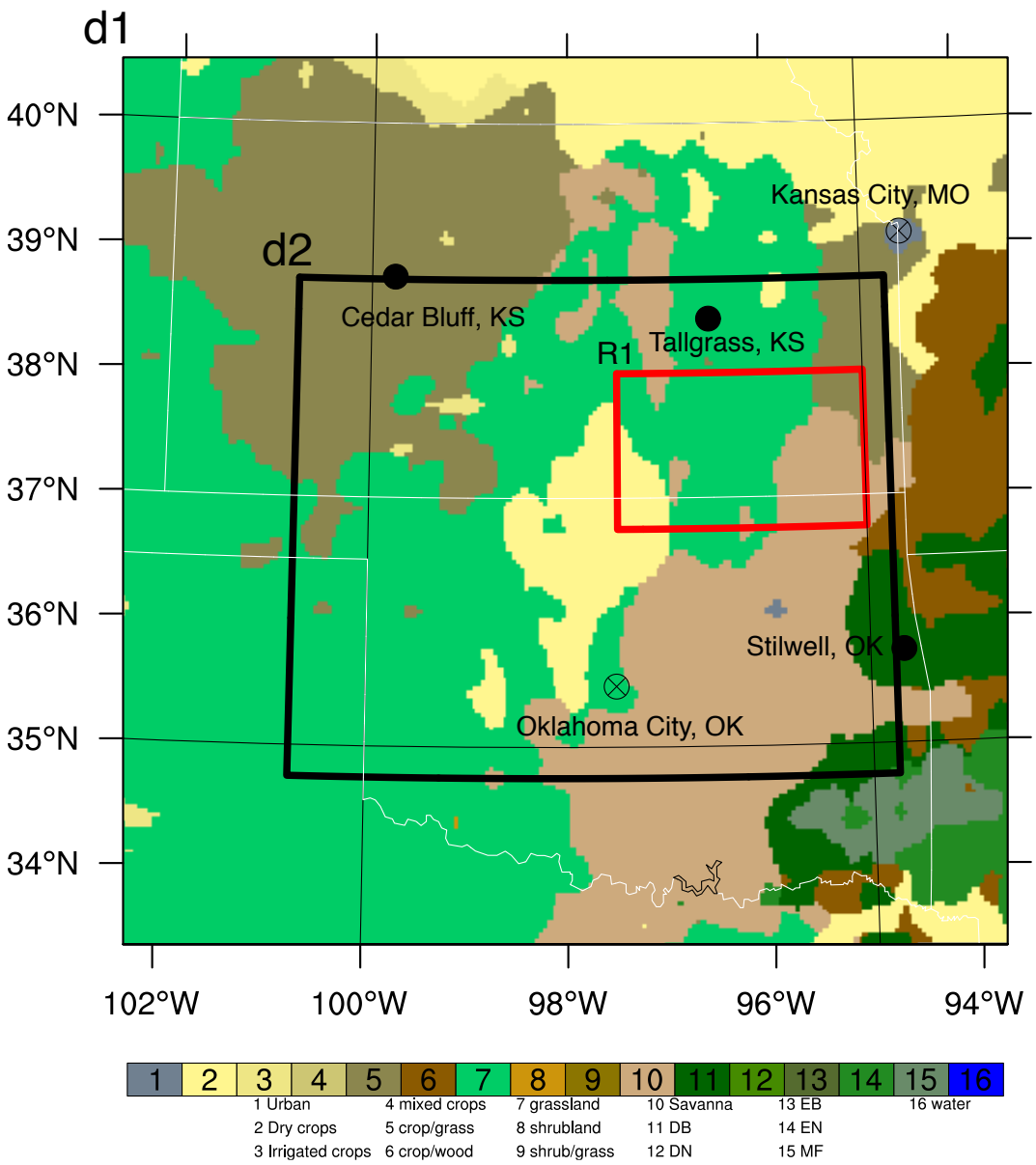

Figure 4.1: Land use category for simulated 4-km coarse domain (d1). The black line indicates the 1.33-km domain (d2). The red line encompasses the averaging region used in later figures (R1). Fill black circles are IMPROVE stations, circles with X's indicate cities.

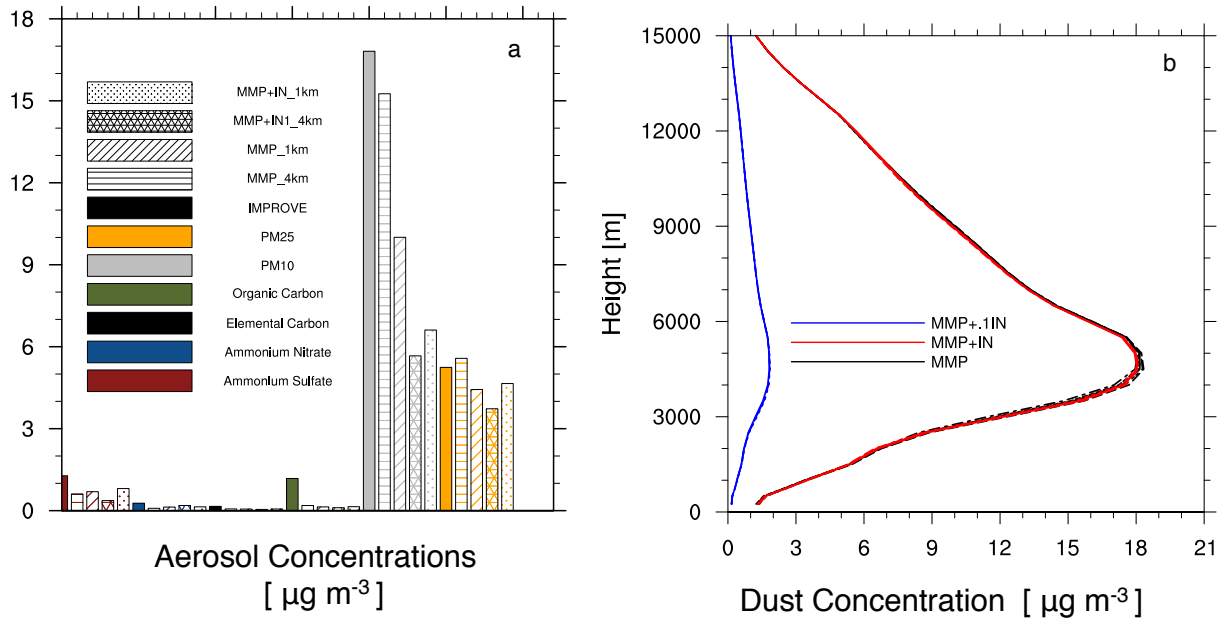

Figure 4.2: a) Aerosol concentrations averaged from IMPROVE sites (Tallgrass, KS; Stilwell, OK; and Cedar Bluff, KS) for May 30, 2012. Solid bars are averaged IMPROVE values. Hashed fills indicate modeled boundary layer averages from May 29 09:00 UTC – May 30 09:00 UTC. Horizontal lines are the MMP 4km model values, slanted lines are the MMP 1km model values, star hashing is the MMP+0.1IN model values and dot fill is the MMP+0.1IN model values. b) Vertical profile of dust (soila) concentrations from the MMP members (1-5, black lines), MMP+IN members (red lines), and MMP+0.1IN members (blue lines).

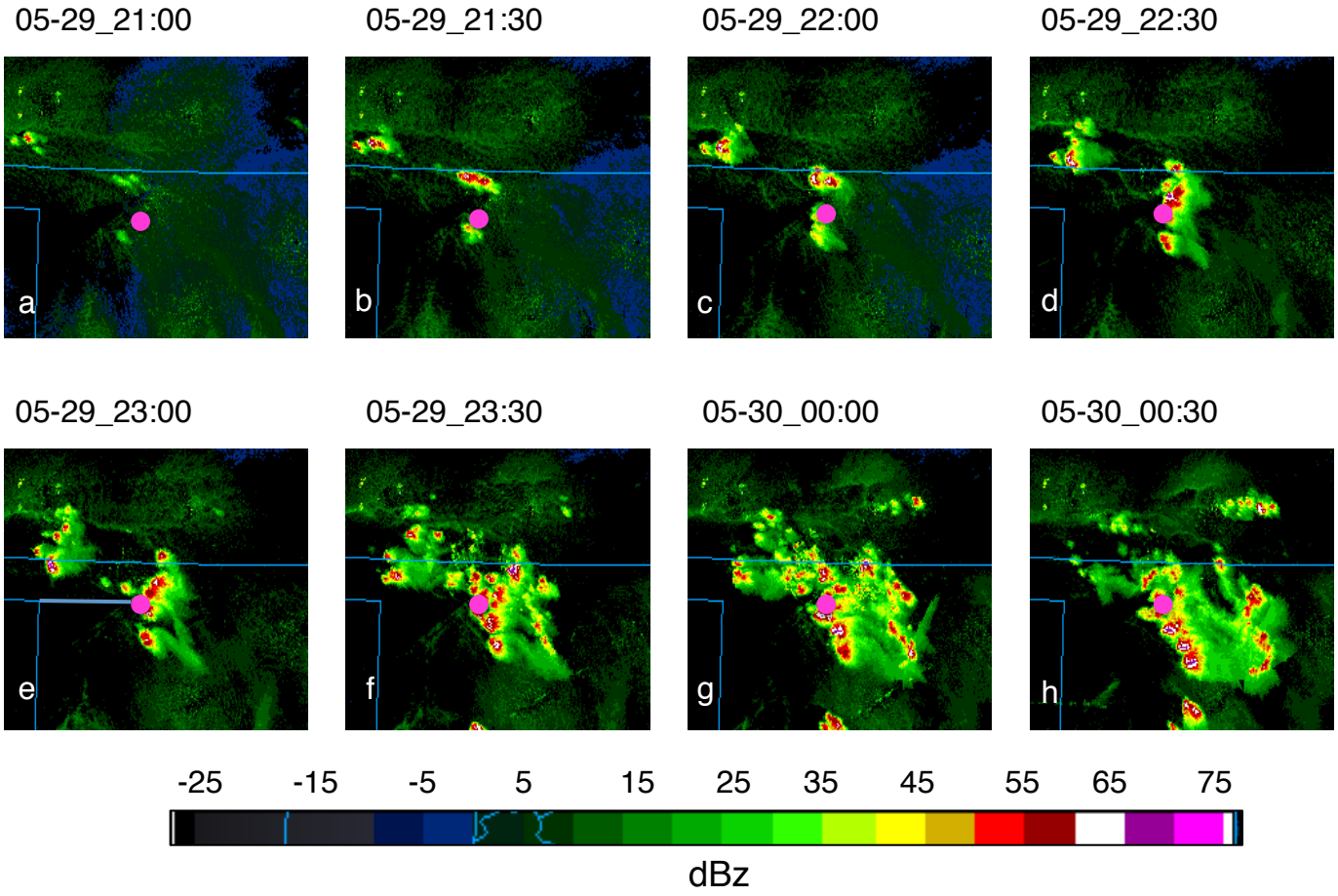

Figure 4.3: Archived radar images from www2.mmm.ucar.edu.imagearchive from May 29 (21:00 UTC) – 30 (00:30 UTC), 2012.The pink dot denotes Enid, OK.

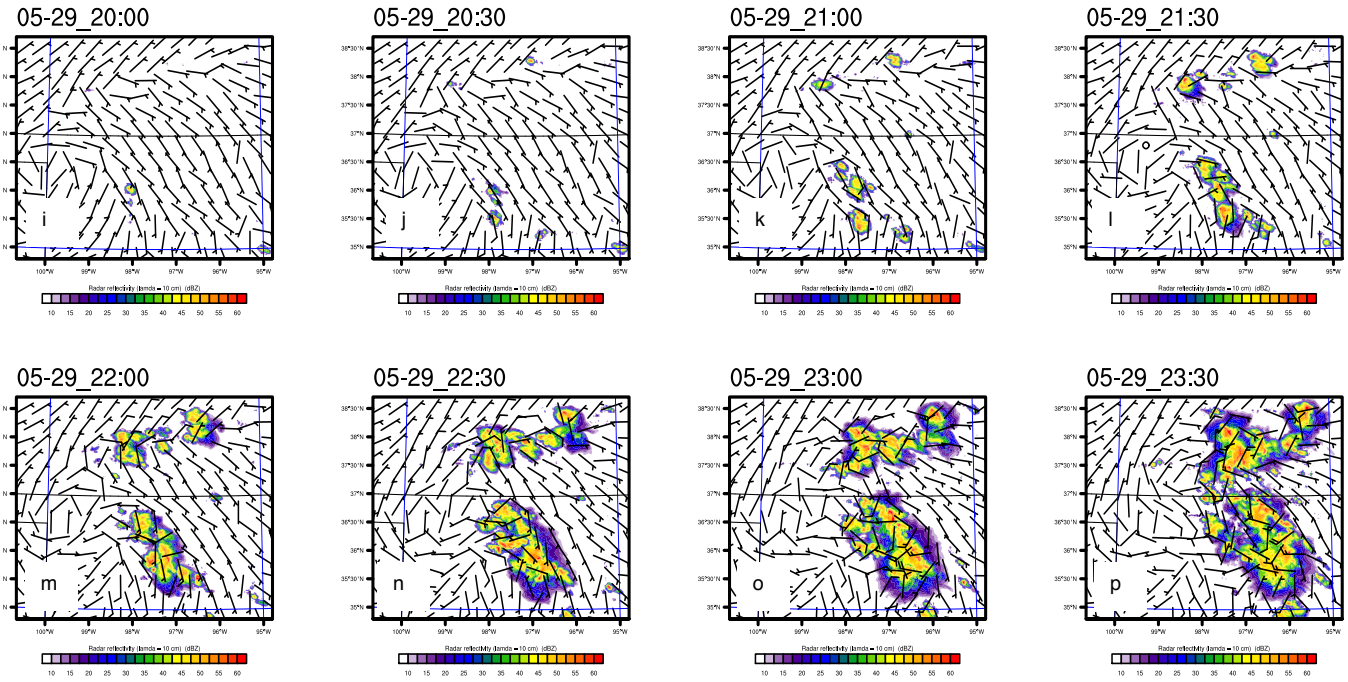

Figure 4.4: MMP4, 1.33 km domain simulated maximum radar reflectivity from May 29 (20:00 UTC – 23:30 UTC), 2012. Vectors indicate surface winds.

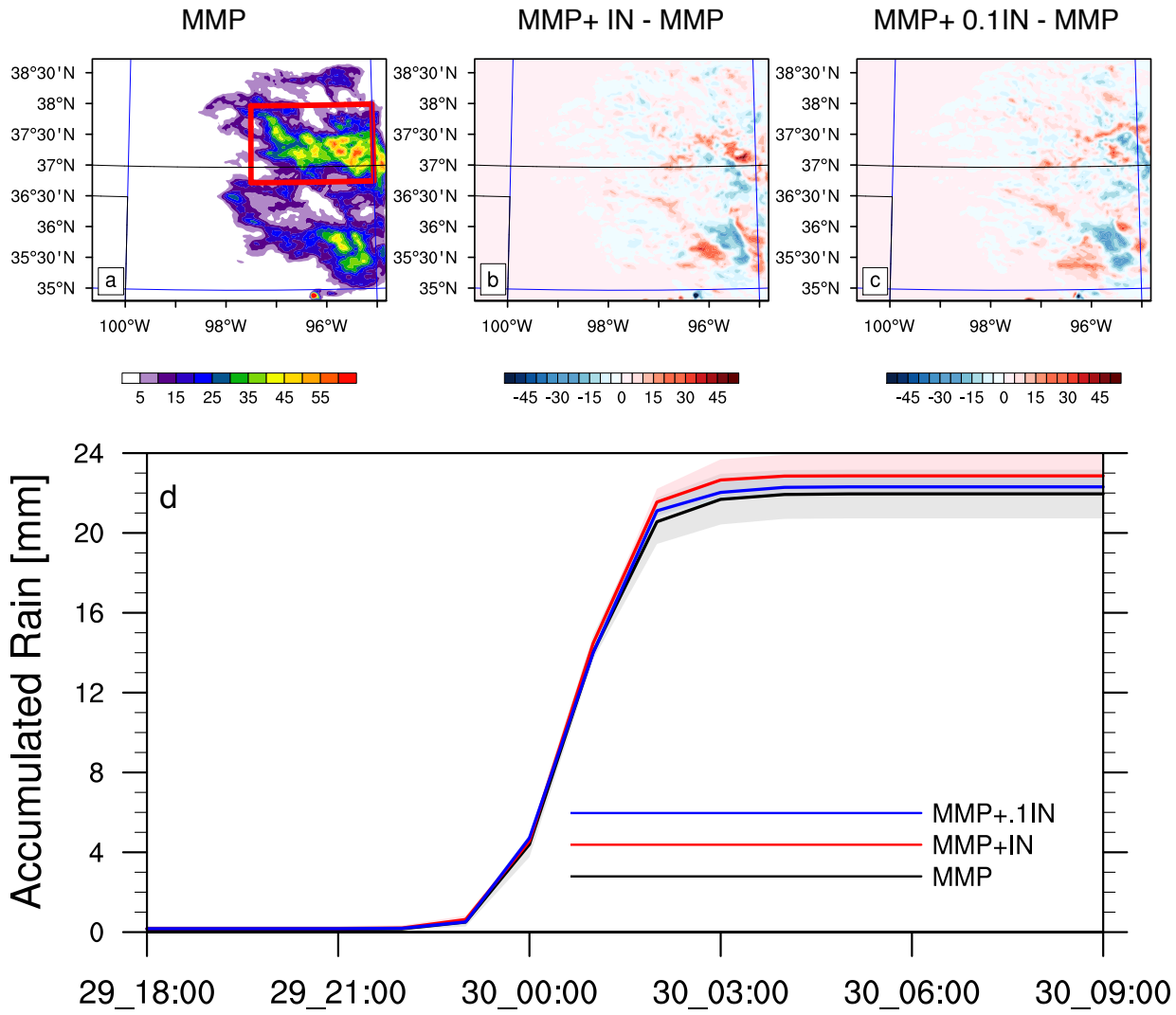

Figure 4.5: Accumulated for the time period May 29 18:00 UTC – May 30 09:00 UTC. a) MMP (1-5) ensemble mean accumulated rain (mm), red box (R1) indicates averaging region for 5d. b) difference of MMP+IN (1-3) ensemble mean accumulated rain (mm) and MMP ensemble mean. C) difference of MMP+0.1IN (1-3) ensemble mean accumulated rain (mm) and MMP ensemble mean. d) R1 averaged time series of accumulated rain (mm). Solid lines (black for MMP, red for MMP+IN, and blue for MMP+0.1IN) indicate ensemble means. Associated color shading indicates ensemble max and min.

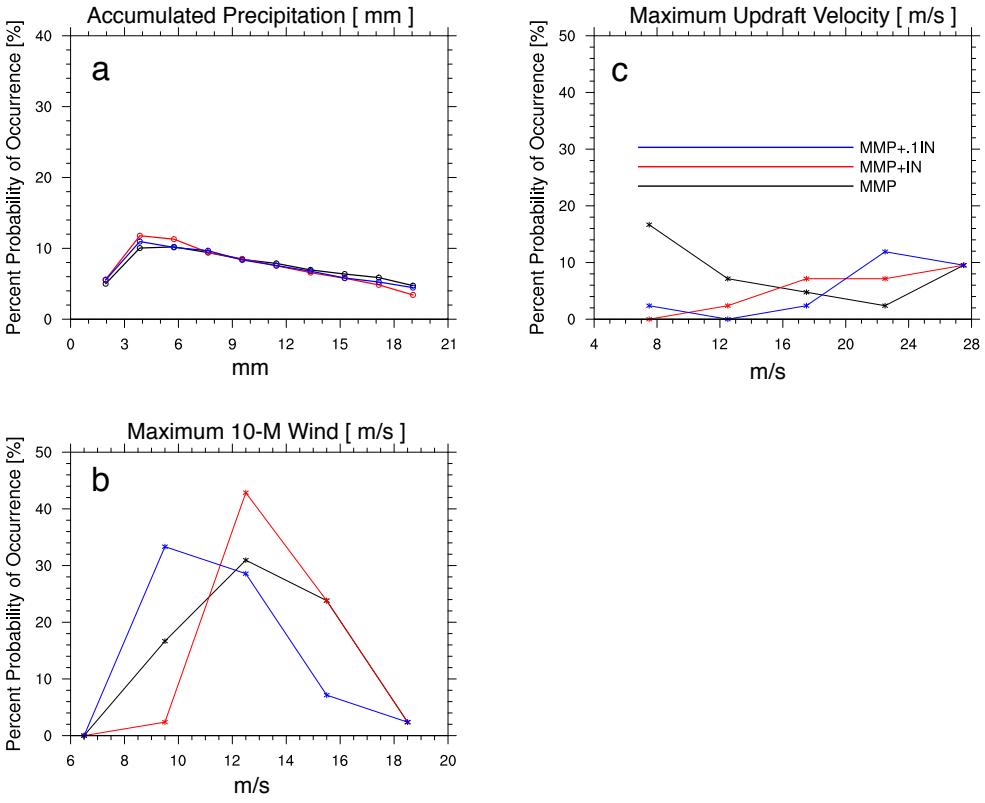

Figure 4.6: Inner domain, ensemble average probability density functions for a) accumulated rain (mm), b) 10-m horizontal maximum wind speeds, and c) maximum updraft velocities. Black lines indicate the MMP ensemble mean, red lines indicate the MMP+IN ensemble means, and blue lines indicate the MMP+0.1IN ensemble means.

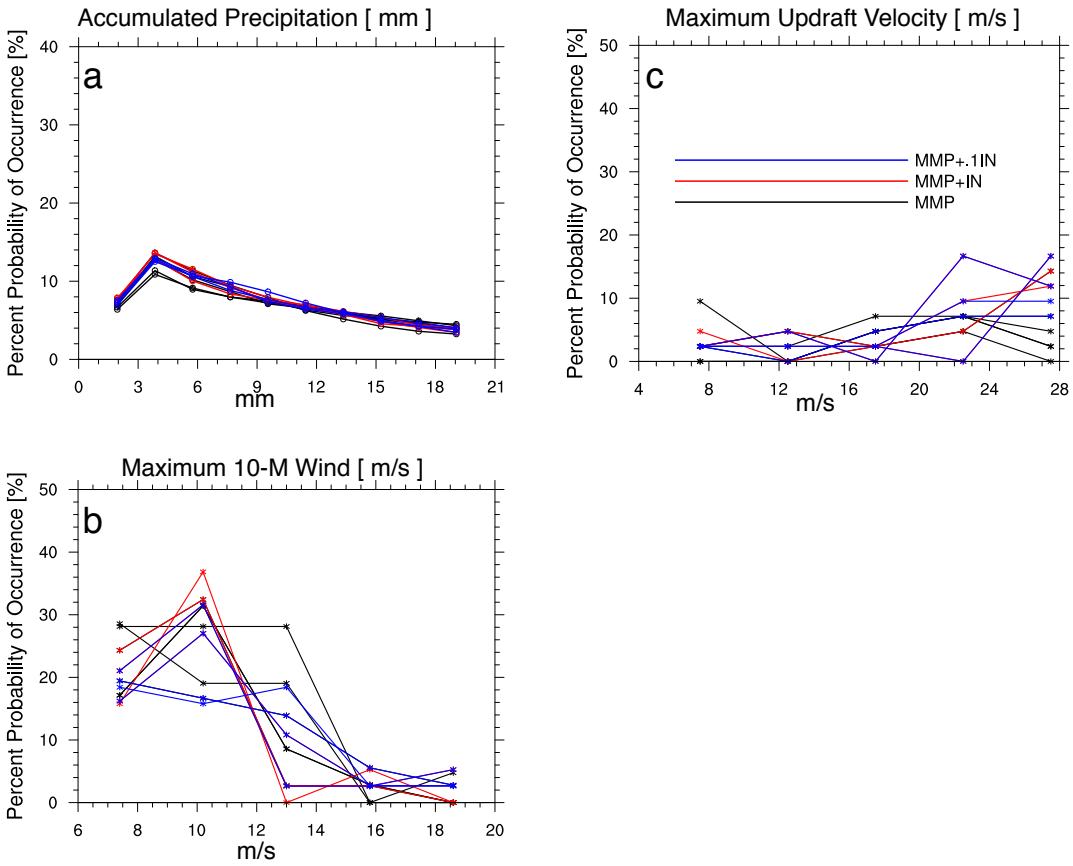

Figure 4.7: Inner domain, ensemble members probability density functions for a) accumulated rain (mm), b) 10-m horizontal maximum wind speeds, and c) maximum updraft velocities. Black lines indicate the MMP ensemble members, red lines indicate the MMP+IN ensemble members, and blue lines indicate the MMP+0.1IN ensemble members.

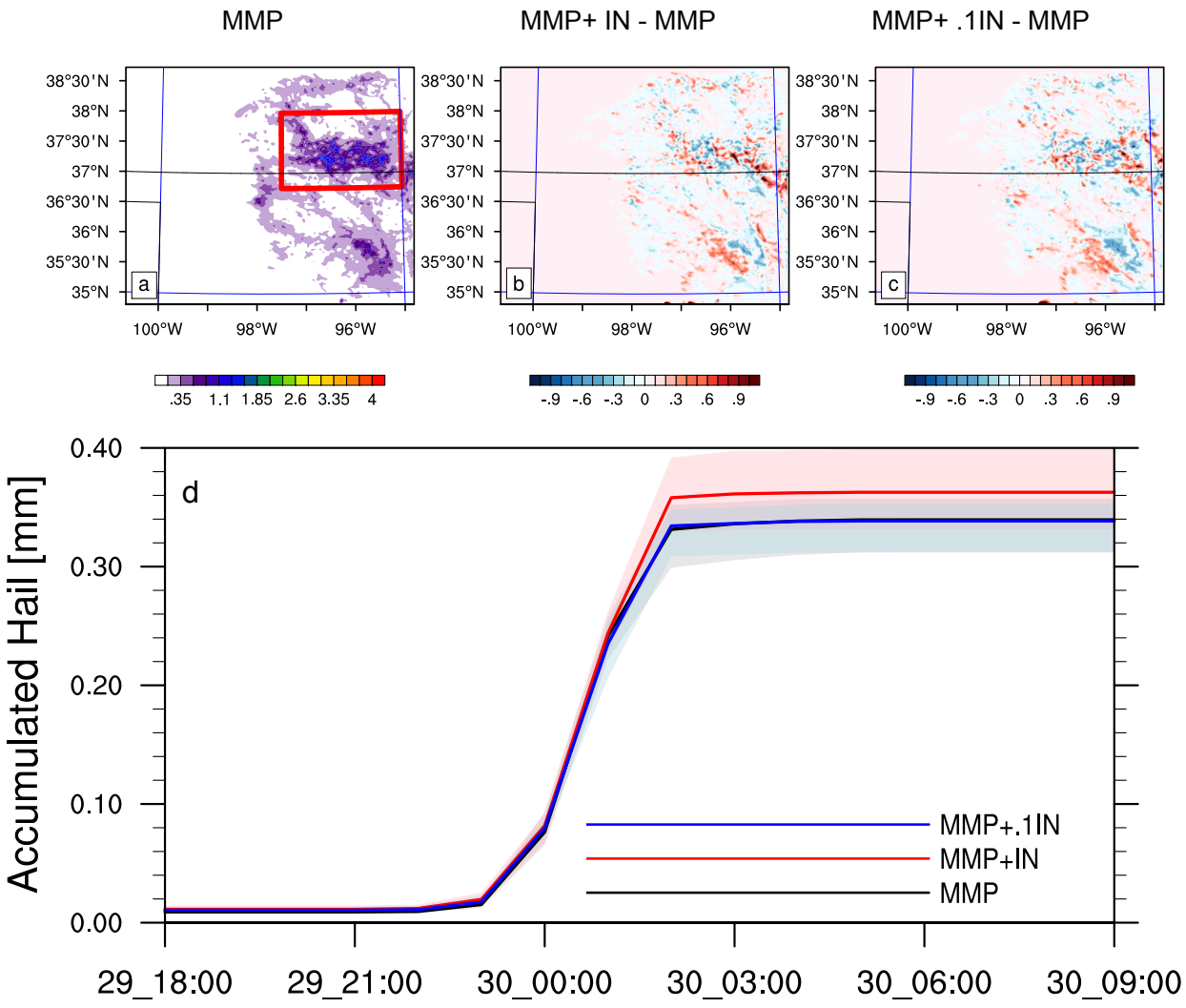

Figure 4.8: as in Figure 5, but for accumulated hail (mm).

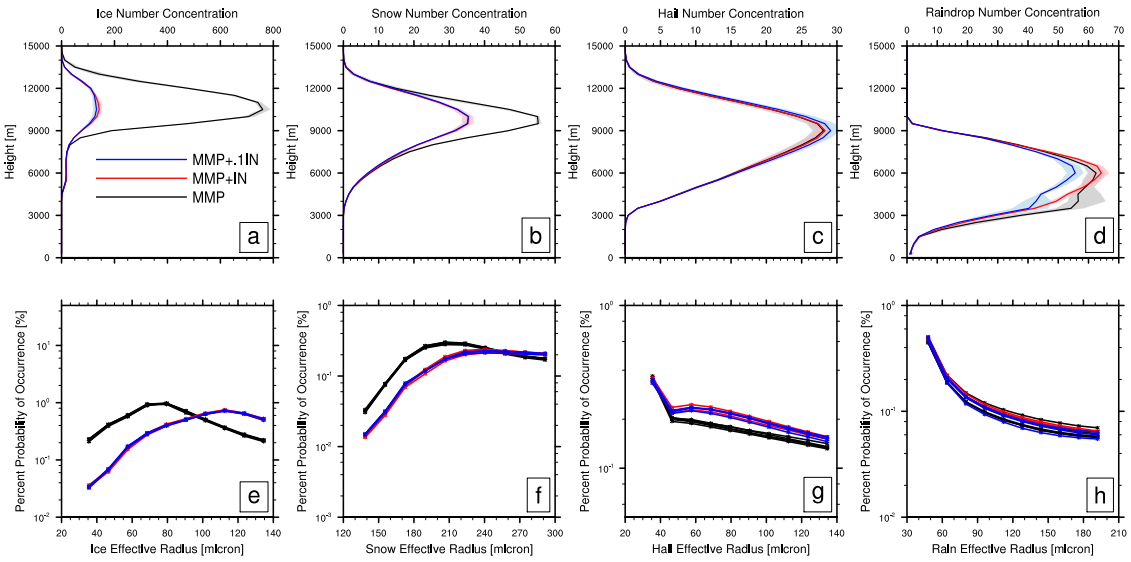

Figure 4.9: Vertical profiles of hydrometeor number concentrations (# L-1; a-d) averaged spatially over R1 region and temporally from May 29, 18:00 UTC – May 30, 09:00 UTC. a) Ice, b) snow ,c) hail, and d)rain. Probability density functions of effective size from May 29 18:00 UTC to May 30 09:00 UTC (microns; e-h) for R1 and all model levels, e) ice, f) snow, g) hail, h) rain. Solid lines indicate ensemble means: black for MMP, red for MMP+IN, and blue for MMP+0.1IN. Shading indicates ensemble max and min values.

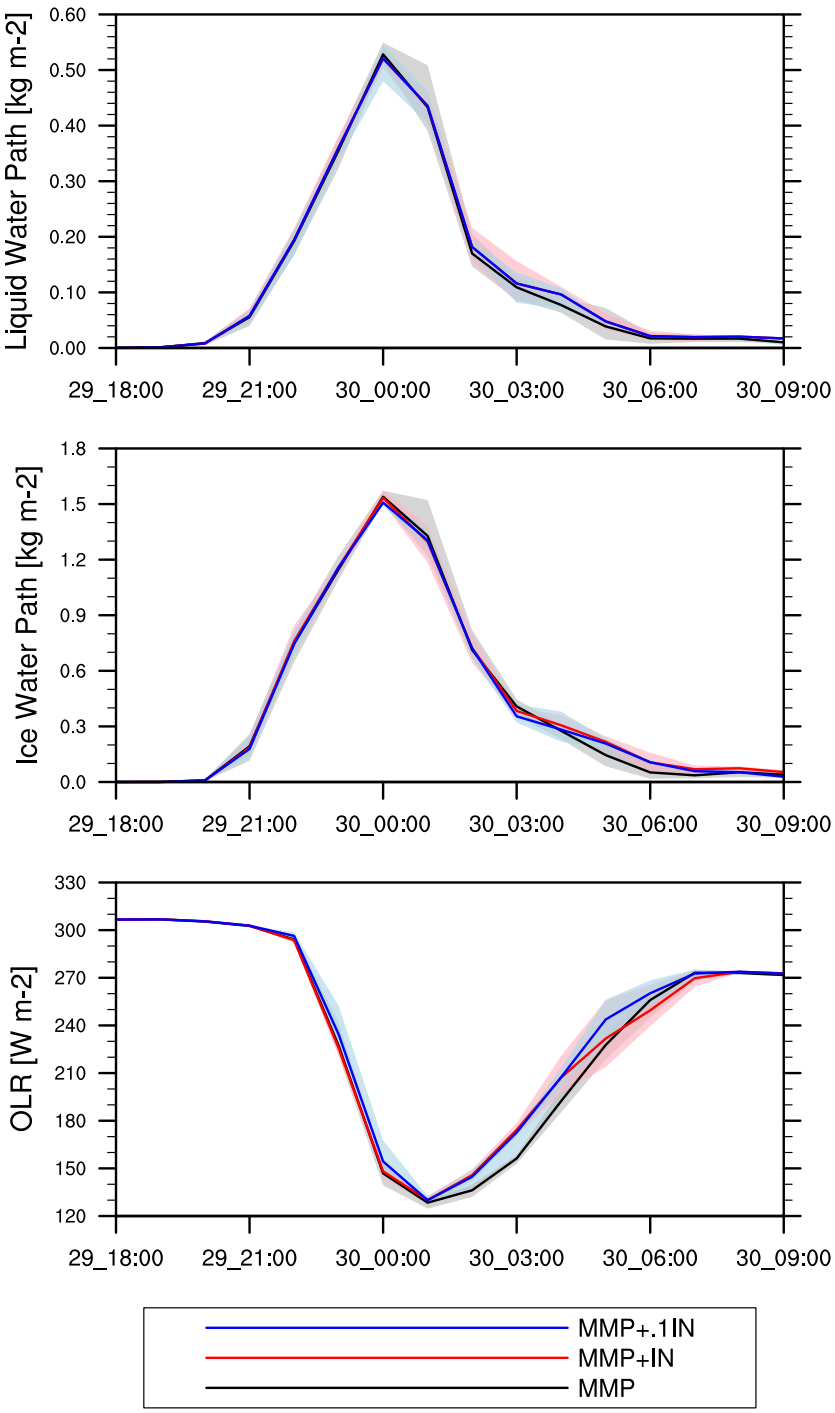

Figure 4.10: R1 spatially averaged a) Liquid water path (LWP, kg m^{-2}), b) Ice water path (IWP, kg m^{-2}) and c) Outgoing long-wave radiation (OLR, W m^{-2}). Solid lines indicate ensemble means: black for MMP, red for MMP+IN, and blue for MMP+0.1IN. Shading indicates ensemble max and min values

Ensemble Member	Microphysics	Dust Concentration Scaling Factor	Parent Domain
MMP1, MMP2, MMP3, MMP4, MMP5	Morrison (original)	100	MMP (4km)
MMP+IN1, MMP+IN2, MMP+IN3	Modified Morrison	100	MMP+IN (4km)
MMP+0.1IN1, MMP+0.1IN2, MMP+0.1IN3	Modified Morrison	10	MMP+0.1IN (4km)

Table 4.1: Ensemble members and experimental set up

Chapter V

5.0 Conclusions

Overall, aerosol-cloud interactions are known to impact climate via radiation effects and weather via microphysical processes. Understanding these interactions on regional scales is imperative to gaining insight for the global scale (Regayre et al. 2014). Because these relationships are known to be extremely complex, the treatment of aerosols over various spatial and temporal scales in models is a key element contributing to uncertainty in climate feedbacks (Seinfeld et al. 2016). Aerosol-cloud processes vary over a range of temporal and spatial scales, and this dissertation focuses on the interactions between aerosols and clouds during severe weather events. This includes a focus on the role of the magnitude of urban emissions on a squall line (Chapter 2), the role of chemical composition and model representation of hygroscopicity (Chapter 3), and the importance of dust as an ice nucleating particle (INP) in a supercell (Chapter 4). These results are summarized here and followed by a discussion examining further applications and the implications of this work.

5.1 Effects of urban aerosols on a mesoscale convective system.

In chapter 2, we investigated the effects of urban anthropogenic aerosols on a squall line. Specifically, we investigated the influence of urban emissions on a squall line that crossed Kansas City, MO on May 27, 201using the WRF-Chem model. The first set of experiments used the 2011 National Emissions Inventory to quantify anthropogenic emissions from Kansas City

emissions (BASE). We then scaled the emissions by a factor of two (2X) and one-half (HALF) to understand the sensitivity of the aerosol effect to the magnitude of urban emissions. For each case, we ran three ensemble members and evaluated changes based on the ensemble means and variability. Overall, we found that the magnitude of urban aerosols can affect a mesoscale convective system. Increasing emissions led to an increase in storm intensity, quantified by a larger and stronger cold pool and an increase in squall line precipitation. Decreasing emissions led to a decrease in storm intensity, earlier rainout of hydrometeors, and a smaller cold pool that advanced south more quickly than the precipitation, effectively weakening the system. These changes in the dynamics of the squall line are a function of the changes to the microphysics and are a direct result of the differences in urban aerosol loading. While these are model sensitivity tests, they do provide some insight into the role of urban areas in a severe weather location such as the Central Great Plains. Increasing the understanding of urban aerosol and meteorology interactions is important from a public safety perspective, a weather forecasting perspective, and the climate perspective. Gaining insight into where the heaviest precipitation might occur or where the most severe weather is more likely to occur is helpful to city planners and susceptible/vulnerable populations. This work highlights that the inclusion of urban aerosols and aerosol-cloud interactions in numerical weather prediction may lead to more accurate forecasts of severe weather, allowing longer warning lead times that can reduce property damage and potentially save lives.

5.2 The influence of aerosol hygroscopicity on precipitation intensity during a mesoscale convective event.

In chapter 3, we investigated the sensitivity of precipitation generated by a squall line to aerosol hygroscopicity (i.e,. the same event as simulated in Chapter 2 on May 27, 2013). There

are a suite of default hygroscopicity values prescribed in WRF-Chem, and these default values are used in the baseline simulation (BASE). We then perform an additional four simulations that perturb these default values to match laboratory-derived values. For the second simulation (SULF), we increase the sulfate hygroscopicity from 0.5 to 0.71, reflecting a substantial increase in anthropogenic aerosol hygroscopicity. In the third simulation (ORGO), we decrease the hygroscopicities of four of the anthropogenic organic aerosol species. The fourth simulation (SWITCH) implements a hygroscopicity dependency for ammonium. The ammonium ion can form either ammonium sulfate or ammonium nitrate depending on the ratio of ammonium to sulfate; if this ratio is higher than 2, then ammonium is allowed to partition to ammonium nitrate, leading to an increase in the ammonium ion hygroscopicity value. Finally, we perform an additional simulation (ALL) that incorporates all three the above changes (SULF, ORGO and SWITCH). Overall, we find hydrometeor sizes are more sensitive to hygroscopicity changes than hydrometeor number concentrations, which affects the formation of raindrop rates and precipitation. However, these changes in size lead to changes in precipitation patterns. Increasing hygroscopicity (SULF and SWITCH) increases the frequency of high intensity precipitation events (e.g., > 70 mm d^{-1}), while decreasing mid-range (30-70 mm d^{-1}) intensity events. Decreasing the hygroscopicity (ORGO) greatly increases the likelihood of weak intensity (< 20 mm d^{-1}) events, a decrease in mid-range intensity events, and an increase in strong intensity events. Including all the changes leads to a precipitation intensity distribution that best matches the observations, suggesting that the representation of aerosol composition is an important factor in determining precipitation intensity. Performing ensembles of this particular event would allow us to place this simulated improvement into the context of internal model variability, which can be large in this type of simulation. Additional case studies using different synoptic meteorology,

such as a wintertime extra-tropical cyclone, would allow us to evaluate the impact of aerosol composition on multiple meteorological scales.

We note that the mix of aerosol composition is an important component of the overall impact of the aerosol hygroscopicity sensitivity tests. For example, the Central Great Plains region has a relatively large amount of ammonium nitrate compared to ammonium sulfate, due to power primarily generated from natural gas instead of coal burning (EPA 2011). Because of the relatively small urban areas and vast amounts of agriculture and rangeland, the CGP has a different aerosol composition than other more populated regions of the United States. While this work shows that assumptions about composition are clearly important in determining precipitation patterns and intensity, there may be important regional differences that require further investigation.

5.3 Dust as ice nuclei: Implications for a mesoscale convective event in the Central Great Plains.

In contrast to the prior two chapters that focus on anthropogenic emissions, Chapter 4 focuses on dust in the Central Great Plains of the United States. Dust is an important aerosol component in the region due to the large amount of agricultural area, and observations show that there is significant inter-annual variability in dust concentrations (Prospero et al. 2002; Ginoux et al. 2012). Additionally, the intense meteorology in the region leads to severe weather such as squall lines and supercell formation, whose mesoscale dynamics include the formation, maintenance and dissipation of mixed phase and cold clouds. Because dust is an important ice nuclei, these aerosols may play an important role in the development and maintenance of supercell systems. However, many existing model parameterizations do not include the role of

dust as INP in these systems, and Chapter 4 describes new model development that supports this capability.

Chapter 4 includes a new dust INP parameterization to explore the role of dust on a supercell thunderstorm. In the prior studies described in this dissertation, the Morrison microphysics ice nucleation rate (Morrison et al. 2005) depends only on temperature and ice supersaturation and the role of interactive dust is not included in the interactions between aerosols and deep convection. In this chapter, we develop a new parameterization that uses the simulated and dynamic dust concentrations from the chemistry portion of the code in the microphysics portion of the code. We use the previously described relationship for deposition nucleation (Phillips et al. 2008) and condensation/immersion freezing (DeMott et al. 2010) to include dust as INPs. To determine the impacts of this INP change on a mesoscale convective event, we simulate a supercell that occurred on May 29-30, 2012 north of Oklahoma City, OK. Including dust as INPs leads to decreases in ice and snow number concentrations by factors of 5 and just under 2 respectively, and also shifts the cold-phase hydrometeors to larger effective radii. Interestingly, these differences do not demonstrate a significant impact on storm severity or precipitation and this is likely because, to a large extent, the strength of a supercell is determined by the synoptic meteorological conditions, such as convective available potential energy (CAPE) and low-level wind shear. Additionally the limited amount of water and water vapor indicates that most of the changes are between hydrometeor species and sizes, meaning there is a limit on the latent heat release. However, there is a notable increase in outgoing long-wave radiation with the new implementation, as a result of the decrease in the solid phase hydrometeor number concentrations. While including dust as INPs does not affect the overall severity of convection in this specific system, the prior work in Chapters 2 and 3 indicate that

squall lines could be modified as a result of changes to the anvil from including dust as INP. Additionally, the significant changes in outgoing long-wave radiation could have potentially important climate feedbacks for these severe weather systems.

5.4 Synthesis

This dissertation demonstrates the role of atmospheric aerosol composition on cloud microphysics, specifically in the context of mesoscale convective systems. While past work has approached this question using idealized simulations, this dissertation focuses on understanding aerosol and deep convective cloud interactions with realistically evolving aerosols and meteorology using a coupled chemistry-meteorology model (WRF-Chem). Overall, we find that squall lines are sensitive to the magnitude and composition of aerosols, and representing these processes within numerical weather prediction could improve forecasts of precipitation placement and intensity. The addition of dust as INP to the microphysics addresses a critical limitation of a popular and widely used numerical weather prediction model, WRF-Chem. The sensitivity studies presented here show that this implementation does not have a large impact on the precipitation processes, but does have a larger and more significant effect on the radiative balance of the mesoscale system. This suggests that the new parameterization does change the amount and size of solid phase hydrometeors, which affect the anvil size and distribution and drive changes in the radiative budget.

There are still many issues to resolve to further understanding of these complex interactions between aerosols and clouds. For example, many physical and chemical processes are competing on the drop level, on the cloud level, and on the system level and disentangling these effects require sensitivity studies as presented here. With this work, we further the

community's understanding of cloud and aerosol interactions and have elucidated the importance of dynamic aerosol simulations on short time scales such as that for severe weather systems.

One aspect that was not addressed in this dissertation is the long-term or climatic response to these changes. The sensitivity tests presented here were relatively short (e.g., 1- 3 days), and longer-term simulations spanning the entire convective season could highlight the climatic impact of cloud-aerosol interactions. This would enable the quantification of aerosol magnitude and composition effects on convective intensity and precipitation patterns on a seasonal scale, which would be invaluable to mitigating the uncertainty surrounding cloud and aerosol interactions with respect to climate and climate change. Additionally, performing experiments varying the water vapor of the squall line system would allow us to apply conclusions from this study to different climatic regions. Other variables can be tested as well, such as lifted condensation level (LCL) and the subsequent convective available potential energy (CAPE). Being able to separate the effects these environmental variables and aerosols have on each other and cloud drop activation would improve the understanding of cloud-aerosol interactions. Finally, performing the aerosol magnitude and composition sensitivity experiments with a supercell case study would provide a spectrum of aerosol effects on storm severity for the different types of mesoscale storms. These additional sensitivity tests would lead to more robust conclusions about how aerosols and squall lines interact with the climate.

Including dust concentrations in the ice nucleation parameterization did not change storm severity, yet changed the resulting radiation. The lack of severity change is likely because powerful mesoscale features drive supercell thunderstorms. However, different mesoscale systems interact differently with the environment. Squall lines can have a measurable feedback with radiation at the top of the anvil cloud. Simulating a squall line with this new

parameterization would allow an evaluation of how important dust is in squall line generation, formation, and propagation. Incorporating the new dust as INP parameterization into a WRF-Chem model release would allow others to address questions of changes in anvil characteristics and the associated climate and shorter-term feedbacks.

Finally, this work investigates realistic incidents that have direct applications to the current world. While the simulations are designed as sensitivity tests, the use of the dynamic aerosol populations and a complex mixture of composition introduces an aspect of realism to the simulations that have not been included in other case studies. While this dissertation focuses on the meteorological impacts of aerosols, both urban and agricultural populations are susceptible to pollution effects from aerosols because fine and coarse particulate matter play a key role in air quality. Modeling experiments such as those presented here should be considered when examining potential public health, environmental justice, and societal impacts.

References

DeMott, P. J., and Coauthors, 2010: Predicting global atmospheric ice nuclei distributions and their impacts on climate. *Proceedings of the National Academy of Sciences*, **107,** 11217-11222.

EPA, 2011: National Emissions Inventory.

Ginoux, P., J. M. Prospero, T. E. Gill, N. C. Hsu, and M. Zhao, 2012: Global‐scale attribution of anthropogenic and natural dust sources and their emission rates based on MODIS Deep Blue aerosol products. *Reviews of Geophysics*, **50**.

Morrison, H., J. Curry, and V. Khvorostyanov, 2005: A new double-moment microphysics parameterization for application in cloud and climate models. Part I: Description. *Journal of the Atmospheric Sciences*, **62,** 1665-1677.

Phillips, V. T. J., P. J. DeMott, and C. Andronache, 2008: An Empirical Parameterization of Heterogeneous Ice Nucleation for Multiple Chemical Species of Aerosol. *Journal of the Atmospheric Sciences*, **65,** 2757-2783.

Prospero, J. M., P. Ginoux, O. Torres, S. E. Nicholson, and T. E. Gill, 2002: Environmental characterization of global sources of atmospheric soil dust identified with the Nimbus 7 Total Ozone Mapping Spectrometer (TOMS) absorbing aerosol product. *Reviews of geophysics*, **40**.

Regayre, L., and Coauthors, 2014: Uncertainty in the magnitude of aerosol‐cloud radiative forcing over recent decades. *Geophysical Research Letters*, **41,** 9040-9049.

Seinfeld, J. H., and Coauthors, 2016: Improving our fundamental understanding of the role of aerosol− cloud interactions in the climate system. *Proceedings of the National Academy of Sciences*, **113,** 5781-5790.